2016

Conditional Cardiac-Specific Akap13 Knockout Induces Sex Dependent Biventricular Dilated Cardiomyopathy with Sarcomeric and Mitochondrial Defects

Kimberlyn M. Baig-Ward
Virginia Commonwealth University

CONDITIONAL CARDIAC-SPECIFIC AKAP13 KNOCKOUT INDUCES SEX DEPENDENT BIVENTRICULAR DILATED CARDIOMYOPATHY WITH SARCOMERIC AND MITOCHONDRIAL DEFECTS

A Dissertation submitted in partial fulfillment of the requirements for the degree of Doctor of Philosophy at Virginia Commonwealth University.

by

KIMBERLYN MARAVET BAIG-WARD
B.S., Molecular and Cell Biology, Texas A&M University, 2007
B.S., Biomedical Science, Texas A&M University, 2007

Advisor: JAMES H. SEGARS, M.D.
ADJUNCT PROFESSOR, DEPARTMENT OF BIOCHEMSITRY AND MOLECULAR BIOLOGY, VIRGINIA COMMONWEALTH UNIVERSITY SCHOOL OF MEDICINE
HOWARD W JONES, JR AND GEORGEANNA JONES PROFESSOR AND DIRECTOR DIVISION OF REPRODUCTIVE SCIENCES,
JOHNS HOPKINS SCHOOL OF MEDICINE

Advisor: JEROME F. STRAUSS, III, M.D., PH. D
PROFESSOR, DEPARTMENT OF BIOCHEMISTRY AND MOELCULAR BIOLOGY
DEAN, VIRGINIA COMMONWEALTH UNIVERSITY SCHOOL OF MEDICINE

Virginia Commonwealth University
Richmond, Virginia
August 2017

Acknowledgement

This dissertation is dedicated to my grandmother, Hancel E. Cochran (1937-2014). She was the wind beneath my wings and a light in the darkness. This world is a better place because she was here. I miss you and will always love you.

I could fill another dissertation with acknowledgments alone. First and foremost, I want to thank God for His immense blessings. I want to thank my parents (M.K. “Kim” and Connie) without whom I would never have been able to pursue my dreams. They taught me that no dream was too big, no mountain too high, no endeavor too challenging that hard work and determination can’t accomplish. I also want to thank my children, Camden and Amerlyn Ward. You two make everything worthwhile. Everything I do, I do it for you guys.

Dr. Jim Segars, what can I even say? I can’t even begin to thank you enough for your unwavering support, dedication to my project and belief in me. You never stopped pushing me and never stopped raising the bar. When you relocated to Johns Hopkins University School of Medicine after 20+ years at the National Institute of Child Health and Human Development at the National Institutes of Health, I followed you. I would have followed you no matter where you relocated because a true mentor is worth their weight in gold. I look forward to many years of collaboration and spurring each other on

to further our science, ask challenging research questions, and continue to pursue AKAP13's integral physiologic role. I'm an AKAP13 lady for life!

Dr. Jerome Strauss, III, Dr. Gordon Archer, Dr. Ross Mikkelsen, and Sandra Sorrell of the Virginia Commonwealth University School of Medicine and VCU MD/PhD program, thank you, thank you, from the bottom of my heart thank you for the opportunity to pursue the combined degree program at VCU School of Medicine. Thank you for the steadfast support that you give to each one of your students. The one thing, in my opinion, that separates VCU School of Medicine from every single medical school in the country is YOU and the VCU student-centric environment. You don't aim to fit square pegs in round holes. You treat your students as individuals to help them accomplish their goals, and do whatever it takes to help your students not only succeed, but craft a degree and training program that is ideally suited for everyone. You knew I wanted to participate in the Graduate Partnership Program at the National Institutes of Health, and you helped make that happen. I cannot thank you enough. Any student trained at VCU School of Medicine is a student that was cherished and given the best training and support for success. You were each a wonderful mentor to me along this journey. Thank you again.

It has been said that it takes a village to bring up a child, similarly it takes a village of dedicated scientists to bring up a Ph.D. I would like to thank the many, many colleagues, collaborators, and committee members that helped make this project possible,

my amazing scientific village: Dr. Tomasz Kordula, Dr. Joyce Lloyd, Dr. Alan DeCherney, Dr. Tomoshige Kino, Dr. Suzanne Barbour, Dr. Hisashi Koide, Dr. “Cat” Guo, Tiffany Chu, Caroline Quaglieri, Dr. Stasia Anderson, Dr. Alessandra Broferrio, Vivian Diaz, Su-Chi Su (Caine), Dr. Sunni Mumford, Dr. Julian Liu, Dr. Kamaria Cayton, Dr. Sinnie Ng, Dr. Minnie Malik, Dr. Joy Brittan, Dr. Mones Abu-Asab, Dr. Uri Manor, and all Segars’ lab members (former and present). There were many, many others who were an integral part of this project and without whom, this endeavor would not have been possible. Thank you all again for your dedication, guidance, and friendship. Finally, I would like to thank the National Institutes of Health (NIH) Graduate Partnership Program for allowing me to pursue an individual GPP.

Table of Contents

Page

List of Tables

Page

List of Figures

Page

Abstract

CONDITIONAL CARDIAC-SPECIFIC AKAP13 KNOCKOUT INDUCES SEX DEPENDENT BIVENTRICULAR DILATED CARDIOMYOPATHY WITH SARCOMERIC AND MITOCHONDRIAL DEFECTS

By K. Maravet Baig-Ward, Ph.D.

A Dissertation submitted in partial fulfillment of the requirements for the degree of Doctor of Philosophy at Virginia Commonwealth University.

Virginia Commonwealth University, 2016

Major Director: Dr. James H. Segars, MD
Adjunct Professor, Biochemistry and Molecular Biology

Heart disease is a complex and heterogeneous disease. Notably, studies have demonstrated gender differences in the expression and types of cardiovascular disease, such as dilated cardiomyopathy (DCM), a major underlying cause of heart failure. Previously we showed that loss of A-Kinase Anchoring Protein 13 (*Akap13)*, a unique proto-oncogene and estrogen receptor modulator, resulted in enlarged embryonic hearts, defective cardiac sarcomere formation, and embryonic lethality in mice. Data have also

shown cAMP-dependent Protein Kinase A (PKA) to be involved in DCM pathophysiology. Given the established role of AKAP13 in cell signaling, its ability to bind and modulate ligand-activated nuclear hormone receptors and transcription factors, and its association with actin and other cytoskeletal components, **we hypothesized that a functional AKAP13 protein was required for cardiomyocyte function in the adult heart; defective function of AKAP13 could promote DCM.** To this end, we established an inducible, cardiac-specific *Akap13* conditional knockout (*Akap13*^{cKO}) mouse model using a Cre-lox recombination strategy with two separate Cre-recombinase expressing mouse models (α-MHC-MerCreMer and *Tnnt2*-rtTA; TetO-Cre).

Cardiac functional examination of *Akap13*^{cKO} mice revealed significant biventricular dilated cardiomyopathy with compensatory hypertrophic remodeling of the left ventricle and left atrial enlargement, decreased left and right ventricular systolic function, and abnormal left ventricular diastolic function. Of note, female *Akap13*^{cKO} mice displayed a more pronounced cardiac phenotype and were more likely to die post-recombination.

CHAPTER1: Introduction to AKAP13

Introduction

Cells process a vast array of diverse stimuli and differentiate a multitude of signals based on multiple factors, including the cells' internal and external milieu. Cyclic adenosine monophosphate (cAMP), a commonly used, generic second messenger, is involved in many, and often disparate, signaling pathways. A-Kinase Anchoring Proteins (AKAPs) rectify cAMP signaling pathways by tethering cAMP-dependent Protein Kinase A (PKA) to sub-cellular microdomains, such as organelles and other membranes (Colledge, 1999) (Welch, 2010). Within these sub-cellular niches, AKAPs act as engaged scaffolding proteins or "signaling centers," confining PKA, or other signaling enzymes, closer to their biological substrates, downstream signaling enzymes, supplemental molecules, and co-factors. Notably, AKAP13, found on human chromosome 15q25.3 and mouse chromosome 7D2 (Pruitt, 2013), is the only known AKAP with Guanine Nucleotide Exchange Factor (GEF) activity and the ability to modulate nuclear hormone receptors such as Estrogen Receptors α and β (ER α and ER β) (Rubino, 1998) (Driggers, 2001).

A-Kinase Anchoring Proteins (AKAPs) are essential signaling pathway rectifiers. As a family, AKAPs share a common function: to bind and sequester cAMP-dependent Protein Kinase A to discrete subcellular microdomains thereby enhancing downstream signaling to PKA targets, and affecting gene expression (Wong, 2004) (Colledge, 1999).

(Fig.1.1). It is hypothesized that these sub-cellular microdomains may be niches with transiently increased levels of cAMP (Scott, 2010) (Bacskai, 1993) (Hempel, 1996).

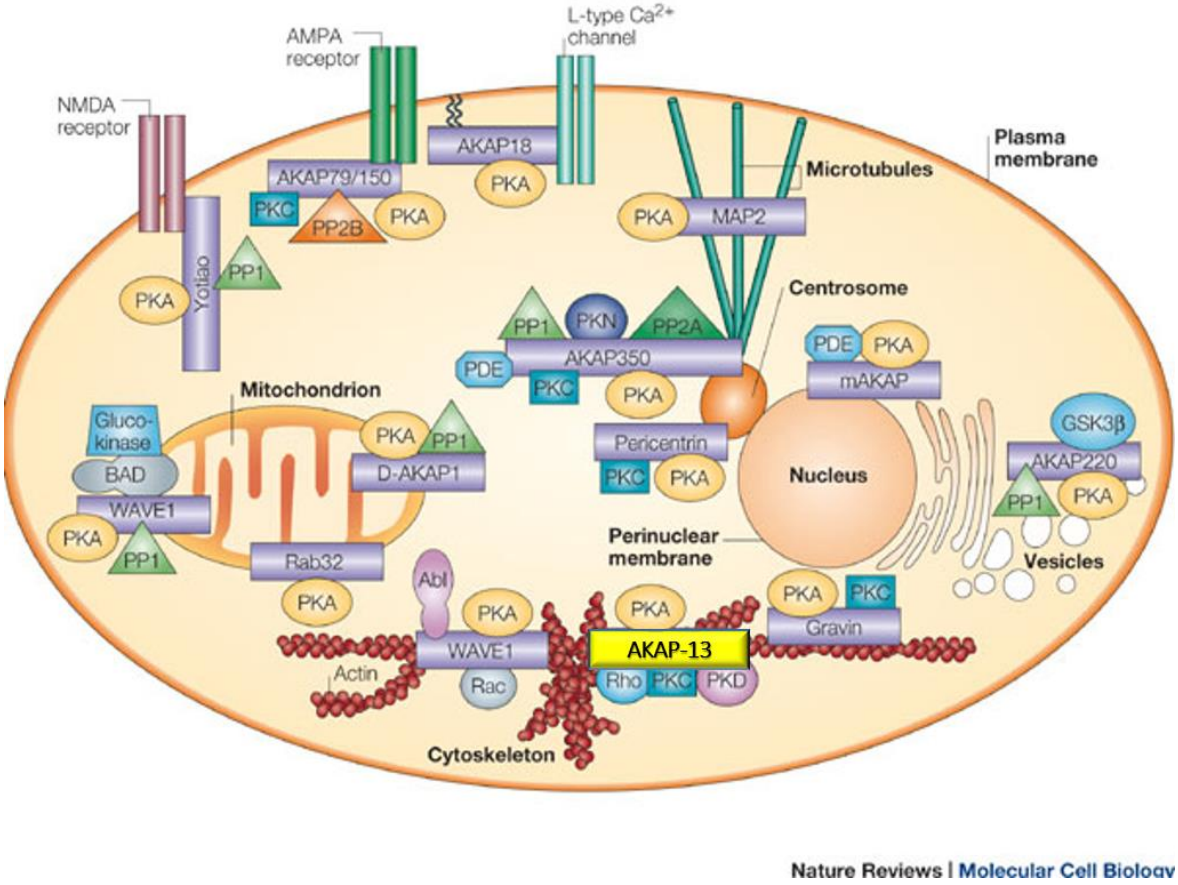

Nature Reviews | Molecular Cell Biology

Figure 1.1| **AKAPs in cell signaling.** AKAPs have significant roles in cell signaling from the membrane to the nucleus. AKAPs often associate with organelles and other cellular components to rectify signaling pathways for spatiotemporal fidelity (modified from: Wong, 2004).

While AKAPs have a common function, they are structurally heterogeneous except for a conserved 14-18 amino acid residue amphipathic helix (Baisamy, 2005) (Welch, 2010). This helical region anchors Protein Kinase A. AKAPs also act as scaffolding proteins; they can bind a variety of enzymes and associated substrates, both directly and indirectly, to enhance signal transduction for timely action by the cell (Welch, 2010) (Mauban, 2009). To date, there are more than 50 reported AKAPs; this number includes AKAP splice variants (Carnegie, 2009) (Welch, 2010). AKAP13, also known as Brx and AKAP-Lbc, is unique. In addition to classic AKAP function, tethering PKA to sub-cellular locations and acting as a scaffolding protein, AKAP13 contains a Rho- Guanine Nucleotide Exchange Factor (GEF) activity domain and binds to other signaling proteins including ligand-activated nuclear receptors (Rubino, 1998) (Diviani, 2001) (Fig. 1.2). GEFs, such as Epac, are known to refine cAMP signaling (Pereira, 2007). Specifically, AKAP13 has been shown to bind to nuclear receptors such as Estrogen Receptors (ER), retinoid X receptor (RXR), thyroid hormone receptor (THR), peroxisome proliferator-activated receptor (PPAR) and cAMP response element binding protein (CREB) (Rubino, 1998) (Driggers, 2001). Since AKAP13 has characteristic AKAP activity as well as Rho-GEF activity and the ability to bind nuclear hormone receptors, it is essential that pathways involving AKAP13 are tightly regulated and serve to promote cellular actions that are regulated both spatially and temporally.

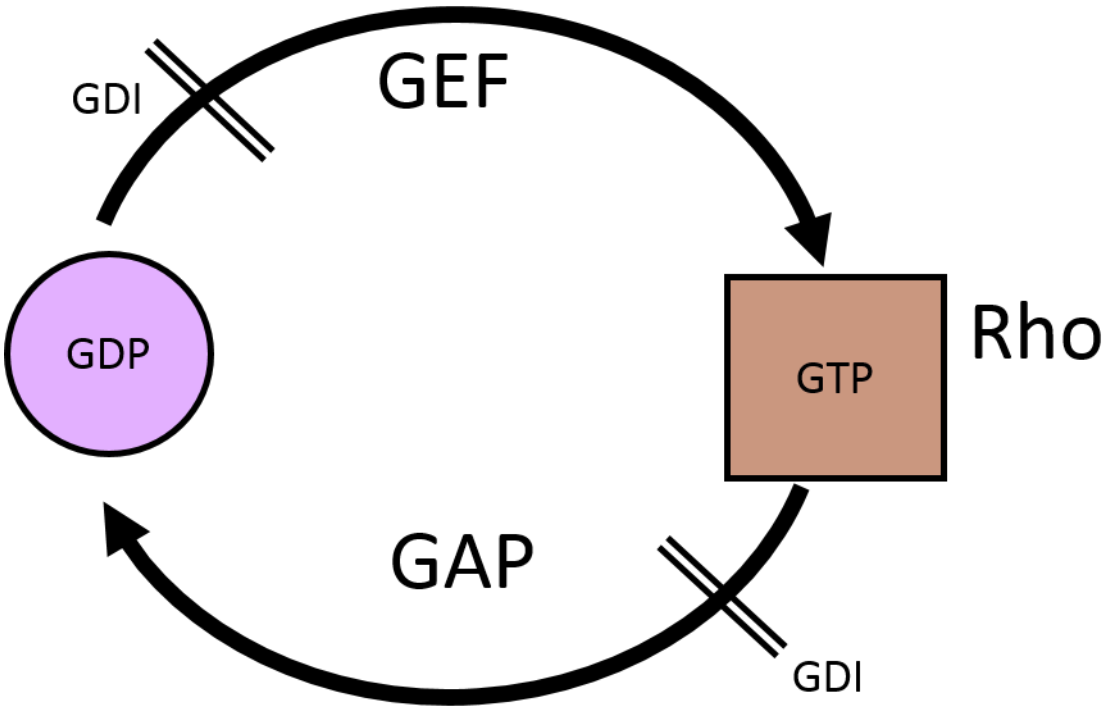

Figure 1.2| Guanine Nucleotide Exchange Factor Activity. Guanine Nucleotide Exchange Factor Activity (GEF) facilitates GTP-exchange on small G-Proteins. RhoA (GTPase) is activated with the binding of GTP. GTPase Activating Proteins (GAPs) and Guanine Nucleotide Dissociation Inhibitors (GDIs) affect the GDP and GTP binding state of the small G-protein.

Initial characterization of AKAP13: Brx

Previous *in vitro* studies demonstrated the presence of an auxiliary protein that bound the retinoid x receptor (RXR) and demonstrated involvement in the inhibition of estrogen-responsive genes (Segars, 1993). These findings led to the hypothesis that an auxiliary protein(s) also involved in estrogen-responsive breast cancer *in vivo* (Anzano, 1994) (Rubino, 1998). To this end, a breast cancer expression library was probed using a cloning strategy that took advantage of the unknown auxiliary protein's ability to bind RXR. From this, a novel cDNA was isolated. Further analyses identified the novel auxiliary protein to be the smallest and first AKAP13 gene product fully characterized, the 170kDa protein often referred to as Brx: **b**reast cancer nuclear **r**eceptor-binding au**x**iliary protein (Rubino, 1998). This isoform was found to directly associate with Estrogen Receptor α (ER α) as exhibited by far-Western analysis (Rubino, 1998). Northern blot analysis suggested that AKAP13 gene products were highly expressed in reproductive tissues including tissues from the ZR 75-1 breast carcinoma cell line (Rubino, 1998). Due to Brx's presence in reproductive tissues, ability to bind nuclear hormone receptors via the LXXLL (specifically LYELL) domain including ERs (Rubino, 1998) (Driggers 2001), and the role of estrogen in some forms of breast and endometrial cancers, our group, and others continued to pursue this isoform's role in estrogen-responsive tissues. More recently, AKAP13 has also been shown to bind Progesterone Receptor (PR) and the Vitamin D receptor (VDR) among others (unpublished data).

In 2006, Wirtenberger and colleagues revealed a genetic polymorphism (Lys526Gln) in AKAP13 with statistically significant association with familial breast

cancer (OR=1.58, 95% CU=1.07-2.88). This single nucleotide polymorphism (SNP) was found to be even more significantly linked to high-risk familial breast cancer (OR=1.85, 95% CI= 1.19-2.88). These data suggested that women with the AKAP13 Lys526Gln SNP if diagnosed with breast cancer, were more likely to have high-risk breast cancer (Wirtenberger, 2006).

Functional and structural regions within AKAP13

AKAP13 is a unique cAMP-dependent Protein Kinase A Anchoring Protein (AKAP) member of the Dbl family of oncoproteins (Rubino, 1998). As the name suggests, AKAP13 acts to bind and sequester PKA in order to bring it closer to its biological substrates (Michel and Scott, 2002). While AKAP13 can bind other isoforms of PKA, such as type I PKA, it preferentially binds type II PKA (Diviani, 2004). Additionally, AKAP13 contains a single Dbl Homology domain (DH) with a single, flanking Pleckstrin Homology domain (PH). Together these domains comprise the Guanine Nucleotide Exchange Factor (GEF) activity region of the protein (Rubino, 1998) (Wirtenberger, 2006). While AKAP13 as a whole has not been crystallized, the GEF domain has been crystallized (Fig. 1.3) (Azeez, 2014). This characteristic is shared by other oncogenic Dbl family members, such as Lbc. AKAP13 is often reported as AKAP-Lbc in the literature because of the shared sequence homology. AKAP13 has also been reported as a truncated form of Ht31 and has even been called Ht31 (Klussmann, 2001). This, however, is not the case. Ht31 is a partial cDNA is that likely a truncated form of AKAP13, and not vice versa. Therefore, AKAP13 is the preferred, and more accurate, name.

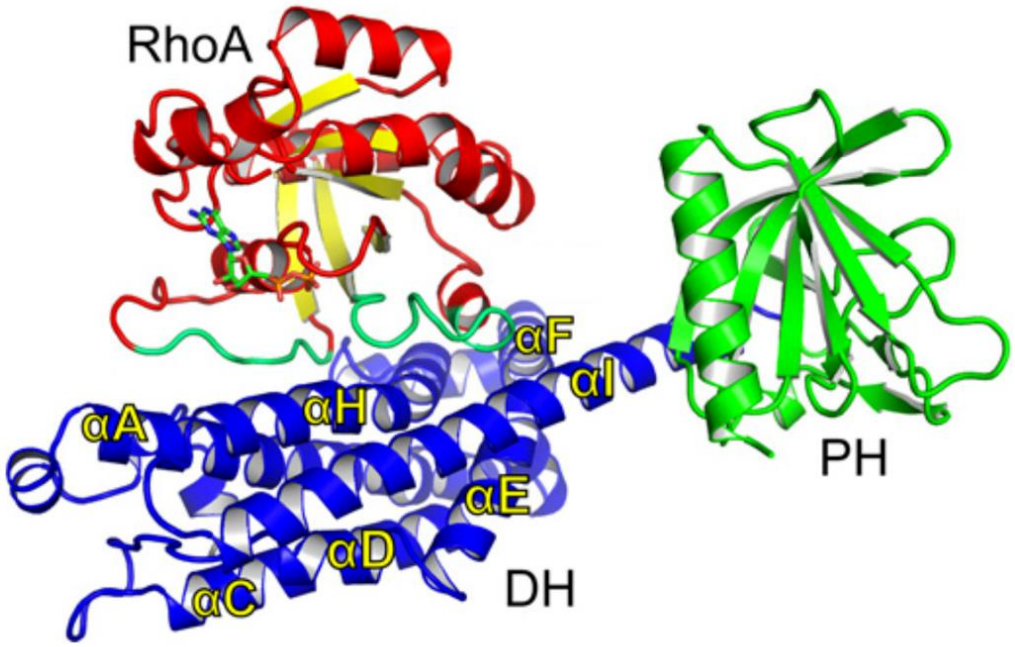

Figure 1.3| AKAP13 transcripts and Guanine Nucleotide Exchange Factor (GEF) crystal structure. a) AKAP13 is alternatively spliced. Some of the more common transcripts are depicted above. **b)** The RhoA and AKAP13 complex is depicted in structural form. RhoA is depicted with red α-helices and yellow β-strands. AKAP13 DH domain is depicted by the blue α-helices, and the PH domain is depicted by the green α-helices and β-strands (modified from: Azeez, 2014).

It has been reported by our laboratory and others that AKAP13 is a RhoA-specific GEF (Diviani, 2001) (Mayers, 2010). AKAP13's GEF domain may have modest activity with Rac and Cdc42 (Rubino, 1998) (O'Connor, 2012). However, AKAP13 also interacts with small GTPases, such as Cdc42, in other capacities (Rubino, 1998).

AKAP13 Rho-GEF activity is regulated by the homodimerization of the AKAP13 carboxyl terminus (Baisamy, 2005). Similarly, AKAP13 has two putative 14-3-3 binding sites; PKA bound to AKAP13 can phosphorylate serine residues within the 14-3-3 binding sites thereby recruiting 14-3-3, and inhibiting AKAP13's Rho-GEF activity (Diviani, 2004; Baisamy, 2005). Therefore, it is hypothesized that AKAP13 is maintained in a basal, resting state through homodimerization of the carboxyl terminus and binding of 14-3-3 (Baisamy 2005). Binding of dimeric 14-3-3 prevents RhoA association with AKAP13 (Baisamy, 2005; Diviani, 2004). However, 14-3-3 only functions as an inhibitor of Rho-GEF activity when AKAP13 is in an oligomeric state (Baisamy, 2005). With appropriate activating stimuli, such as LPA or thrombin, the α subunit of the $G_{\alpha 12}$ signaling molecule stimulates AKAP13 Rho-GEF activity (Diviani, 2001), preventing 14-3-3 binding, and thereby assisting in the transformation of AKAP13 from a basal, resting state into a multimolecular signaling rectifier. PKA acts as an inhibitor of RhoA and serum response factor (SRF) and activator of cAMP-response element binding protein (CREB) (Sauzeau, 2000) (Ellerbroek, 2003). Conversely, RhoA activates SRF and therefore induction of serum response element (SRE) driven genes, many of which are implicated in heart disease (Mayers, 2010) (Seeger, 2010) (Montaner, 1999). Consequently, AKAP13 is central to the

balance between CRE responsive genes and SRE responsive genes depending on the physiologic and temporal needs of the cell including the developmental stage (Fig. 1.4).

As an active, modular protein platform, AKAP13 integrates upstream factors with downstream signaling to affect gene expression and cell response (Rubino, 1998). In order to do this, AKAP13 must bind or interact with an assortment of proteins with often disparate family linkages. One such family is the Nuclear Hormone Receptor (NHR) family, specifically Estrogen Receptor (ER) α (Rubino, 1998) and Estrogen Receptor (ER) β (Driggers, 2001). AKAP13's novel and somewhat enigmatic carboxyl terminus separately bind ERα and ERβ, and in doing so, augments the ERs function. In vitro studies have shown that AKAP13 also binds the retinoid x receptor (RXR) (Segars, 1993), the peroxisome proliferator-activated receptor (PPAR), and the thyroid hormone receptor (Rubino, 1998).

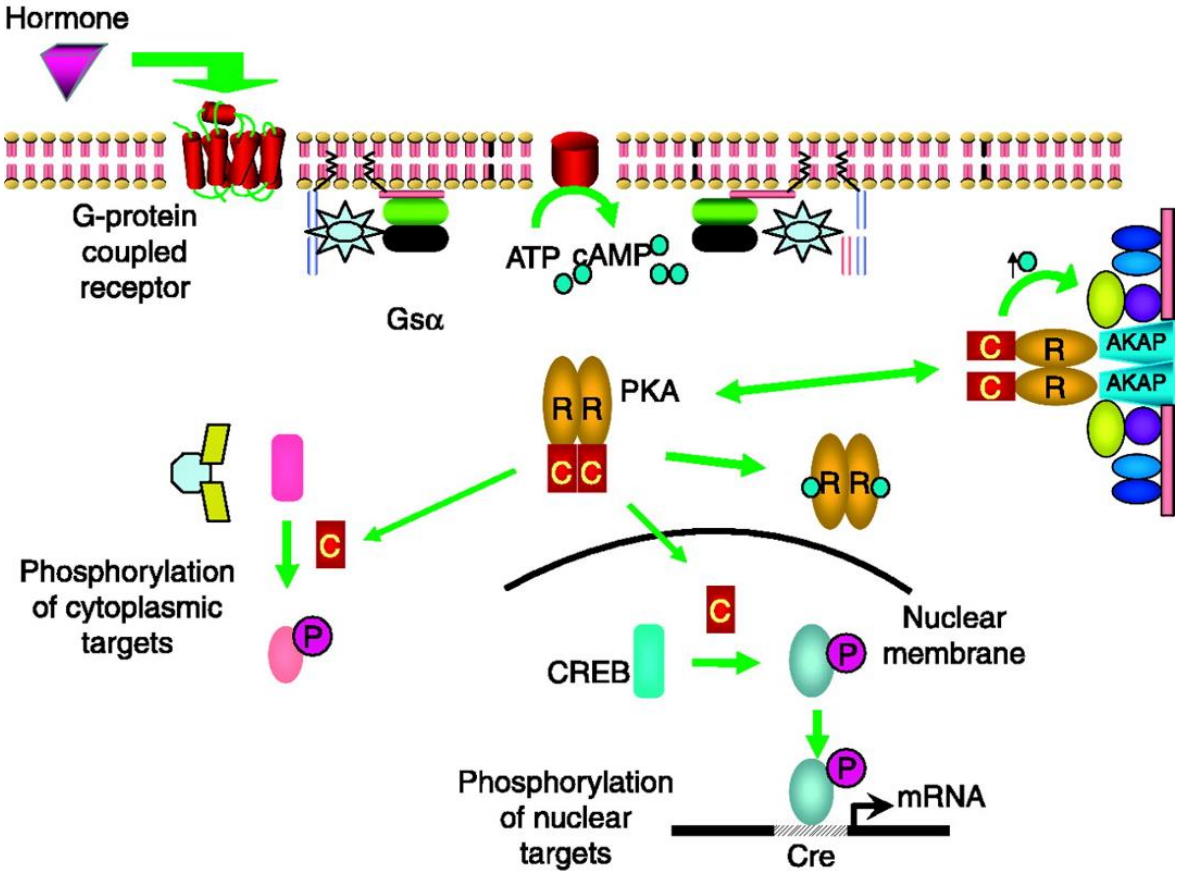

Figure 1.4| AKAP13 involved in PKA signaling pathway. Ligand binding of G-protein coupled receptors (GPCRs) stimulates the Gα subunit thereby increasing production of cAMP via Adenylyl Cyclase (AC). cAMP binds to PKA releasing the catalytic (C) subunits which phosphorylate downstream effectors such as cAMP response element binding protein (CREB). AKAP13 is shown tethered to PKA; AKAP13 localizes to discrete subcellular micro-domains thereby focusing the generic signaling molecules to specific downstream targets (Kirschner, 2009).

Due to AKAP13's interaction with NHRs, it should come as no surprise that AKAP13 is found to be highly expressed in reproductive and immune tissues. Additionally, AKAP13 is found to be highly expressed in the heart, skeletal muscle, hematopoietic cells, pancreas, and lungs (Rubino, 1998). Given AKAP13's diverse tissue expression and role as a pathway rectifier, one can hypothesize that AKAP13's role in each of the tissues is not identical. In fact, AKAP13 can bring common second messengers and widely used signaling cascades to a focused endpoint depending on the needs of the cell (Welch, 2010) (Scott, 2010).

AKAP13 isoforms

The *AKAP13* gene is alternatively spliced and encodes several splice variants. Of these, three mRNA transcripts have been well characterized: 5.3kb, 8.5kb, and 10.0kb. These AKAP13 transcripts, and subsequent proteins are not ubiquitous in human body tissues. The proteins' roles vary depending on the tissue of expression, and the cellular context. Some transcripts are found highly expressed in some tissues while having less expression in other tissues (Toksoz and Willams, 1994) (Uhlen, 2015) (Fig. 1.5a-c).

The 5.3kb transcript encodes a 170kDa protein (Brx) and is highly expressed in human breast and reproductive tissue. Northern blot data has also shown this isoform to be present in human heart muscle, breast cancer, and reproductive tissues (Rubino 1998). The expression pattern of Lbc, as described in 1994 by Toksoz and Williams, is similar to, but not exactly like AKAP13's. Notably, the cDNA called Lbc was found to be a fusion of 2 products encoded by two different genes. AKAP13 is present in the tissues that Lbc is present, but is also present in tissues where Lbc is not, such as breast and reproductive tissue. Brx has a predicted nuclear localization signal (NLS) and can be found in both the nucleus and cytoplasm, with the latter being the more common location (Rubino 1998).

The 8.5kb transcript encodes a ~220kDa protein and is expressed in the following tissues: spleen, thymus, ovary, peripheral leukocytes, pancreas, skeletal muscle, lung, placenta, and heart muscle (Rubino, 1998). This AKAP13 isotype is found in the cytoplasm. Less is known about this particular isoform since most research has focused on other splice variants.

The 10.0kB transcript is translated into the ~310 kDa AKAP13 protein; this splice variant is found to be highly expressed in heart tissue and binds actin and myosin filaments in the cytoplasmic compartment of the cell. Further characterization of this isoform showed that AKAP13 was required for murine heart development (Mayers, 2010). In the absence of AKAP13, mice homozygous for the AKAP13 null allele died by embryonic day 10.5-11.0 (Mayers, 2010). This transcript is also found highly expressed in the following tissues: placenta, lung, skeletal muscle, pancreas, and ovary. Details for the role of AKAP13 in the heart will be discussed in Chapter 2.

a

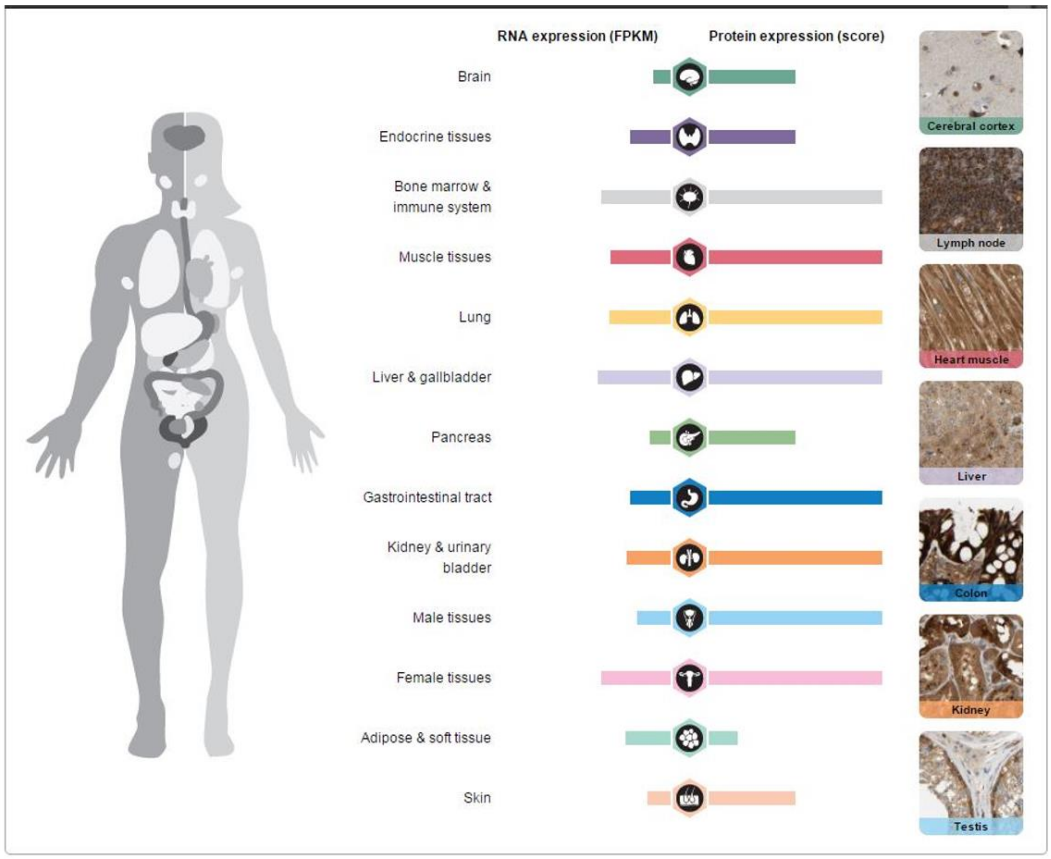

Figure 1.5| AKAP13 protein and transcript distribution in humans. a) Schematic showing full length AKAP13 RNA (left of organ icon) and protein (right of organ icon) expression in selected organs and tissues. Colored bars represent individual tissues. From top to bottom they are as follows: Brain (dark green), Endocrine tissues (dark purple), Bone marrow and immune system (grey), Muscle tissues (red), Lung (yellow), Liver and gallbladder (violet), Pancreas (green), Gastrointestinal tract (dark blue), kidney and urinary bladder (orange), male tissues (light blue), female tissues (pink), adipose and soft tissue (light green), skin (tan).

b

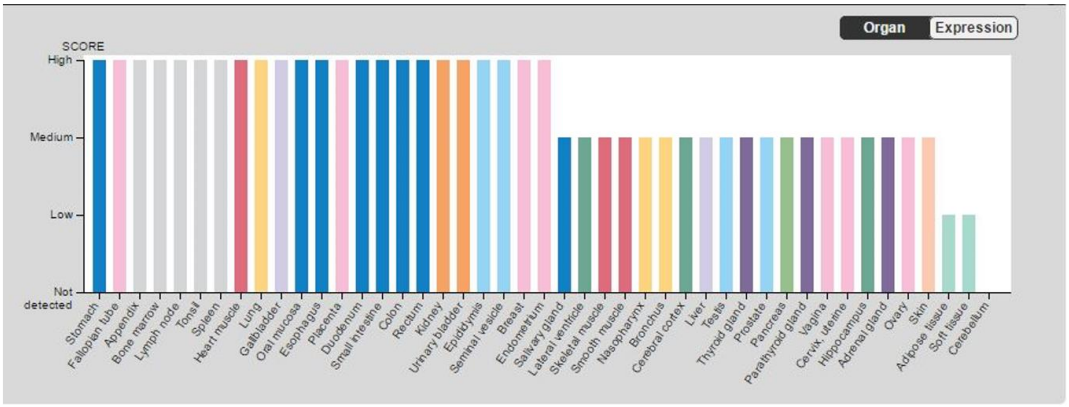

c

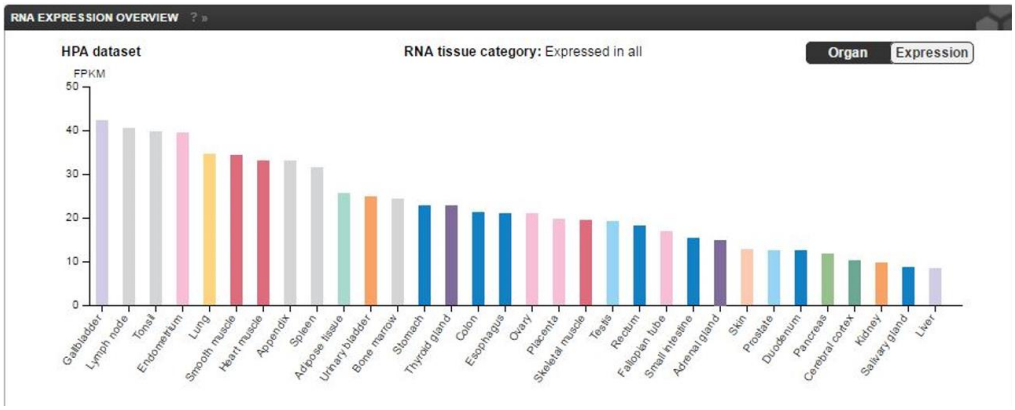

Figure 1.5 cont.| AKAP13 protein and transcript distribution in humans. b) Full length AKAP13 protein levels scored from no expression to High protein levels throughout various organs and tissues. Colors are as in a). c) RNA expression levels scored from low to high expression, colors as in a) Fragments per Kilobase of transcript per Million mapped reads (FPKM) throughout various organs and tissues (Uhlen, 2015) (Uhlen, 2010).

CHAPTER 2: Results

Introduction

Like many complex diseases, heart disease can vary in presentation, severity, and even outcome contingent upon the sex of the individual. Females commonly present to the clinic later and with atypical symptoms and differences exhibited upon initial cardiac examination, such as with electrocardiogram (ECG) (Curtis et al., 2012; Meyer et al., 2014). Because of this, a better understanding of the mechanism and progression of heart disease is of utmost importance in women's health and sexual disparity research; failure to do so has broad and far reaching health and economic implications (Fig. S.1) (Heron, 2009) (Pilote , 2007) (Heidenreich, 2011).

Heart disease is a complex, heterogeneous disease with many additional factors indicated in its development including a complex hormonal milieu, and environmental influences, such as diet and alcohol use. Furthermore, many studies have demonstrated gender differences in the expression and types of cardiovascular disease, such as dilated cardiomyopathy (DCM), a major underlying cause of heart failure (Frazao, 1999) (Pilote, 2007) (Konhilas, 2007) (Hershberger, 2010) (Wilson, 2007), stress cardiomyopathy (Virani, 2007), and others. Nevertheless, reports have shown up to 50% of cardiomyopathy cases can be considered idiopathic since the causative agent is unknown (Hershberger, 2010) (Hazebroek, 2012). The underlying complexity and pathway integration involved in cardiomyocyte signaling, both inter- and intracellularly makes pathway analyses difficult

at best (Wheeler-Jones, 2005) (Feliciello, 2001). While certain pathway components, such as RhoA, PKA, CREB, and intracellular Ca^{2+} dynamics are understood to be important factors in cardiac function and signaling, sarcomere formation, and cell differentiation, all pieces of the signaling puzzle have yet to be identified (Diviani D, 2001) (Teramoto, 2003) (Sahai, 1998) (Mauban, 2009) (Mayers, 2010) (Greenstein, 2011). It is likely that common signaling pathways are engaged by multiple entities (Wheeler-Jones, 2005) (Feliciello, 2001) (Mayers, 2010). Therefore, key to understanding heart pathologies such as DCM, especially as they are related to sex differences, lies in the elucidation of common genetic, hormonal, or pathway defects. This common defect may involve permutations or dysfunction in A Kinase Anchoring Protein (AKAP) 13.

AKAP13 is a nuclear hormone receptor modulator, dynamic scaffolding protein, and pathway integration center with a conserved PKA-binding domain and Rho-GEF activity (Rubino, 1998) (Mayers, 2010). AKAP13 not only possesses additional functionality that surpasses any other known AKAP, but is of unique importance to the medical and research communities due to its central and regulatory roles in familial breast cancer, uterine fibroid development, immune response, and heart development (Rubino, 1998) (Mayers, 2010) (Rogers, 2008). In the heart disease literature, AKAP13 was implicated as a major component of the PKD signaling pathway involved in cardiac hypertrophy (Carnegie, 2008) (Taglieri, 2014). Notably, AKAP13 was up-regulated in hypertrophic cardiomyocytes and was found to have important roles in activation and localization of proteins involved in myocyte enhancer factor (MEF), specifically MEF2 signaling and transcriptional reprogramming (Carnegie, 2008). Previously our group

showed that AKAP13 was essential for cardiac development and proper cardiomyocyte differentiation. Global loss of *Akap13* caused embryonic lethality by E10.5 to 11.0. Embryos exhibited DCM with pericardial effusion, trabecular defects, and dysregulation of key cardiac developmental genes such as *Mef2* and *Srf*. Cardiac ultrastructural changes showed defective cardiac sarcomere formation (Mayers, 2010) (Mauban, 2009). Similarly, CREB deletion mutants produced dilated cardiomyopathy, mitochondrial dysfunction, and increased female morbidity (Watson, 2010). This is particularly interesting since AKAP13 is known to modulate CREB (Baig, 2017, *In Preparation*).

Briefly, the *AKAP13* gene is an alternatively spliced proto-oncogene located on human chromosome 15q25.3 and on murine chromosome 7D2. AKAPs rectify cAMP signaling pathways by tethering cAMP-dependent Protein Kinase A (PKA) to subcellular micro-domains, such as organelles and other membranes (Welch, 2010). Within these sub-cellular niches, AKAPs act as engaged scaffolding proteins or signaling centers, holding PKA, or other signaling enzymes, closer to substrates, downstream signaling enzymes, and other relevant, supplemental molecules and co-factors. AKAP13 (also known as Brx and AKAP-Lbc), was first isolated by Segars et al., from estrogen-responsive breast cancer cells (Segars, 1993). Further studies by our group showed that the majority of *AKAP13* isoforms modulated estrogen receptors and other nuclear hormone receptors through a conserved carboxyl-terminal LXXLL nuclear receptor-interacting domain (NRID) ultimately affecting the transcriptional program (Rubino, 1998) (Kino, 2006). Both the N-terminal and carboxyl-terminal conserved domains have key regulatory functions.

The protein kinase A (PKA) anchoring motif, whereby AKAP13 was classified, is encoded in the N-terminal region. Interestingly, not all isoforms of the protein include this PKA domain (e.g. 170kDa Brx) (Rubino, 1998). Furthermore, AKAP13 was found to be the only known AKAP with Guanine Nucleotide Exchange Factor (GEF) activity via conserved DH and PH domains (Mayers, 2010). Homodimerization of AKAP13 carboxyl domains have been reported to regulate Rho-GEF activity (Baisamy, 2005). Rho GTPases have been reported to have an important role in sarcomere development in cardiomyocytes. They have also been shown to affect the cell cytoskeleton (Sah, 1999) (Majumdar, 1999) (Kawamura, 2003). Additionally, RhoA, a known target of AKAP13, has been reported to influence downstream components including GATA-4 and Serum Response Factor (SRF) (Park, 2002). GATA-4 and SRF are known to be essential for cardiomyocyte differentiation.

For proper *Srf* gene transcription and actin filament organization to take place, Rho GTPase signaling pathways must be intact and fully functioning (Park, 2002) (Diviani, 2001) (Teramoto, 2003) (Sahai, 1998). Since AKAP13 has been reported to bind and activate RhoA (and other Rho family GTPases such as RhoB and RhoC) via the GEF domain, it is therefore likely that AKAP13 also influences cardiomyocyte differentiation, and may be equally important to previously mentioned factors (Wei, 1998) (Sterpetti, 1999) (Diviani, 2001) (Charron, 2001) (Carnegie, 2008) (Teramoto, 2003) (Sahai, 1998).

Principally, AKAP13 acts as a central pathway integrator for an array of signaling pathways while also providing a means to add specificity and spatiotemporal fidelity to various effectors both upstream and downstream. AKAP13 conveys upstream information

by coordinating signals from cell membrane LPA receptors, thrombin, and osmoreceptors via G-proteins (Diviani, 2001) (Kawamura, 2003) (Huang, 2005). $G\alpha_{12}$ has been one of the G proteins most focused on with regard to interaction with AKAP13. However, AKAP13 has been shown to mediate signaling by the following G-proteins: $G\alpha_{13}$, $G\alpha_{14}$, $G\alpha_{q}$, and $G\alpha_{15}$ (Ruwhof, 2000) (Petroff, 2001) (Schmidt, 2002) (Wei, 1998). Additionally, data have shown AKAP13 action downstream of ET-1, and α- and β- adrenergic receptors (Rubino, 1998) (Taglieri, 2014) (Carnegie, 2008).

Given the role of AKAP13 in cell signaling, its ability to modulate estrogen receptors, transcription factors and PKA, demonstrated effects on SRF and MEF2c expression levels, essential role in proper embryonic cardiac sarcomere development, and its robust expression in the both the human (Fig. S.2a, b) and mouse (Fig. S.2c, d) adult myocardium (Mayers, 2010), **we hypothesized that a functional AKAP13 protein is required for cardiomyocyte function in the adult heart; defective function of AKAP13 may induce ventricular dysfunction and cardiac sarcomeric disorganization**. Moreover, we postulated that the carboxyl region of AKAP13 plays a vital role in the regulation and coupling of PKA and Rho-GEF activity in order to signal and modulate downstream effectors specifically involved in cardiac signaling events. Resent reports have shown an increasingly complex role for AKAP13 in both physiologic and pathophysiologic states. Because of this, investigation of AKAP13's role in the adult heart will provide essential mechanistic insights, open new avenues for therapeutics, and facilitate a better characterization of sex dependent differences in heart disease presentation and progression.

Establishment of conditional cardiac-specific *Akap13* knockout mouse model

To better understand the physiologic role of *Akap13* in adult cardiac function, conditional knockout (*Akap13*^{cKO}) mice were generated using a Cre-Lox deletion strategy targeted to the guanine nucleotide exchange factor (GEF) domain of *Akap13* (Fig. 2.1). Sequencing analysis and polymerase chain reaction (PCR) were used to verify the desired construct in vitro and correct recombination and presence of LoxP sites in vivo (Fig. S.3a-f). In vitro studies confirmed expected Cre-recombination (Fig. S.4a-c). An inducible, tissue-specific Cre approach was used since global *Akap13* knockout resulted in embryonic lethality by embryonic day 10.5-11.0, as previously described by our group (Mayers, 2010). Moreover, the role of *Akap13* in the adult mouse heart could be more precisely studied with the use of an inducible, cardiac tissue-specific Cre-expressing model since multi-organ system involvement and potential off-target effects would be reduced or eliminated (Fig. S.5). The well described Cre-recombinase-expressing mouse model *α-MHC*-MerCreMer (MCM), driven by the *α-MHC* promoter, was used to achieve cardiac tissue specificity (Sohal, 2001). For generation of the conditional knockout model, adult mice at three months of age with homozygous floxed *Akap13* alleles and expressing *α-MHC*-MerCreMer (*Akap13*$^{cKO\text{-}MCM}$) were administered tamoxifen treatment via tamoxifen-laced chow (40mg/kg body weight) for four weeks for induction of Cre-mediated excision. Mice were induced at three months of age for comparison with published data (Sohal, 2001). Assays were performed at least 3 weeks following treatment cessation.

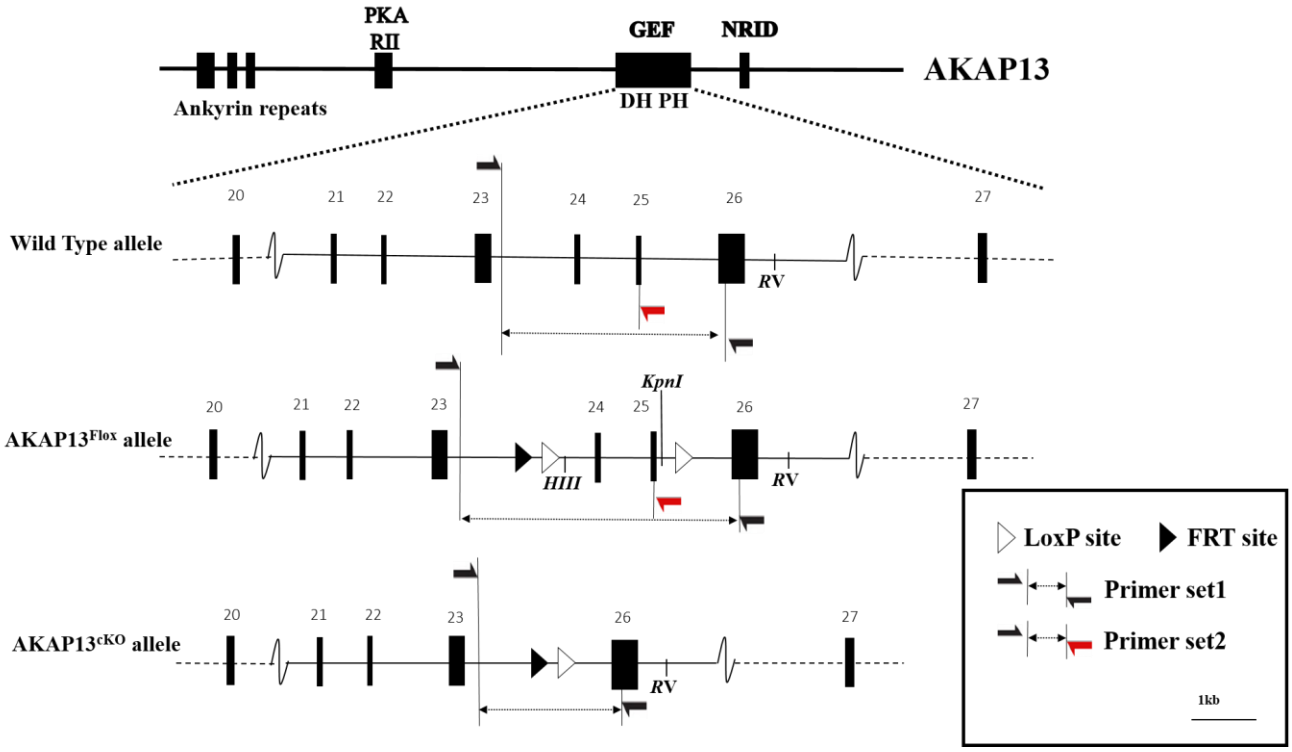

Figure 2.1| **Cre-lox deletion strategy for murine *A Kinase Anchoring Protein 13 (Akap13) gene*.** Shown are the Wild Type (WT), *Akap13*^{Flox}, and *Akap13*^{cKO} alleles. A Cre-lox deletion strategy was used to target the guanine nucleotide exchange factor (GEF) region with flanking Dbl-homology (DH) and pleckstrin homology (PH) conserved domains targeted for deletion. Flippase (FLP) recombinase-recombination target (FRT) site remained from removal of the FRT flanked neomycin cassette. Solid arrows (black and red) indicate binding sites for selected PCR primers used for genotyping analyses.

To control for possible treatment effects, a second inducible, cardiac-specific Cre-expressing mouse model was included in the study: *Tnnt2*-rtTA; TetO-Cre (TOC). The doubly transgenic *Tnnt2*-rtTA promoter was the cardiac specific driver for TOC as described in the literature (Wu, 2010). For generation of the second conditional knockout model, adult mice at three months of age with homozygous floxed *Akap13* alleles and expressing *Tnnt2*-rtTA;TetO-Cre ($Akap13^{cKO\text{-}TOC}$) were administered doxycycline (1mg/mL) via their water source for one to two weeks for induction of Cre-mediated excision. Assays were performed at least 1 week following treatment cessation.

The efficiency of *Akap13* knockdown was monitored through real-time quantitative polymerase chain reaction (RT-qPCR) (Fig. 2.2), *in situ* hybridization (ISH) (Fig. 2.3), immunohistochemistry (IHC) (Fig. 2.4), Western (Fig. 2.5) and Southern blotting (Fig. S.6). Similar outcomes were observed between the two Cre models (MCM and TOC) with comparable gene knockdown. Therefore, both Cre models utilized were efficient and achieved *Akap13* knockdown with tissue specificity, and will hereafter be referred to as $Akap13^{cKO\text{-}MCM}$ or $Akap13^{cKO\text{-}TOC}$ where appropriate. Where $Akap13^{cKO}$ is used, combined results were analyzed or overall conclusions were made for both models. Genotyping was performed via PCR using gDNA isolated from the tail (Fig. S.7). For analytical purposes, background strain was considered, and the two different Cre models were analyzed with their appropriate background except where noted (for combined knockout analyses). For controls, littermates were used where possible, and either expressed the desired Cre and were not given treatment or did not express the Cre and were given treatment. No statistical differences were found between the two (Tables ST.1-ST.3) and will henceforth

be referred to as control mice. In all cases, results for *Akap13*$^{cKO\text{-}MCM}$ mice will be given in the text. References to *Akap13*$^{cKO\text{-}TOC}$ mice will be noted where appropriate. Please note that the *Akap13*$^{cKO\text{-}TOC}$ was introduced later in the project, so were not available for every assay. Additional *Akap13*$^{cKO\text{-}TOC}$data is located in Appendix B.

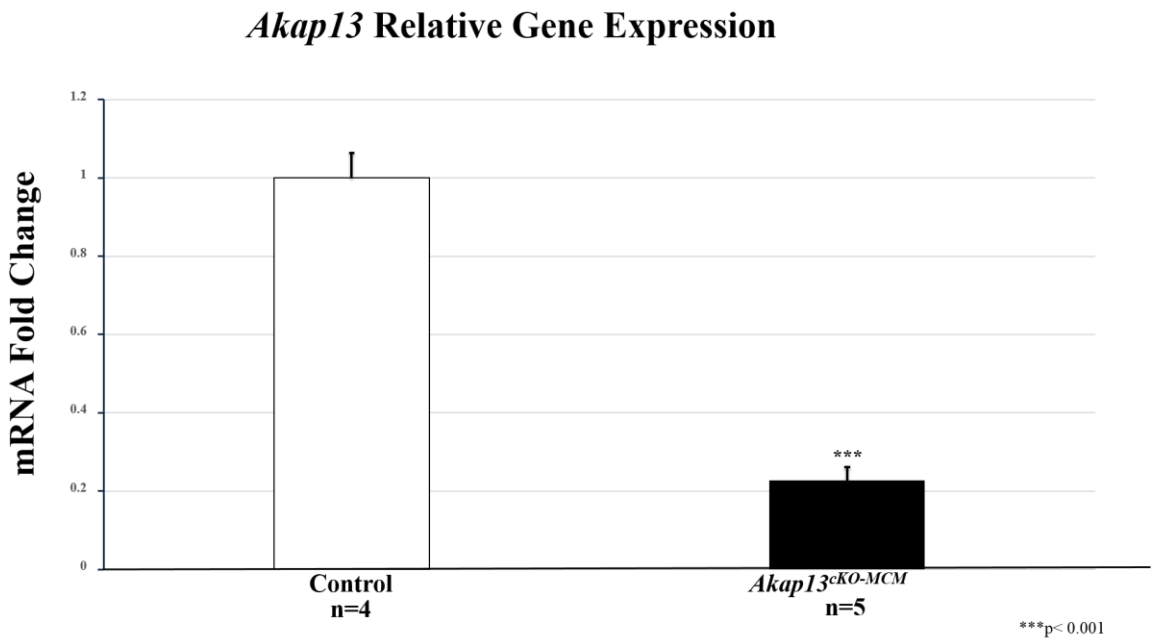

Figure 2.2| **RT-qPCR analyses showed knockdown of *Akap13*.** Here we show qRT-PCR analysis of *AKAP13* expression represented as mRNA fold change comparison between control mice (F/F, MCM-; Tamoxifen diet) (n=5) and *Akap13*$^{cKO-MCM}$ mice (n=5). *Akap13* expression in cKO mice was lower than *Akap13* expression in control mice ($p<0.001$) which demonstrated appropriate gene knockdown. Each biological replicate (single mouse sample) had three technical replicates; results were normalized to GAPDH and 18S housekeeping genes. Three independent experiments were performed to validate results shown; error reported as S.E.M. Student's t-test was performed for statistical analysis.

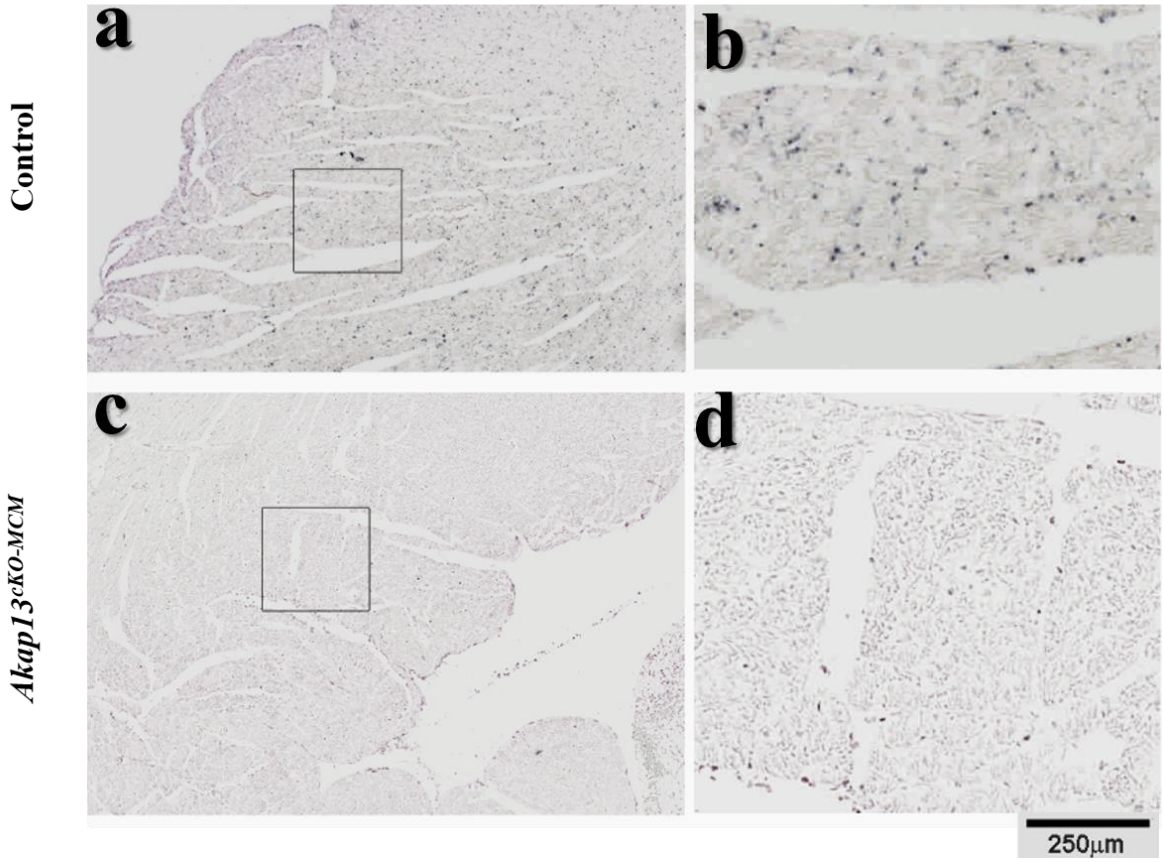

Figure 2.3| ***In situ*** **Hybridization (ISH) with riboprobe showed reduction of *Akap13* transcripts.** Here we demonstrated efficient knockdown of *Akap13* using In Situ Hybridization (ISH) with a riboprobe. The panels on the left (40X) show a) control (n=4) and c) *Akap13*^{cKO} (n=4) in 5 month old adult murine hearts. The panels to the right (100X) are magnifications of the boxed regions b) control and d) *Akap13*^{cKO}, and substantiated the absence of *Akap13* mRNA in the *Akap13*$^{cKO\text{-}MCM}$ mouse hearts.

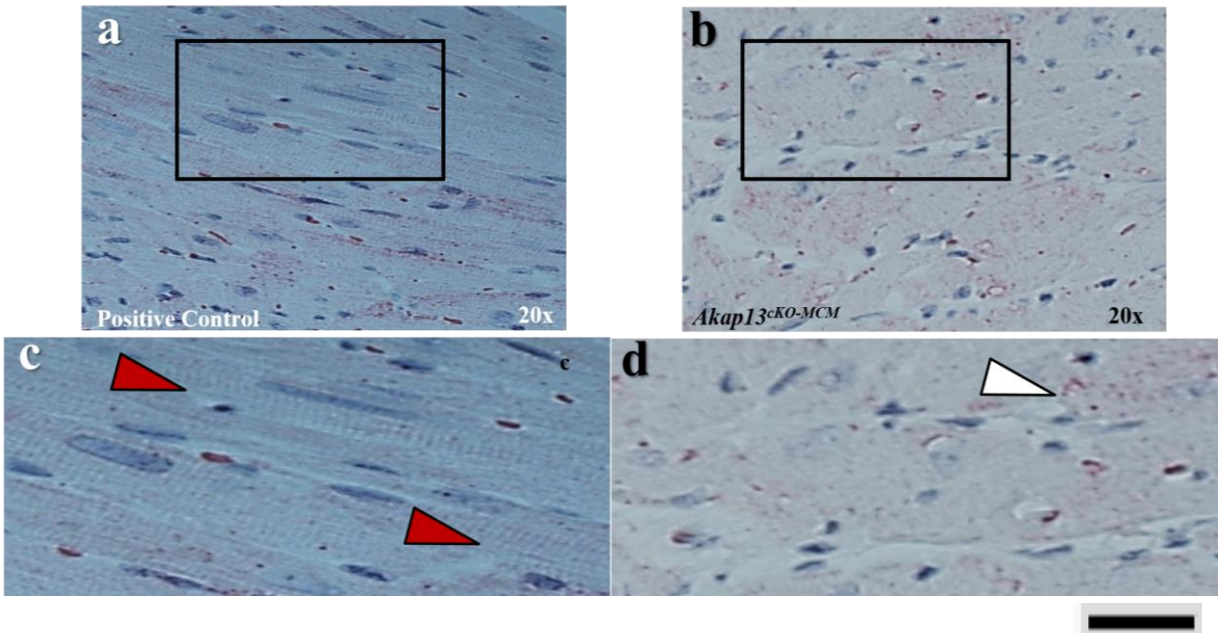

Figure 2.4| **Immunohistochemistry showed reduction in AKAP13 protein levels in *Akap13*$^{cKO\text{-}MCM}$ mouse hearts.** a) Immunohistochemistry (IHC) showed positive anti-AKAP13 staining (pinkish-red) in Control mouse hearts (n=3) b) IHC showed reduced anti-AKAP13 staining in the *Akap13*$^{cKO\text{-}MCM}$ mouse hearts (n=3). c) Enlargement of a) showed a striated pattern in adult control mouse hearts (red arrows). d) Enlargement of b) showed faint and disrupted AKAP13 protein distribution (white arrow) which indicated knockdown was achieved. Scale bar shown is 50µm.

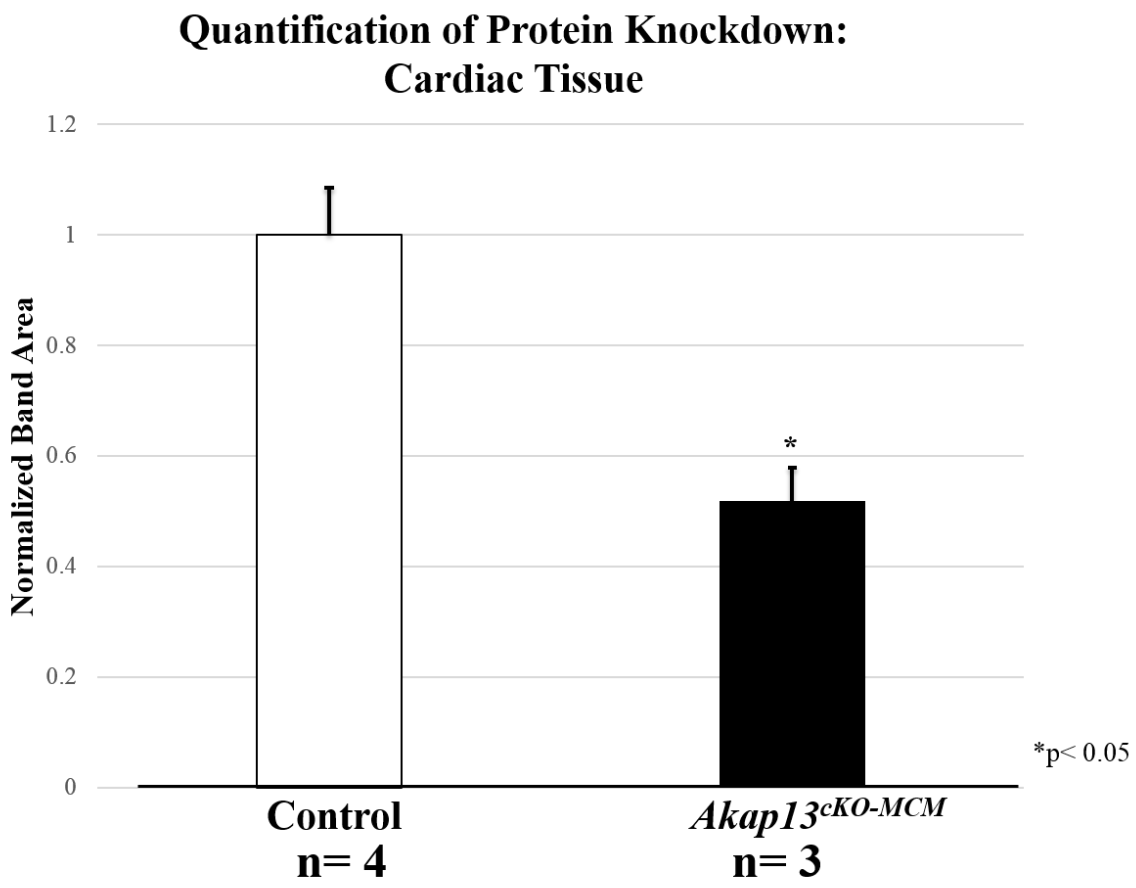

Figure 2.5| **Quantification of Western Blot showed reduced AKAP13 protein levels.** Western blot verified AKAP13 protein knockdown in *Akap13*$^{cKO\text{-}MCM}$ cardiomyocytes. Notably, multiple cell types comprise cardiac tissue. Both Cre models were driven by cardiomyocyte specific promoters, therefore *Akap13* was expressed in fibroblasts which account for more than 50% of cardiac cells. For statistical analysis, Student's *t*-test was used for comparison between control (F/F, MCM-; Tamoxifen diet) (n=3) and *Akap13*$^{cKO\text{-}MCM}$ mice (n=3) (where * indicates significant value $p<0.05$).

Histology revealed dilated ventricular chambers and dysmorphic cardiomyocytes

Histologic examination of formalin fixed hematoxylin and eosin (H&E) stained *Akap13*$^{cKO\text{-}MCM}$ mouse heart tissue cross-sections at the level of the papillary muscles revealed dilated left ventricles in *Akap13*^{cKO} mice (n=4) compared to controls (n=3) (*Akap13*^{cKO}: 196.62cm^2 ± 19.10; control: 127.5cm^2 ± 5.76; $p<0.05$) (Fig. 2.6). Strikingly, areas of less intense eosin staining were observed along with a more granular, disorganized appearance of most of the cardiomyocytes, which also demonstrated pyknotic nuclei, in *Akap13*$^{cKO\text{-}MCM}$ cardiac tissue sections compared to controls which suggested cytoskeletal and potentially organellar changes (Fig. 2.7). *In situ* hybridization with a riboprobe was performed to assess AKAP13 transcript levels in the heart tissue. Areas of more intense and less intense staining were seen. Areas of more intense staining were likely to correspond with normal appearing cardiomyocytes, and areas with less intense, or no staining were likely to correspond with the dysmorphic and likely necrotic cardiomyocytes secondary to the loss of *Akap13* (Fig. 2.8). There were no inflammatory cells or other signs of infection, either acute or chronic in nature. Since many disrupted cardiomyocytes were observed in the *Akap13*$^{cKO\text{-}MCM}$ hearts, terminal deoxynucleotidyl transferase dUTP nick end labeling (TUNEL) was performed to assess apoptosis by fluorescently labeling fragmented DNA. However, apoptosis was not found to be increased in the *Akap13*$^{cKO\text{-}MCM}$ cardiac tissue compared to control tissue (Fig S.8). Since apoptosis was not indicated, other mechanisms of cell death, such as autophagy, remain plausible.

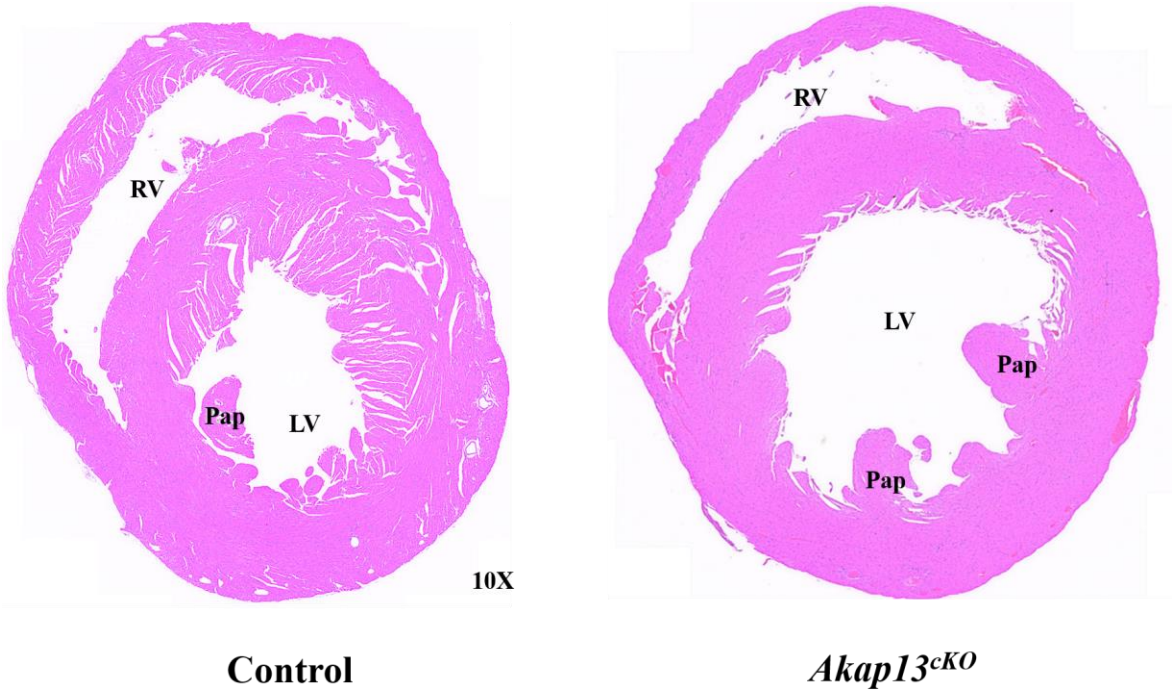

Figure 2.6| **Knockdown of *Akap13* induces ventricular dilation in the adult murine heart.** a,b) (10X) Here we showed haematoxylin/eosin (H&E) stained mid-ventricular cross-sections of murine hearts at the level of the papillary muscles. Controls (F/F, MCM-; Tamoxifen diet) (n=3) and *Akap13*^{cKO} mice (n=4). The *Akap13*^{cKO} hearts had a visibly enlarged left ventricular chamber. The cKO shown here is from an *Akap13*$^{cKO\text{-}TOC}$ mouse, but is representative of both the *Akap13*$^{cKO\text{-}TOC}$ and *Akap13*$^{cKO\text{-}MCM}$ mice.

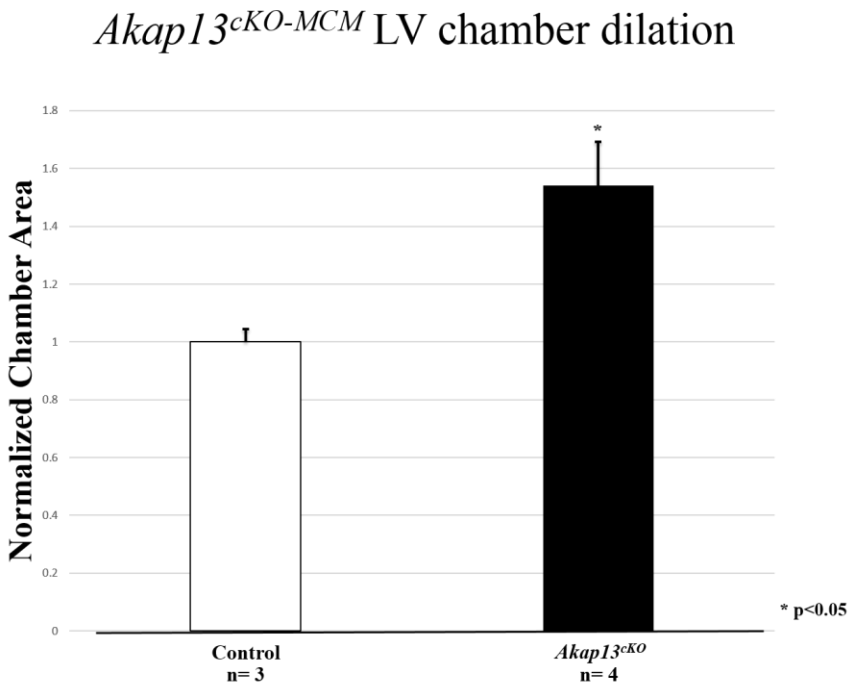

Figure 2.6 cont.| **Knockdown of *Akap13* induces ventricular dilation in the adult murine heart.** c) Quantification of the ventricles of *Akap13*^{cKO} hearts compared to controls (F/F, MCM-; Tamoxifen diet) showed enlarged left ventricular chambers in the *Akap13*^{cKO} hearts compared to the controls ($p<0.05$).

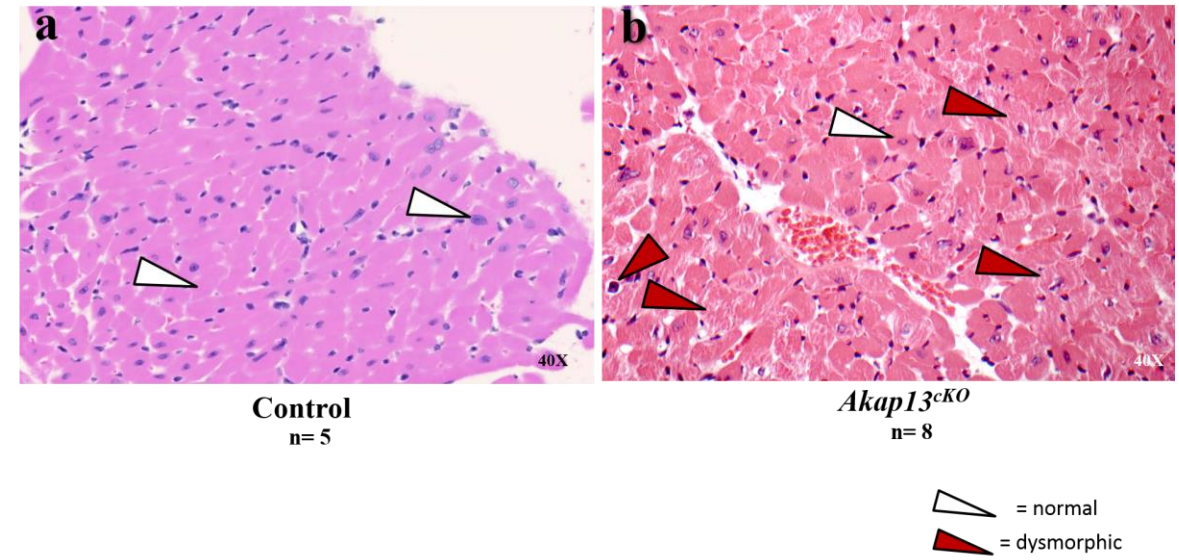

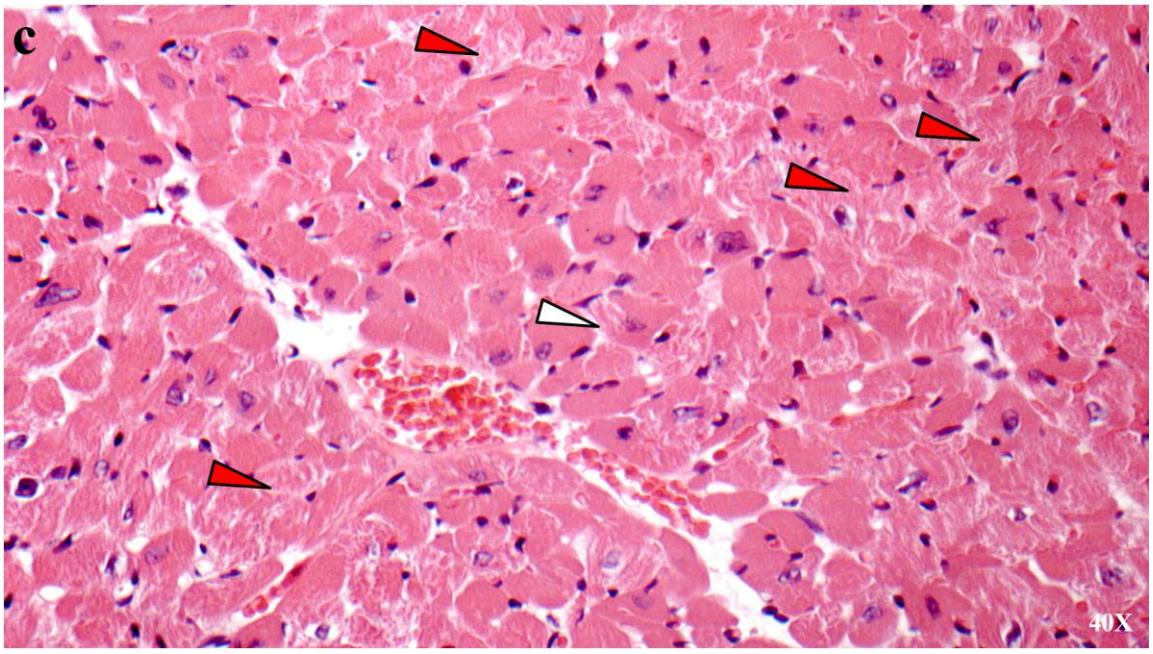

Figure 2.7| **H&E stained *Akap13*$^{cKO\text{-}MCM}$ mouse cardiac tissue sections showed disrupted cardiomyocytes.** a,b) H&E stained cardiac tissue sections (40X) showed disrupted cardiomyocytes with granular and irregular appearing eosinophilic cytoplasmic staining and pyknotic nuclei indicative of necrosis. The white arrows show normal, healthy cardiomyocytes (control-left panel) whereas the red arrows show the dysmorphic cardiomyocytes (*Akap13*$^{cKO\text{-}MCM}$ -right panel). c) Enlargement of b) revealed the majority of cardiomyocytes in the *Akap13*$^{cKO\text{-}MCM}$ were disrupted (red arrows).

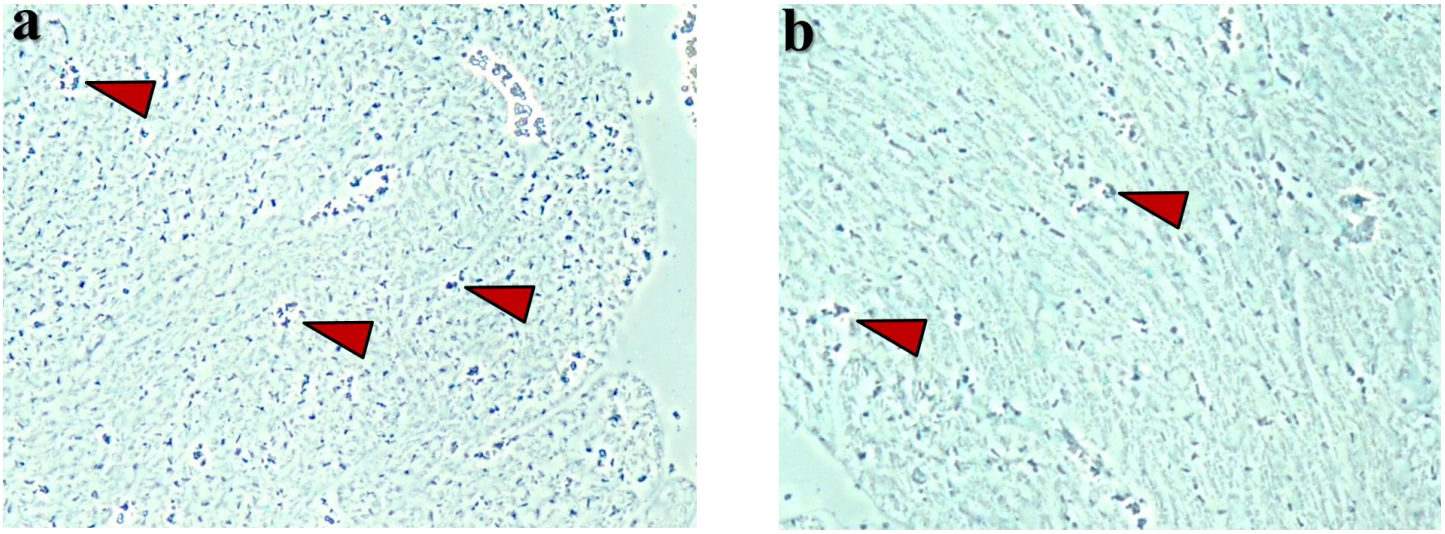

Figure 2.8| ***In situ hybridization (ISH)* showed reduced *Akap13* message in *Akap13*$^{cKO\text{-}TOC}$ mouse hearts.** a,b) *In situ* Hybridization (ISH) with an *Akap13* riboprobe (bluish-purple) showed marked reduction of *Akap13* transcripts in the *Akap13*$^{cKO\text{-}TOC}$ mouse hearts (b) compared to *Akap13*$^{Het\text{-}TOC}$ mouse hearts (a). Persisting *Akap13* expression likely occurred in cardiac fibroblasts or a small subset of cardiomyocytes (20%) where recombination did not occur.

Electron Micrographic analyses showed disrupted sarcomeres and mitochondria

Given the significant histologic changes observed in the *Akap13*^{cKO} mice, we next sought to characterize the cardiac sarcomeres and ultrastructural underpinnings of the *Akap13*^{cKO} cardiac tissue compared to controls. Immunohistochemistry with anti-sarcomeric alpha-actinin revealed disruption of the cardiac sarcomere. Normal sarcomeric banding patterns were seen in control mice (n=3), but not in *Akap13*^{cKO} mice (Fig. 2.9a). Scrutiny of electron micrographic data revealed widespread sarcomeric disorganization in the *Akap13*^{cKO} mice (n=7) compared to controls (n=6) (Fig. 2.9b). Normal sarcomere banding patterns were observed in the controls. The majority of the tissue examined in *Akap13*^{cKO} mice was in complete disarray with severely disrupted sarcomeres, including missing and blind-ended z-discs and abnormal or missing bands (e.g. A-band). Some areas were so severely affected that it was difficult to ascertain the existence of sarcomeres altogether (Fig. S.9). Moreover, mitochondria showed significant pathological changes in *Akap13*^{cKO} mice compared to controls. Mitochondria were increased in number, were swollen or of differing sizes, and partially or completely lacked cristae (Fig. 2.10-2.12). Additional observations included increased lipid droplets, inclusions, and lamellar bodies in the *Akap13*$^{cKO\text{-}MCM}$ mice (Fig. S.10).

In sum, these data indicated widespread sarcomeric and severe mitochondrial disruption in *Akap13*^{cKO} mice. Of note, mitochondria in *Akap13*^{cKO} mouse cardiac tissue were lacking some or all of their cristae, appeared to have increased fusion/fission, and many were swollen and missing their outer mitochondrial membranes. Cardiac sarcomeres

were disorganized and missing some or all of the necessary bands to form an adequate contractile unit. While some electron micrographic sections from the *Akap13*^{cKO} mice had more normal appearing ultrastructure, most of the observed sections had widespread pathological disorganization.

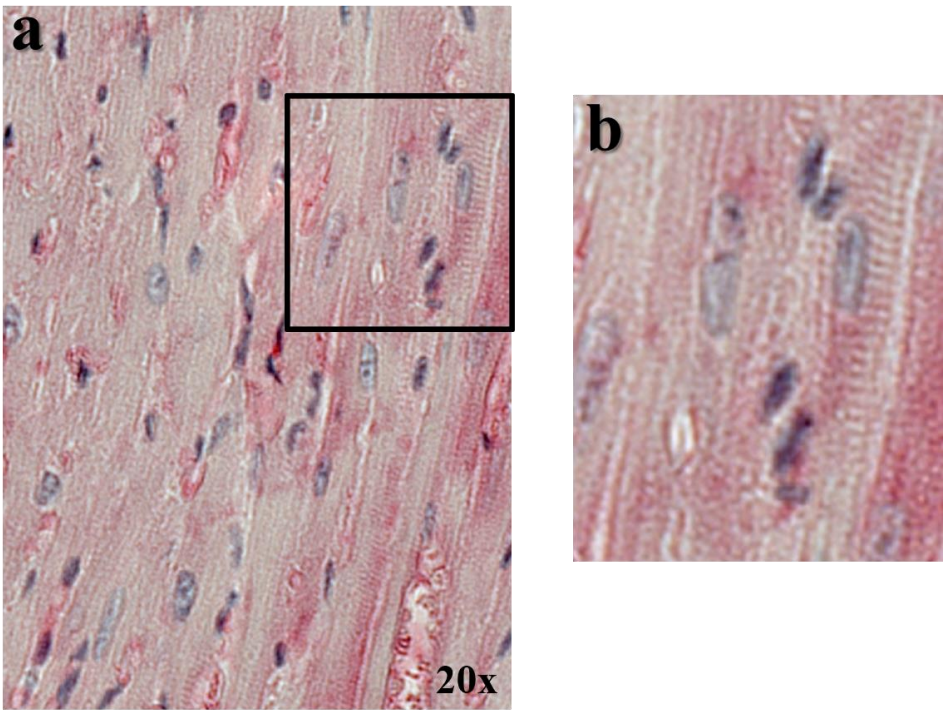

Figure 2.9| **IHC showed disrupted sarcomeric alpha actinin in *Akap13*^{cKO} mouse cardiac tissue sections.** a) Control cardiac tissue sections showed normal staining with anti-sarcomeric alpha actinin (20X). b) Enlargement of a) showed regular, striated sarcomeric banding pattern in the control mouse cardiac tissue.

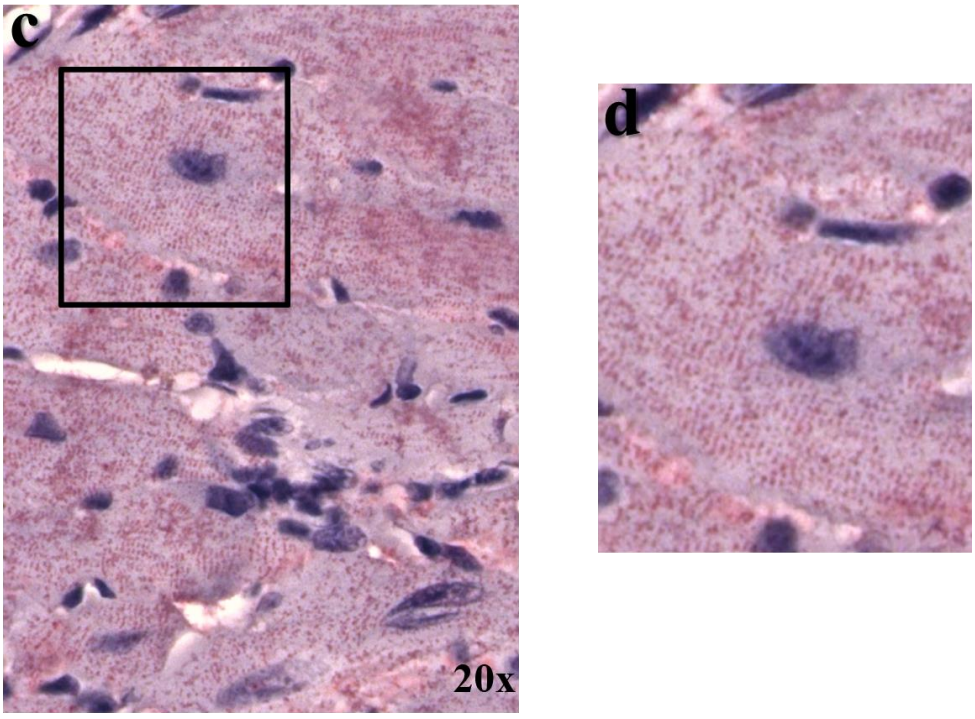

Figure 2.9 cont.| **IHC showed disrupted sarcomeric alpha actinin in *Akap13*^{cKO} mouse cardiac tissue sections.** c) *Akap13*^{cKO} mouse cardiac tissue sections showed disrupted and irregular sarcomeric banding patterns (20X). d) Enlargement of c) highlighted the sarcomeric pathology seen in *Akap13*^{cKO} mouse cardiac tissue sections.

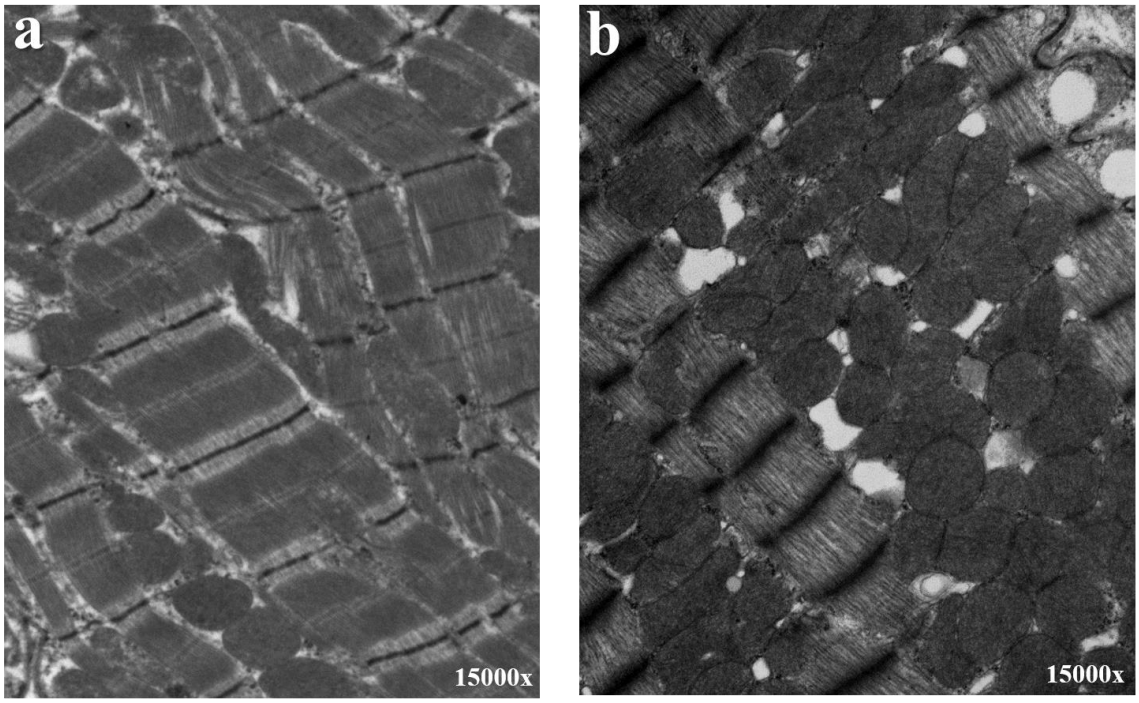

Figure 2.10| **Electron Microscopy revealed significant changes to the cardiac sarcomeres in *Akap13*^{cKO} mouse cardiac tissue.** a) Electron micrograph, Control mouse cardiac tissue (15,000x) showed normal sarcomeric banding patterns. Mitochondria were uniform and aligned along the sarcomeres, as expected. b) Electron micrograph, Akap13^{cKO} mouse cardiac tissue showed significant disruption of the sarcomeres including loss of the normal banding pattern (e.g. A-band).

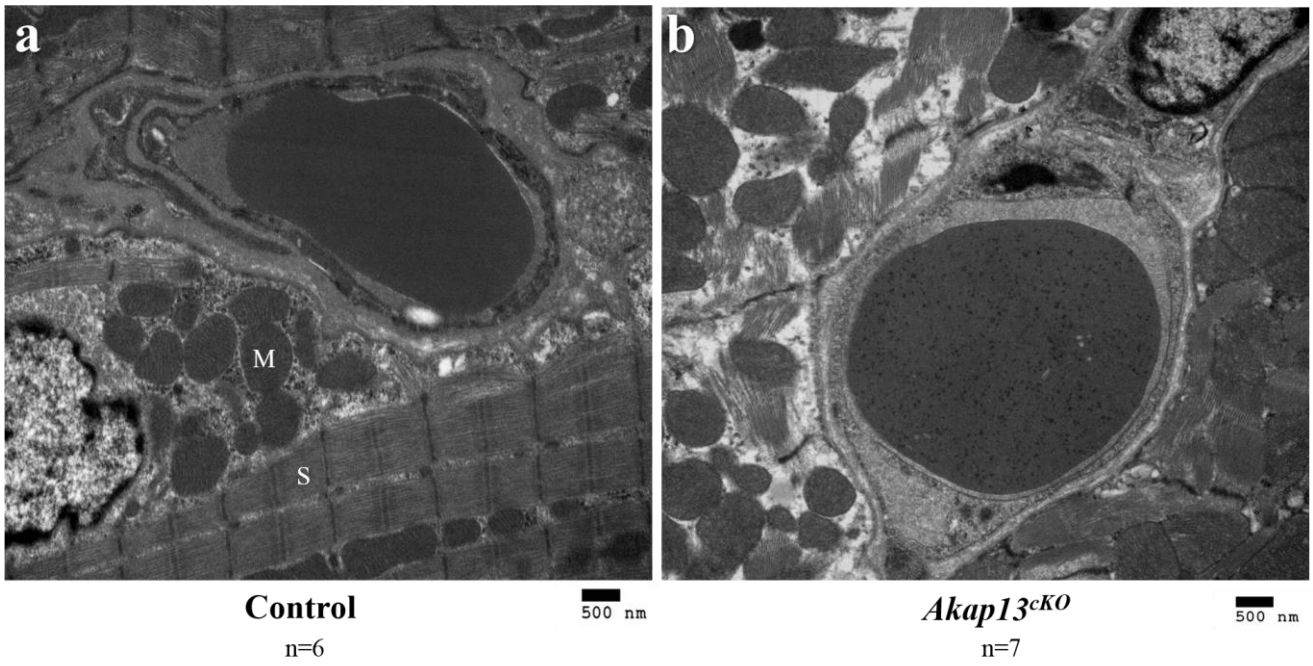

Figure 2.11| **Electron Microscopy showed ultrastructural disarray in *Akap13*^{cKO} mouse cardiac tissue.** a) Electron micrograph, Control mouse cardiac tissue showed typical sarcomeric banding pattern and typical group of mitochondria. b) Electron micrograph, Akap13^{cKO} mouse cardiac tissue showed significant disarray with blind ending sarcomeres, and mitochondria lacking cristae.

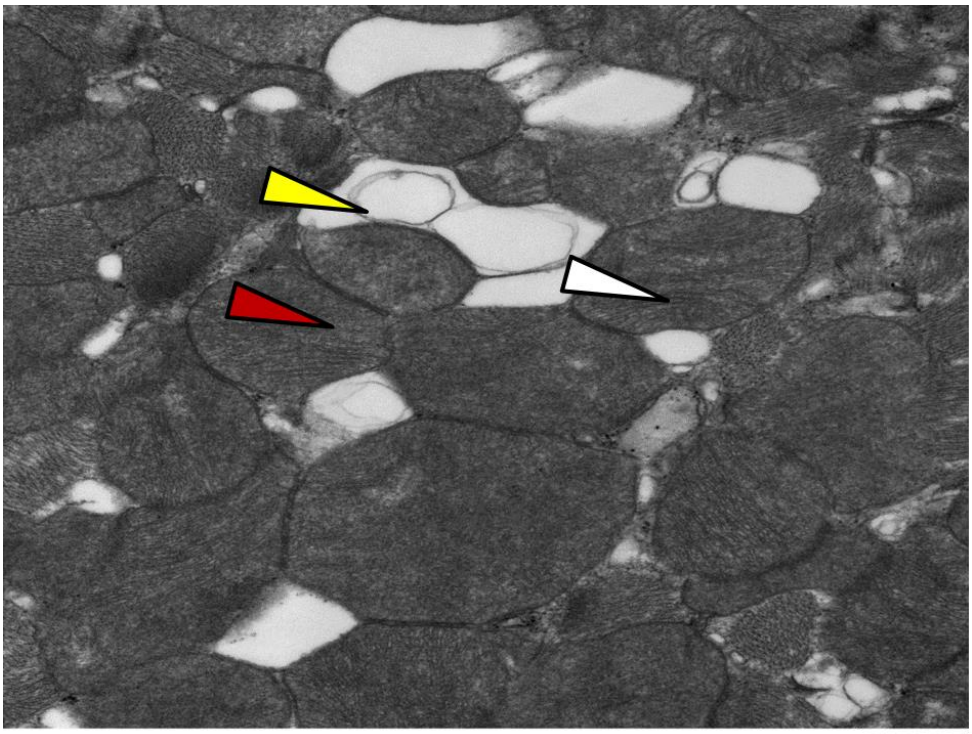

Figure 2.12| **Electron Microscopy showed mitochondria lacking cristae and lamellar inclusions.** Electron micrograph, Akap13^{cKO} mouse cardiac tissue showed an increased number of mitochondria. Mitochondria were either partially or fully lacking cristae. Some cristae were present (white arrow), but most areas were lacking cristae (red arrow). Lamellar inclusions (yellow arrow) were likely cristae extruded from the mitochondria.

Akap13^{cKO} mice developed dilated cardiomyopathy

Magnetic Resonance Imaging (MRI) is considered the gold standard for evaluating cardiac volume due to its ability to quantify a three-dimensional dataset, unlike other imaging modalities. We performed MRI to evaluate the cardiac volumes and function of *Akap13*$^{cKO\text{-}MCM}$ and *Akap13*$^{cKO\text{-}TOC}$ mice (collectively referred to as *Akap13*^{cKO}). Heart rate, body temperature, and respiration rates were monitored for each animal during the procedure. Results for *Akap13*$^{cKO\text{-}TOC}$ mice were not statistically different than *Akap13*$^{cKO\text{-}MCM}$ mice (data not shown). *Akap13*$^{cKO\text{-}MCM}$ mice were imaged in two different time ranges: <8 weeks post-cessation of treatment for Cre-mediated excision (hereafter <8 weeks post-recombination) or ≥8 weeks post-cessation of treatment for Cre-mediated excision (hereafter ≥8 weeks post-recombination).

Left ventricular ejection fraction (LVEF) is the mainstay for assessment of cardiac function and can be calculated from End Diastolic Volume (EDV) and End Systolic Volume as shown in the following equation:

$$\frac{EDV - ESV}{EDV}$$

Akap13$^{cKO\text{-}MCM}$ mice exhibited decreased resting (baseline) LVEF (50.1% ± 2.5) compared to controls (63.75% ± 1.64; $p<0.01$) characteristic of dilated cardiomyopathy (Fig. 2.13-

Fig. 2.14a). Mice were then analyzed based on their time post-recombination. *Akap13*$^{cKO\text{-}MCM}$ mice in the <8-week post-recombination group exhibited lower LVEF at baseline (51.64% ± 3.89) compared to controls (68.01% ± 2.65; $p<0.00001$) (Fig. 2.14b) as did the *Akap13*$^{cKO\text{-}MCM}$ mice in the ≥ 8-weeks post-recombination group (53.56% ± 4.05) compared to controls (65.58% ± 3.16; $p<0.01$) (Fig. 2.14c).

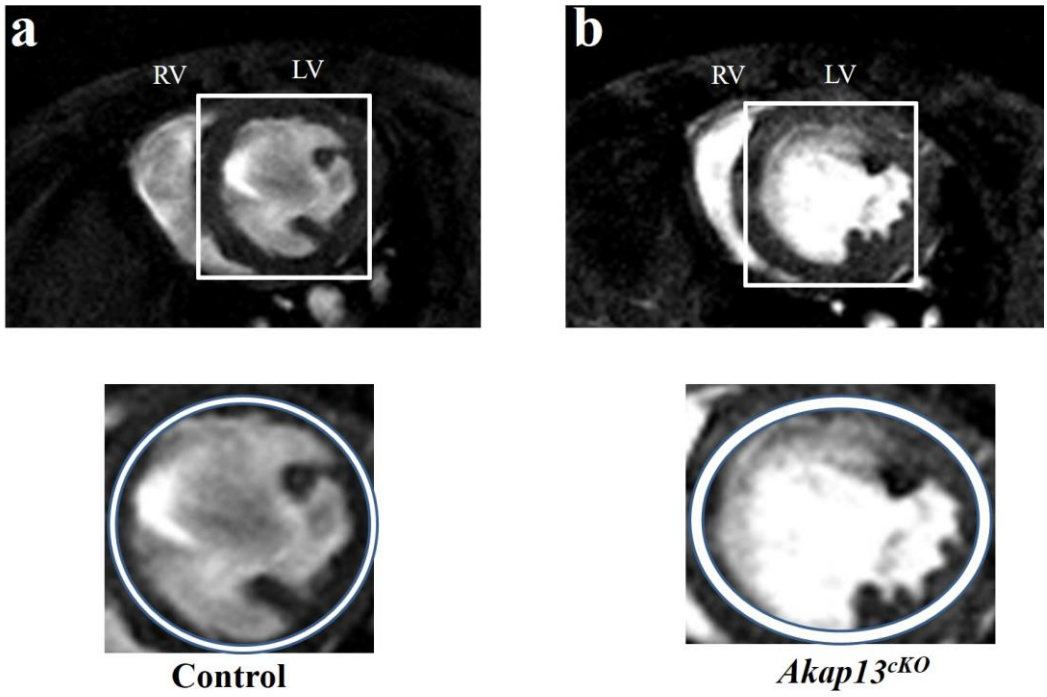

Figure 2.13| ***Akap13*$^{cKO\text{-}MCM}$ mice exhibited dilated left ventricles by magnetic resonance imaging (MRI).** a) MRI with contrast (0.2-0.3 mmol/kg Magnevist), short axis (SAX) slice at the level of the papillary muscles. Control mice (n=9) displayed typical left ventricle (LV) and right ventricle (RV) morphology. Inset shows the enlargement of the boxed region which highlighted the circular shape of the LV. b) MRI with contrast (0.2-0.3 mmol/kg Magnevist), short axis (SAX) slice at the level of the papillary muscles. Akap13$^{cKO\text{-}MCM}$ mice (n=7) showed dilated left ventricles. Inset shows the enlargement of the boxed region which highlighted the elliptical shape of the LV. Student's *t*-test used for statistical analyses.

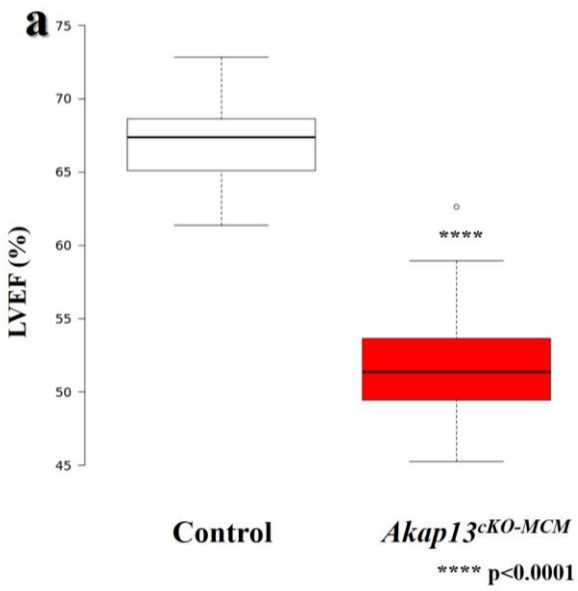

Box plot statistics	Control	Akap13$^{cKO-MCM}$
Upper whisker	72.85	58.95
3rd quartile	68.65	53.65
Median	67.38	51.36
1st quartile	65.09	49.44
Lower whisker	61.37	45.26
n=	15	14

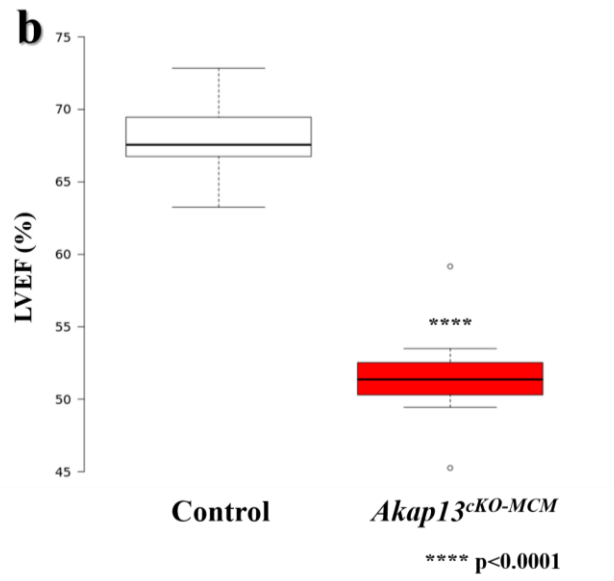

Box plot statistics	Control	Akap13$^{cKO-MCM}$
Upper whisker	72.85	53.5
3rd quartile	69.46	52.53
Median	67.56	51.37
1st quartile	66.75	50.3
Lower whisker	63.26	49.44
n=	9	7

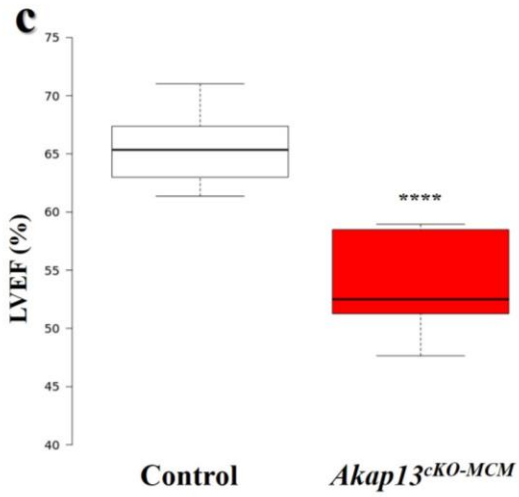

Box plot statistics	Control	Akap13$^{cKO-MCM}$
Upper whisker	71.03	58.95
3rd quartile	67.38	58.49
Median	65.35	52.5
1st quartile	63	51.27
Lower whisker	61.37	47.65
n=	6	6

****** p<0.0001**

Figure 2.14| ***Akap13$^{cKO-MCM}$*** **mice exhibited significantly decreased left ventricular ejection fraction (LVEF).** a) MRI with contrast (0.2-0.3 mmol/kg Magnevist), Normal left ventricular ejection fraction (LVEF) is 55-70%. Overall, *Akap13$^{cKO-MCM}$* mice (n=14) had reduced LVEF compared to control mice (n=15) ($p<0.001$). b) MRI with contrast (0.2-0.3 mmol/kg Magnevist), *Akap13$^{cKO-MCM}$* mice in the < 8 weeks post-recombination group had significantly lower LVEF compared to controls ($p<0.001$). c) MRI with contrast (0.2-0.3 mmol/kg Magnevist), *Akap13$^{cKO-MCM}$* mice in the ≥ 8 weeks post-recombination group had significantly lower LVEF compared to controls ($p<0.0001$). Student's *t*-test used for statistical analyses.

Furthermore, *Akap13*$^{cKO\text{-}MCM}$ mice exhibited an increased left ventricular end diastolic volume index (EDVI) (2.55µL/g ± 0.49) compared to control mice (2.02 µL/g ± 0.21; $p<0.001$), and an increased left ventricular end-systolic volume index (ESVI) (1.21 µL/g ± 0.29) compared to controls (0.67µL/g ± 0.11; $p<0.00001$) (Fig. 2.15a). *Akap13*$^{cKO\text{-}MCM}$ mice also showed increased left ventricular end diastolic mass index (EDMI) values (4.1 mg/g body weight ± 4.4E-4) and end systolic mass index (ESMI) values (4.4 mg/g body weight ± 0.4.8E-4) compared to controls (EDMI: 3.4 mg/g body weight ± 4.4E-4; $p<0.01$) (ESMI: 3.5 mg/g body weight ± 3.1E-4; $p<0.00001$) (Fig. 2.15b). Taken together, these data indicated dilation and hypertrophy of the left ventricle with impaired contractility in *Akap13*$^{cKO\text{-}MCM}$ mice.

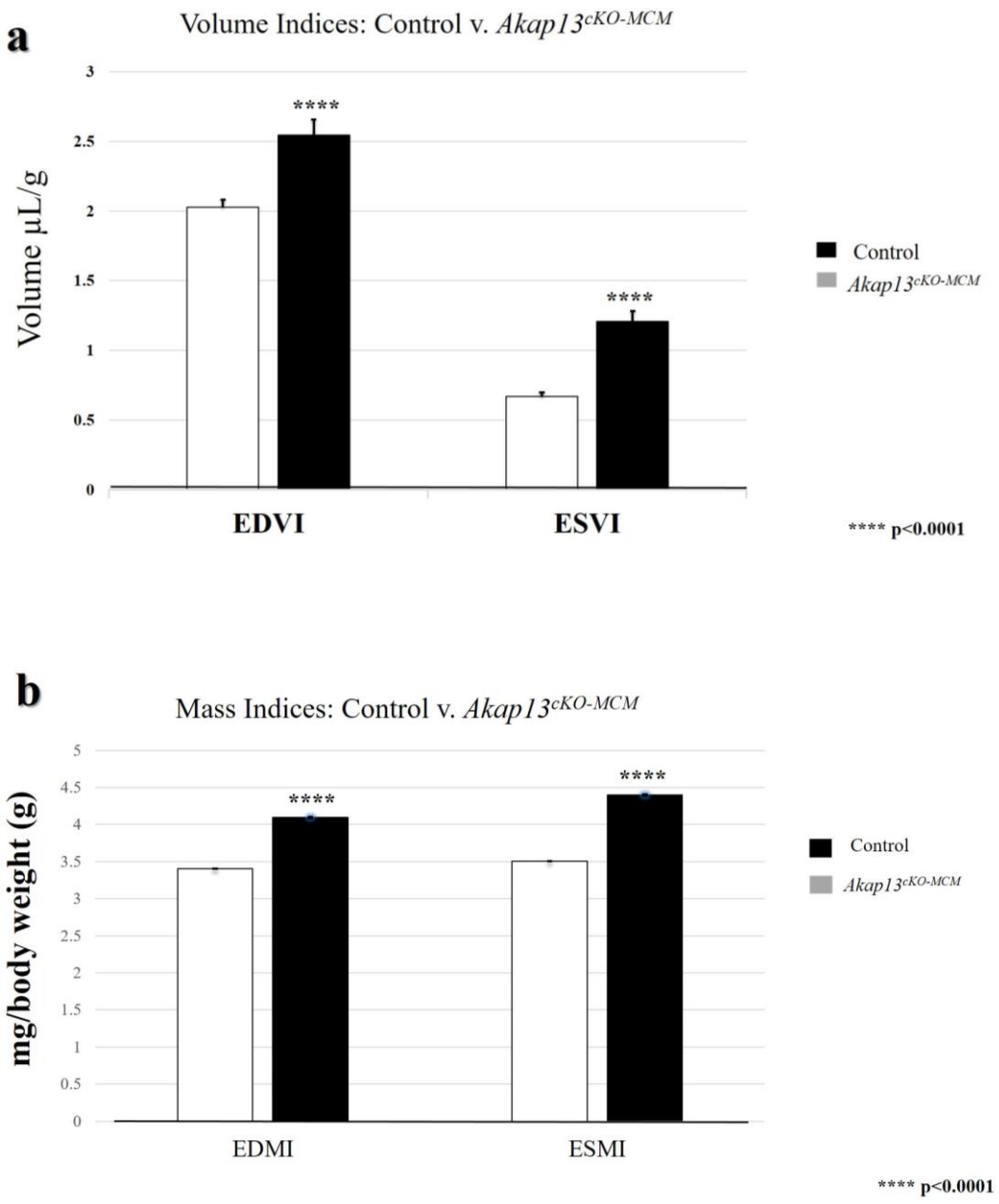

Figure 2.15| ***Akap13$^{cKO\text{-}MCM}$*** **mice had significantly increased volume and mass indices.** a) MRI with contrast (0.2-0.3 mmol/kg Magnevist), Overall, *Akap13$^{cKO\text{-}MCM}$* mice had an increased end diastolic volume index (EDVI) ($p<0.0001$) and end systolic volume index (ESVI) ($p<0.001$) compared to controls. Student's *t*-test used for statistical analyses. b) MRI with contrast (0.2-0.3 mmol/kg Magnevist), Overall, *Akap13$^{cKO\text{-}MCM}$* mice had an increased end diastolic mass index ($p<0.001$) and end systolic mass index (ESMI) ($p<0.0001$). Student's *t*-test used for statistical analyses.

When stratified based on time post-cessation of treatment for Cre-mediated excision, *Akap13*$^{cKO\text{-}MCM}$ mice in the <8 weeks post-recombination group exhibited increased left ventricular EDVI (2.65µL/g ± 0.31) (control: 2.03µL/g ± 0.20; $p<0.0001$) and ESVI (1.29µL/g ±0.23) (control: 0.65µL/g ± 0.094; $p<0.00001$). EDMI was also increased compared to control (3.9 mg/g body weight ± 0.00035) (control: 3.12 mg/g body weight ± 0.00037; $p<0.005$) as was ESMI (4.3 mg/g body weight ± 3.4E-4; control: 3.4 mg/g body weight a 2.7E-4; $p<0.00001$) (Table 2.1). *Akap13*$^{cKO\text{-}MCM}$ mice in the ≥ 8-weeks post-recombination group had increased EDVI (*Akap13*$^{cKO\text{-}MCM}$: 2.53 ± 0.45; control: 2.02 ± 0.21) ($p<0.01$) and EDMI (*Akap13*$^{cKO\text{-}MCM}$: 0.0044 ± 0.0003; control: 0.0038 ± 0.0002) ($p<0.01$), but not ESVI or ESMI ($p>0.05$) (Table 2.2).

	Resting MRI: < 8 weeks post-recombination				
	Akap13 $^{cKO\text{-}MCM}$		Control		p-value
LVEF	51.64	%	68.01	%	0.00000021
EDVI	2.65	µL/g	2.03	µL/g	0.00049
ESVI	1.29	µL/g	0.65	µL/g	0.0000068
EDMI	3.90	mg/g	3.16	mg/g	0.0019
ESMI	4.32	mg/g	3.36	mg/g	0.000042

Table 2.1| **Resting MRI summary table for < 8 weeks post-recombination group.** Summary of data showing significant values for all MRI variables measured.

	Resting MRI: ≥ 8 weeks post-recombination				
	Akap13 $^{cKO\text{-}MCM}$		Control		p-value
LVEF	53.56	%	65.58	%	0.00038
EDVI	2.53	µL/g	2.02	µL/g	0.046
ESVI	1.19	µL/g	0.7	µL/g	0.0062
EDMI	4.42	mg/g	3.77	mg/g	0.0050
ESMI	4.60	mg/g	3.72	mg/g	0.0064

Table 2.2| **Resting MRI summary table for ≥ 8 weeks post-recombination group.** Summary of data showing significant values for all MRI variables measured.

These data suggested dilation and hypertrophy in both the <8 weeks post-treatment and the ≥8 weeks post treatment *Akap13*$^{cKO\text{-}MCM}$ mice. When the *Akap13*$^{cKO\text{-}MCM}$ mice were compared to each other based on time post-treatment, the ≥8 weeks post-treatment group had increased EDMI compared to the group <8 weeks post-treatment group ($p<0.05$). Therefore, *Akap13*$^{cKO\text{-}MCM}$ mice exhibited left ventricular remodeling which resulted in compensatory hypertrophy concomitant with time post- *Akap13* excision.

Female *Akap13*^{cKO} mice exhibited more severe DCM than male *Akap13*$^{cKO\text{-}MCM}$ mice

When stratified based on sex, both male (Fig. 2.16a) and female (Fig. 2.16b) *Akap13*$^{cKO\text{-}MCM}$ mice had decreased LVEF at rest (male: 55.5% ± 4.46, female: 50.99% ± 3.80) compared to their respective controls (male: 68.5% ± 2.22; female: 66.25% ± 2.72; all $p<0.01$). However, when female *Akap13*$^{cKO\text{-}MCM}$ mice were compared to male *Akap13*$^{cKO\text{-}MCM}$ mice, females had lower LVEF than *Akap13*$^{cKO\text{-}MCM}$ male mice ($p<0.05$, one-way). This was striking since reports in humans have shown that women have higher LVEF than men (Chung, 2006). Similarly, *Akap13*$^{cKO\text{-}TOC}$ female mice exhibited decreased LVEF (59.55% ± 3.49) at rest compared to female controls (69.8 ± 5.24; $p<0.05$).

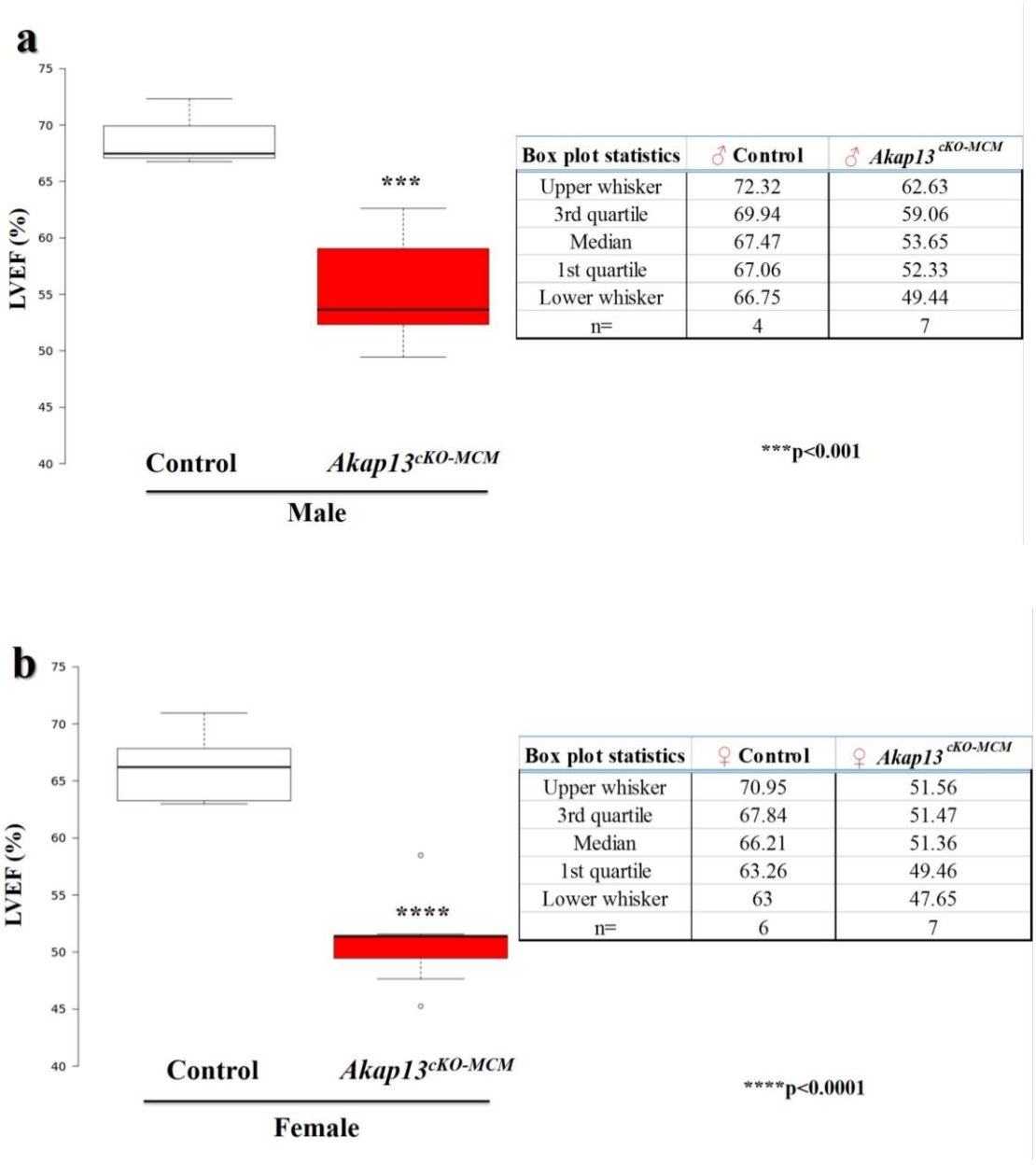

Box plot statistics	♂ Control	♂ *Akap13* $^{cKO\text{-}MCM}$
Upper whisker	72.32	62.63
3rd quartile	69.94	59.06
Median	67.47	53.65
1st quartile	67.06	52.33
Lower whisker	66.75	49.44
n=	4	7

Box plot statistics	♀ Control	♀ *Akap13* $^{cKO\text{-}MCM}$
Upper whisker	70.95	51.56
3rd quartile	67.84	51.47
Median	66.21	51.36
1st quartile	63.26	49.46
Lower whisker	63	47.65
n=	6	7

Figure 2.16| **Male and female *Akap13*$^{cKO\text{-}MCM}$ mice showed significantly reduced LVEF.** a) MRI with contrast (0.2-0.3 mmol/kg Magnevist), Male *Akap13*$^{cKO\text{-}MCM}$ mice (n=7) had significantly reduced LVEF compared to control mice (n=4) ($p<0.001$). b) MRI with contrast (0.2-0.3 mmol/kg Magnevist), Female *Akap13*$^{cKO\text{-}MCM}$ mice (n=7) showed significantly reduced LVEF compared to control mice (n=6) ($p<0.001$). Student's *t*-test was used for statistical analyses. Student's *t*-test used for statistical analyses.

When the male and female mice were stratified based on time post-recombination, male *Akap13*$^{cKO\text{-}MCM}$ mice in the <8 weeks post-recombination group also exhibited reduced LVEF at rest (53.32% ± 3.67) compared to controls (baseline: 68.82% ± 2.21; $p<0.001$). However, male *Akap13*^{cKO} mice ≥ 8 weeks post-recombination exhibited only a reduced LVEF trend at baseline (58.41% ± 3.69) compared to controls (64.33% ± 2.45; $p>0.05$). On the other hand, female *Akap13*$^{cKO\text{-}MCM}$ mice at both time points showed statistically significant reduction in LVEF at rest (<8 weeks: 47.86 ± 4.50; ≥8 weeks: 52.95% ± 2.94) compared to respective controls at rest (<8 weeks: 66.48 ± 4.37; ≥8 weeks: 69.89% ± 3.62) (<8 weeks $p=0.0025$; ≥8 weeks $p<0.01$).

Furthermore, male and female *Akap13*$^{cKO\text{-}MCM}$ mice had increased left ventricular EDVI (male: 2.38µL/g ± 0.36; female: 2.72µL/g ± 0.38) and ESVI (male: 1.07 ± 0.26; female: 2.72 ± 0.38) compared to controls (EDVI: male: 1.84µL/g ± 0.21; female: 2.19µL/g ± 0.14) (ESVI: male: 0.585 ± 0.098; female: 0.74 ± 0.087) (EDVI: male: $p<0.05$; female: $p<0.05$) (ESVI: male: $p<0.05$; female: $p< 0.001$). Male and female *Akap13*$^{cKO\text{-}MCM}$ mice also had increased left ventricular EDMI (male: 3.84µL/g ± 3.9E-4; female: 4.4µL/g ± 3E-4) compared to controls (male: 3.2 µL/g ± 4E-4; female: 3.3 µL/g ± 4E-4) (male: $p<0.05$; female: $p<0.001$) and increased ESMI (male: 4.1 ± 0.00014; female: 4.7 ± 0.00016) compared to controls (male: 3.3 ± 0.00014; female: 3.6 ± 0.00012) (male: $p<0.01$; female: $p<0.001$). It is well established in the literature that females typically have lower EDMI than males. However, female *Akap13*$^{cKO\text{-}MCM}$ mice had increased EDMI

compared to male *Akap13*$^{cKO\text{-}MCM}$ mice ($p<0.05$). This suggested that female *Akap13*$^{cKO\text{-}MCM}$ mice had increased ventricular remodeling compared to males (Table 2.3).

a

Resting MRI: Male					
	Akap13$^{cKO\text{-}MCM}$		Control		p-value
LVEF	55.50	%	68.5	%	0.00081
EDVI	2.38	µL/g	1.84	µL/g	0.036
ESVI	1.07	µL/g	0.59	µL/g	0.010
EDMI	3.84	mg/g	3.20	mg/g	0.04
ESMI	4.14	mg/g	3.30	mg/g	0.0068

b

Resting MRI: Female					
	Akap13$^{cKO\text{-}MCM}$		Control		p-value
LVEF	50.99	%	66.25	%	0.000011
EDVI	2.72	µL/g	2.19	µL/g	0.014
ESVI	1.34	µL/g	0.74	µL/g	0.00039
EDMI	4.40	mg/g	3.30	mg/g	0.00084
ESMI	4.70	mg/g	3.36	mg/g	0.00044

Table 2.3| **Resting MRI summary table stratified by sex.** a) Summary of male data showing significant values for all MRI variables measured. b) Summary of female data showing significant values for all MRI variables measured.

When the <8 weeks and ≥8 weeks groups were stratified based on sex, males in the <8 weeks post-recombination group demonstrated increased EDVI (2.5 ± 0.337) (control: 1.92 ± 0.21) (p=0.27) and ESVI (1.18 ± .24) (control: 0.62 ± 0.093) (p<0.01). EDMI values were modestly increased (p>0.05) (supplemental), but ESMI was increased (4.2 mg/g body weight ± 2.6E-4) (control: 3.3 ± 3.2E-4) (p<0.01). At ≥8 weeks post-recombination, male *Akap13*$^{cKO\text{-}MCM}$ mice only showed modest increases in EDVI, ESVI, EDMI and ESMI (supplemental) (all p>0.05). Moreover, female *Akap13*$^{cKO\text{-}MCM}$ mice **at <8** weeks post-recombination showed increased EDVI (2.84 ± 0.09) (control: 2.16 ± 0.09) (p<0.001), and ESVI (1.44 ± 0.12) (control: 0.71 ± 0.051) (p<0.001). EDMI was also increased (4.24 mg/g body weight ± 1.6E-4) (control: 3.1 mg/g body weight ± 2.3E-4) (p<0.01) as was ESMI (4.5 mg/g body weight ± 3.2E-4) (control: 3.44 ± 1.6E-4) (p<0.01). Female *Akap13*$^{cKO\text{-}MCM}$ mice at ≥8 weeks post-recombination had modestly increased EDVI (2.62 ± 0.48) (control: 2.13 ± 0.24) (p=0.11), but maintained an increased ESVI (1.26 ± 0.30) (3.8 ± 2.9E-4) (p=0.029/0.059). Additionally, EDMI was increased (4.44 a 3.6) (control: 3.8 ± 2.8E-4) (p=0.059 one-way) as was ESMI (4.8 mg/ g body weight ± 4.6E-4) (control: 3.8 mg/g body weight ± 2.9E-4) (p<0.05).

Female *Akap13*$^{Het\text{-}MCM}$ exhibited dilated cardiomyopathy

Mice haploinsufficient (n=11) for the conditional null allele (hereafter *Akap13*$^{Het\text{-}MCM}$) had lower LVEF at baseline (59.66% ± 6.6) compared to controls (66.66% ± 3.88; $p<0.05$). When *Akap13*$^{Het\text{-}MCM}$ mice were stratified based on sex, female *Akap13*$^{Het\text{-}MCM}$ mice exhibited decreased LVEF compared to controls at rest (57.3% ± 7.78) (control: 65.87% ± 2.68) ($p<0.05$). However, no left ventricular phenotype was seen with male *Akap13*$^{Het\text{-}MCM}$ mice ($p>0.05$) at rest (Fig. 2.17). These data showed that females were more affected than males associated with *Akap13* gene disruption, even in the haploinsufficient state.

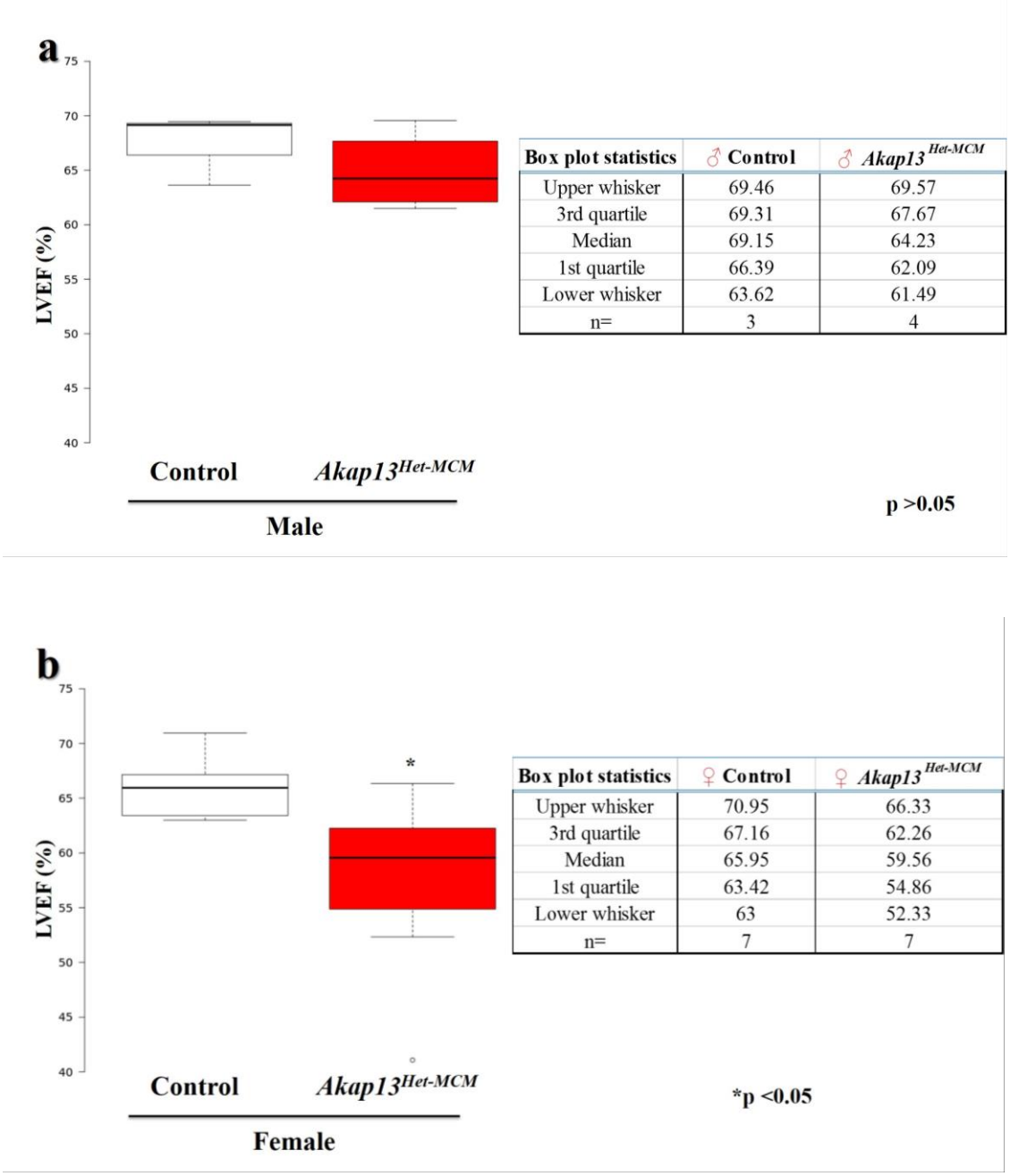

Box plot statistics	♂ Control	♂ *Akap13*$^{Het-MCM}$
Upper whisker	69.46	69.57
3rd quartile	69.31	67.67
Median	69.15	64.23
1st quartile	66.39	62.09
Lower whisker	63.62	61.49
n=	3	4

Box plot statistics	♀ Control	♀ *Akap13*$^{Het-MCM}$
Upper whisker	70.95	66.33
3rd quartile	67.16	62.26
Median	65.95	59.56
1st quartile	63.42	54.86
Lower whisker	63	52.33
n=	7	7

Figure 2.17| **Male and female *Akap13*$^{Het-MCM}$ mice showed differences in LVEF.** a) MRI with contrast (0.2-0.3 mmol/kg Magnevist), Male *Akap13*$^{Het-MCM}$ mice (n=3) showed no changes in LVEF compared to control mice (n=4) ($p>0.05$). b) MRI with contrast (0.2-0.3 mmol/kg Magnevist), Female *Akap13*$^{Het-MCM}$ mice (n=7) had significantly lower LVEF compared to control mice (n=7) ($p<0.05$). Student's *t*-test used for statistical analyses.

Overall, *Akap13*$^{Het\text{-}MCM}$ mice demonstrated no significant changes to left ventricular EDVI, ESVI, EDMI, or ESMI (Table ST.5) compared to controls (n=5), however, sex-dependent changes were observed. Female *Akap13*$^{Het\text{-}MCM}$ mice demonstrated a modestly increased left ventricular EDVI (2.52µL/g ± 0.43) (control: 2.22 ± 0.14; p=0.13), and increased ESVI (1.1 µL/g ± 0.39) (control: 0.76 µL/g ± 0.09; p=0.057). Additionally, female *Akap13*$^{Het\text{-}MCM}$ mice showed increased left ventricular EDMI (4.0 mg mass/g body weight ± 7E-4) (control: 3.3 mg/g body weight ± 4E-4; p=0.057), and modestly increased ESMI (4.0 mg/g body weight ± 6E-4) (control: 0.0036 ± 2.9E-4; p=0.15) (Table 2.4).

Resting MRI: *Akap13* haploinsufficient Female

	Akap13$^{Het\text{-}MCM}$		Control		p-value
LVEF	57.32	%	65.87	%	0.02600
EDVI	2.52	µL/g	2.22	µL/g	0.13
ESVI	1.10	µL/g	0.76	µL/g	0.057
EDMI	4.00	mg/g	3.23	mg/g	0.057
ESMI	4.00	mg/g	3.60	mg/g	0.15

Table 2.4| **Resting MRI summary *Akap13* haploinsufficient female.** Female *Akap13*$^{Het\text{-}MCM}$ mice had significant differences in cardiac function whereas male *Akap13*$^{Het\text{-}MCM}$ mice did not.

Akap13^{cKO} mice failed to increase LVEF with stress testing

After resting cardiac MRI, stress testing with dobutamine, a β_1-adrenergic receptor agonist, and positive inotropic agent, was conducted. Dobutamine was administered at a low dose (10ug/kg/min; hereafter LVEF-10) and a high dose (40ug/kg/min; hereafter LVEF-40) to assess cardiac response. LVEF should increase with inotropic stimulation during stress. *Akap13*$^{cKO\text{-}MCM}$ mice failed to mount an appropriate response to the dobutamine stress; LVEF for *Akap13*$^{cKO\text{-}MCM}$ mice was decreased (LVEF-10: 56.99% ±8.12; LVEF-40: 63.13% ± 10.31) compared to control LVEF (LVEF-10: 77.09% ± 5.89; LVEF-40: 83.47% ± 4.17) at both the low ($p<0.00001$) and high doses ($p<0.00001$) of dobutamine (Fig. 2.18).

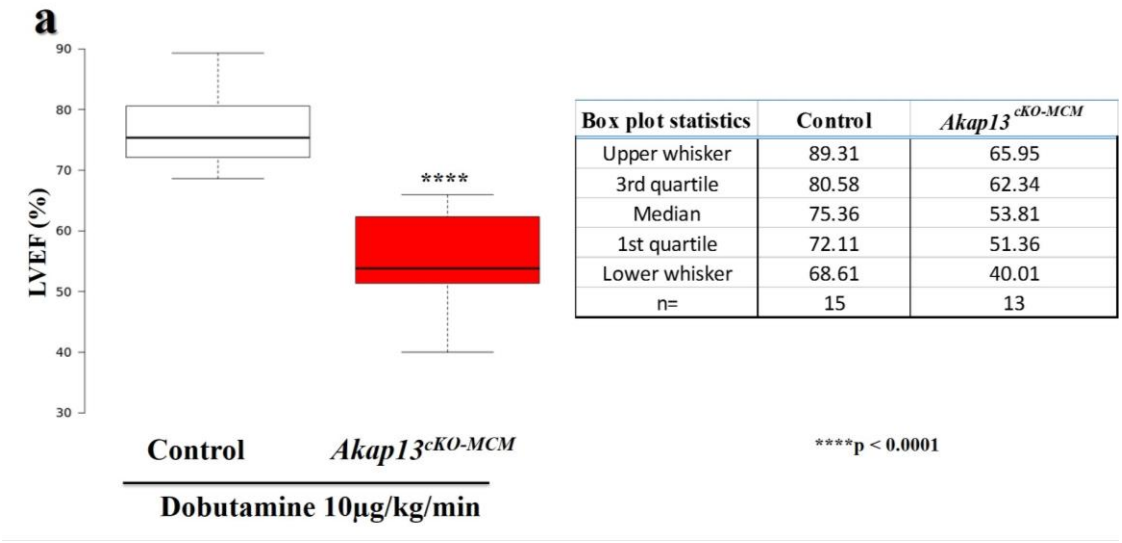

Box plot statistics	Control	*Akap13* $^{cKO-MCM}$
Upper whisker	89.31	65.95
3rd quartile	80.58	62.34
Median	75.36	53.81
1st quartile	72.11	51.36
Lower whisker	68.61	40.01
n=	15	13

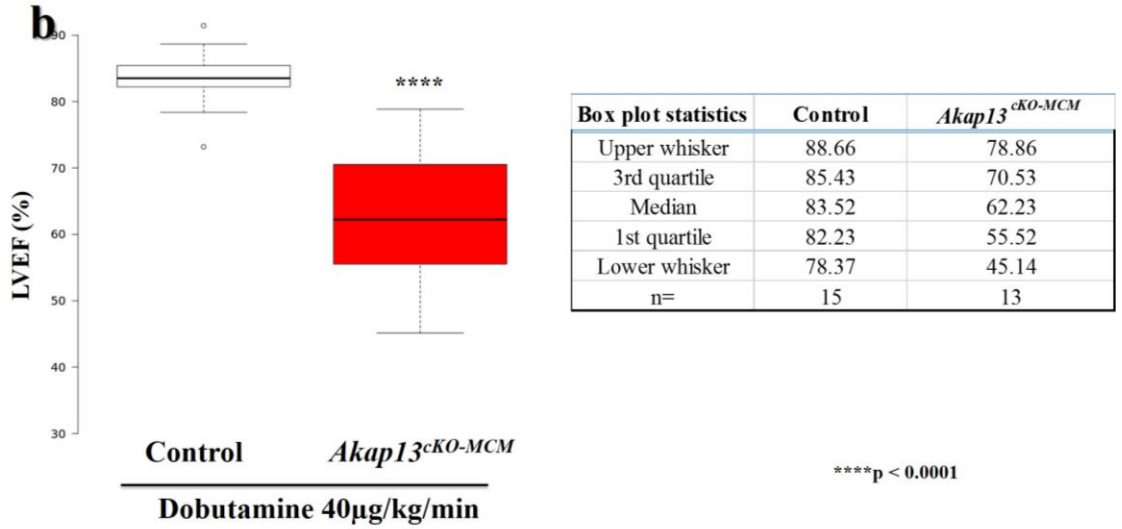

Box plot statistics	Control	*Akap13* $^{cKO-MCM}$
Upper whisker	88.66	78.86
3rd quartile	85.43	70.53
Median	83.52	62.23
1st quartile	82.23	55.52
Lower whisker	78.37	45.14
n=	15	13

Figure 2.18| ***Akap13*** $^{cKO-MCM}$ **mice exhibited decreased LVEF with dobutamine MRI stress testing.** a) Stress MRI with contrast (0.2-0.3 mmol/kg Magnevist), *Akap13* $^{cKO-MCM}$ mice (n=13) had lower LVEF than control mice (n=15) with 10µg/kg/min dobutamine MRI stress testing ($p<0.001$). b) Stress MRI with contrast (0.2-0.3 mmol/kg Magnevist), *Akap13* $^{cKO-MCM}$ mice (n= 13) had lower LVEF than control mice (n=15) with 40µg/kg/min dobutamine MRI stress testing ($p<0.001$). Student's *t*-test used for statistical analyses.

When stratified based on sex, both male and female *Akap13*$^{cKO\text{-}MCM}$ mice failed to increase their LVEF with low dose dobutamine (male LVEF-10: 57.38% ± 8.98; female LVEF-10: 56.65% ± 7.27) and high dose dobutamine (male LVEF-40: 61.53% ± 12.27; female LVEF-40: 65.50% ± 8.03) compared to their respective controls [(male LVEF-10: 77.83% ± 5.76; female LVEF-10: 76.43% ± 5.91) and (male LVEF-40: 83.13% ± 4.29; female LVEF-40: 83.76 ± 4.03)] (all $p<0.01$) (Fig. 2.19).

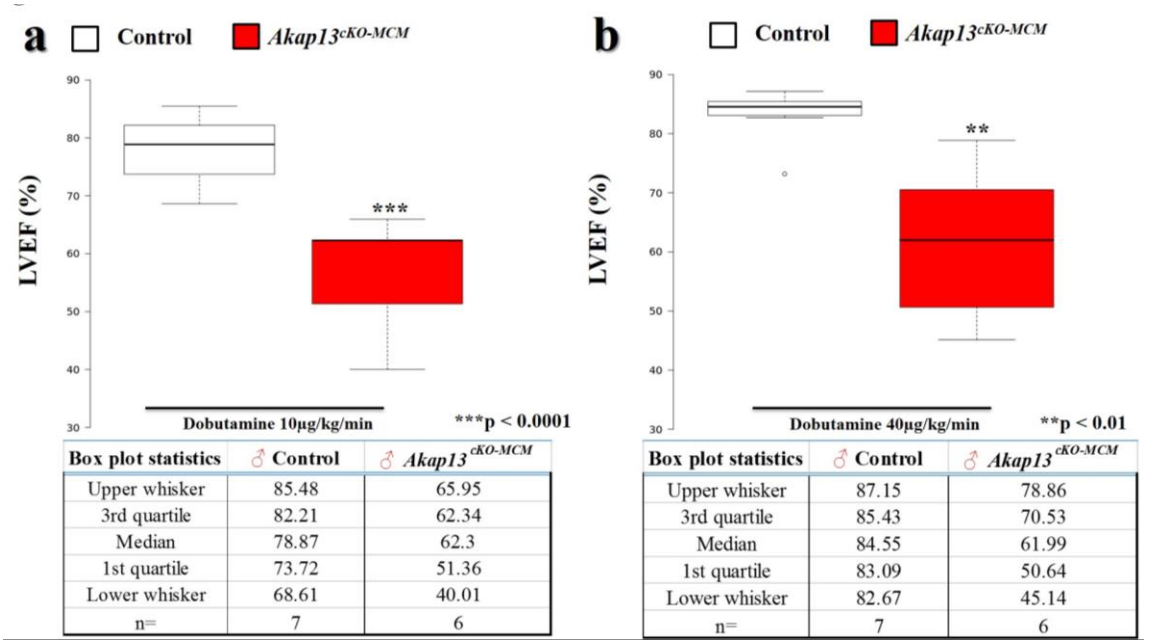

Box plot statistics	♂ Control	♂ *Akap13* $^{cKO\text{-}MCM}$
Upper whisker	85.48	65.95
3rd quartile	82.21	62.34
Median	78.87	62.3
1st quartile	73.72	51.36
Lower whisker	68.61	40.01
n=	7	6

Box plot statistics	♂ Control	♂ *Akap13* $^{cKO\text{-}MCM}$
Upper whisker	87.15	78.86
3rd quartile	85.43	70.53
Median	84.55	61.99
1st quartile	83.09	50.64
Lower whisker	82.67	45.14
n=	7	6

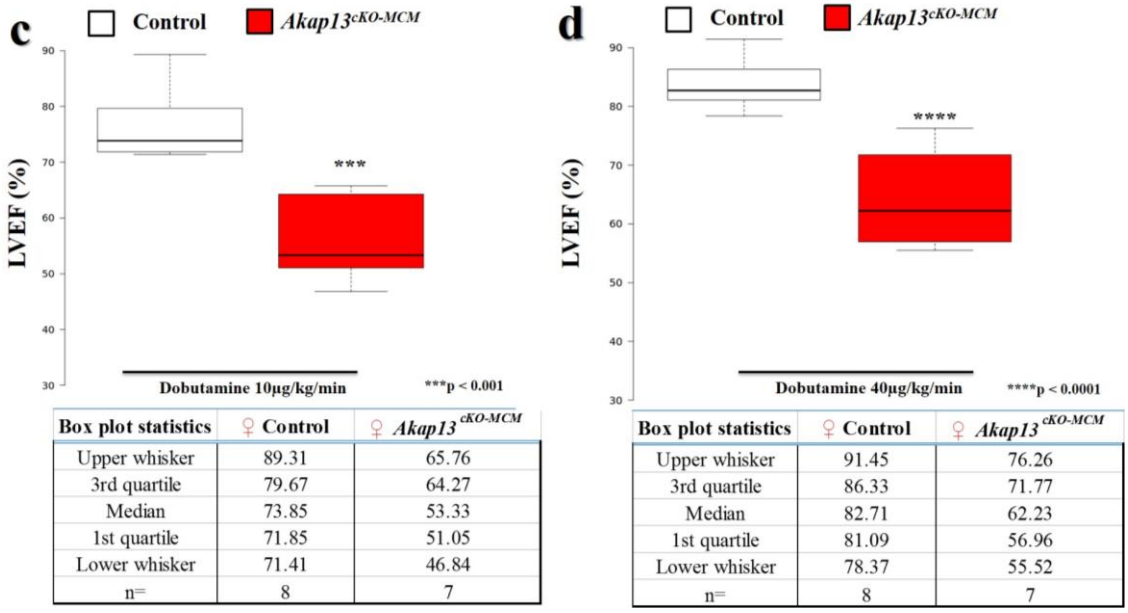

Box plot statistics	♀ Control	♀ *Akap13* $^{cKO\text{-}MCM}$
Upper whisker	89.31	65.76
3rd quartile	79.67	64.27
Median	73.85	53.33
1st quartile	71.85	51.05
Lower whisker	71.41	46.84
n=	8	7

Box plot statistics	♀ Control	♀ *Akap13* $^{cKO\text{-}MCM}$
Upper whisker	91.45	76.26
3rd quartile	86.33	71.77
Median	82.71	62.23
1st quartile	81.09	56.96
Lower whisker	78.37	55.52
n=	8	7

Figure 2.19| **Female and male *Akap13*$^{cKO\text{-}MCM}$ mice exhibited decreased LVEF with dobutamine MRI stress testing.** a,b) Stress MRI with contrast (0.2-0.3 mmol/kg Magnevist), Male *Akap13*$^{cKO\text{-}MCM}$ mice had lower LVEF compared to control mice with both 10µg/kg/min ($p<0.001$) and 40µg/kg/min Dobutamine stress MRI ($p<0.001$). c,d) Stress MRI with contrast (0.2-0.3 mmol/kg Magnevist), Female *Akap13*$^{cKO\text{-}MCM}$ mice had lower LVEF compared to control mice with both 10µg/kg/min ($p<0.001$) and 40µg/kg/min Dobutamine stress MRI ($p<0.001$). Student's *t*-test used for statistical analyses.

Similarly, *Akap13*$^{cKO\text{-}MCM}$ mice in the <8 weeks post-recombination group failed to increase their LVEF with stress testing (LVEF-10: 52.66% ± 8.21; LVEF-40: 59.68% ± 10.46) compared to controls (LVEF-10: 75.67% ± 4.32; LVEF-40: 82.79 ± 2.16; $p<0.001$, both). *Akap13*$^{cKO\text{-}MCM}$ mice in the ≥8 weeks post-recombination group also failed to increase their LVEF with stress testing (LVEF10: 62.04% ±4.09; LVEF40: 67.14% ± 8.45) ($p<0.01$) compared to control mice at the same time point (LVEF10: 79.2% ± 7.15; LVEF40: 84.49% ± 5.89).

When the <8 weeks post-recombination group and the ≥8 weeks post-recombination groups were stratified based on sex, male *Akap13*$^{cKO\text{-}MCM}$ < 8 weeks post-recombination showed statistically lower LVEF at both dobutamine dosages (LVEF-10: 54.92% ± 10.15; LVEF-40: 62.08% ± 13.31) compared to controls (LVEF-10: 78.00% ± 4.90; LVEF-40: 84.23% ± 1.31) ($p<0.05$, both). The ≥ 8 weeks post-recombination group was able to respond at the lower dose of dobutamine (LVEF-10: 65.97% ± 5.20) ($p=0.064$ one-way), but failed to respond at the higher dose of dobutamine, with an actual drop in LVEF to a lower level than their resting LVEF (LVEF-40: 56.80% ± 9.48) compared to controls (LVEF-10: 77.46% ± 6.73; LVEF-40: 81.67% ± 6.08) (LVEF-40: $p< 0.05$). However, female *Akap13*$^{cKO\text{-}MCM}$ showed decreased LVEF at both time points and both dobutamine dosages (<8 weeks: LVEF-10: 49.65% ± 2.05; LVEF-40: 56.48% ± 1.07; ≥8weeks: LVEF-10: 60.62 ± 5.17; LVEF-40: 68.59 ± 4.69) compared to respective controls (<8 weeks: LVEF-10: 73.72 ± 2.42; LVEF-40: 81.63 ± 2.01 ; ≥8 weeks: LVEF-

10: 80.94 ± 7.14) ; LVEF-40: 87.31 ± 4.05) (<8 weeks: LVEF-10: p=1.61E-5 ; LVEF-40: p=2.35E-6) (≥8 weeks: LVEF-10: p<0.05 ; LVEF-40: p<0.05).

Moreover, *Akap13*$^{Het\text{-}MCM}$ mice showed a lower LVEF trend with the lower dose of dobutamine (LVEF 10: 65.33% ± 10.5) (p=0.05, one-way), but a significantly reduced LVEF with the higher dose of dobutamine (LVEF40: 71.63% ± 8.97) (p<0.05 one way) compared to controls (LVEF 10: 73.81% ± 3.68; LVEF 40: 80.25% ± 3.89), and thereby demonstrated decompensation at the higher dobutamine dose. When *Akap13*$^{Het\text{-}MCM}$ mice were stratified based on sex, female *Akap13*$^{Het\text{-}MCM}$ mice showed significantly reduced LVEF at both dobutamine dosages (LVEF-10: 61.1% ± 10.42; LVEF-40: 68.01% ± 8.02) (control: LVEF-10: 73.81% ± 3.68; LVEF-40: 80.85% ± 3.89) (LVEF-10 p<0.05; LVEF-40: p<0.05). However, male *Akap13*$^{Het\text{-}MCM}$ mice showed no statistical changes with stress testing (Table ST.6).

These data showed increased severity of cardiac phenotype in female *Akap13*$^{cKO\text{-}MCM}$ mice compared to male *Akap13*$^{cKO\text{-}MCM}$ mice, and a different cardiac response to stress once the heart is compromised. Moreover, male mice could partially remodel over time, but decompensated with stress. Females were less able to remodel with time and did not show any inotropic response with stress. These data also showed that females were more affected than males associated with *Akap13* gene disruption, even in the haploinsufficient state (Table 2.5).

Resting MRI												
	Male						Female					
	<8 weeks post- knockout			≥8 weeks post-knockout			<8 weeks post- knockout			≥8 weeks post-knockout		
	Akap13^{cKO}	Control	p-value	*Akap13*^{cKO}	Control	p-value	*Akap13*^{cKO}	Control	p-value	*Akap13*^{cKO}	Control	p-value
n	5	4	-	3	3	-	3	5	-	4	3	-
LVEF (%)	53.32	68.82	0.00023	58.41	64.33	0.13	49.40	67.00	0.0010	52.19	66.83	0.0069
EDVI (µL/g)	2.51	1.92	0.027	2.21	1.92	0.29	2.84	2.16	0.00035	2.62	2.13	0.23
ESVI (µL/g)	1.18	0.60	0.0034	0.93	0.68	0.21	1.44	0.71	0.00023	1.26	0.72	0.0294
EDMI (mg/g B.W.)	3.65	3.24	0.17	4.10	3.65	0.22	4.24	3.08	0.0013	4.44	3.89	0.12
ESMI (mg/g B.W.)	4.17	3.30	0.0067	4.10	3.67	0.28	4.53	3.44	0.0040	4.76	3.77	0.040

Table 2.5| **Summary of resting left ventricular MRI values.** Summary of resting left ventricular MRI values stratified based on sex and time post-recombination. *Akap13*$^{cKO\text{-}MCM}$ mice exhibited dilated cardiomyopathy with compensatory hypertrophy. Females had more significant MRI pathology than males.

Akap13^{cKO} mice developed right ventricular dilation and hypertrophy

The function of the right ventricle was assessed to determine any contribution to the cardiac phenotype (Table 2.6). The right ventricular ejection fraction (RVEF) for *Akap13*$^{cKO\text{-}MCM}$ mice was reduced (59.2% ± 3.93) compared to control mice (65.55% ± 5.03) ($p<0.05$). When stratified based on time post-recombination, *Akap13*$^{cKO\text{-}MCM}$ mice in the <8 weeks post-recombination group showed the same pattern of right ventricular dysfunction seen in overall genotype comparisons (60.07 ± 1.93) compared to controls (68.45 ± 3.08; p=1.64E-5). Likewise, *Akap13*$^{cKO\text{-}MCM}$ mice in the ≥8 weeks group had reduced RVEF (58.21 ± 5.20) compared to controls (65.37 ± 2.28) ($p<0.05$).

Resting MRI												
	Male						Female					
	<8 weeks post- knockout			≥8 weeks post-knockout			<8 weeks post- knockout			≥8 weeks post-knockout		
	Akap13^{cKO}	Control	p-value	*Akap13*^{cKO}	Control	p-value	*Akap13*^{cKO}	Control	p-value	*Akap13*^{cKO}	Control	p-value
n	**5**	**4**	**-**	**3**	**3**	**-**	**3**	**5**	**-**	**4**	**3**	**-**
RVEF (%)	60.24	66.82	0.0061	58.05	64.00	0.32	59.82	69.76	0.0034	58.34	65.57	0.041
EDVI (µL/g)	1.72	1.56	0.62	1.73	1.47	0.06	1.98	1.33	0.033	1.80	1.71	0.77
ESVI (µL/g)	0.69	0.51	0.17	0.74	0.53	0.20	0.76	0.40	0.00066	0.75	0.85	0.25

Table 2.6| **Summary of resting right ventricular MRI values.** Summary of resting right ventricular MRI values stratified based on sex and time post-recombination. Females have more significant MRI pathology than males.

Right ventricular assessment of male *Akap13*$^{cKO\text{-}MCM}$ mice compared to female *Akap13*$^{cKO\text{-}MCM}$ mice demonstrated sex-dependent differences. Right ventricular ejection fraction was reduced in both male *Akap13*$^{cKO\text{-}MCM}$ mice (59.42 ± 4.58) and female *Akap13*$^{cKO\text{-}MCM}$ mice (58.97 ± 3.00) compared to control mice (male: 66.23 ± 2.72; $p<0.05$; female: 68.19 ± 3.25; $p<0.001$). Male *Akap13*$^{cKO\text{-}MCM}$ mice in the <8 weeks post-recombination group showed reduced RVEF (60.24 ± 1.69) compared to respective controls (66.82 ± 2.77) ($p<0.01$). However, male *Akap13*$^{cKO\text{-}MCM}$ mice in the ≥8 weeks post-recombination group showed modestly reduced RVEF (58.05 ± 6.95) (63.96 ± 2.37) ($p>0.05$). Conversely, female *Akap13*$^{cKO\text{-}MCM}$ mice in the < 8 weeks post-recombination group exhibited markedly decreased RVEF (59.82 ± 2.26) compared to controls (69.76 ± 2.65; $p<0.01$). Moreover, female *Akap13*$^{cKO\text{-}MCM}$ mice in the ≥8 weeks post-recombination group continued to exhibit significant reduction of RVEF (58.33 ± 3.32) compared to respective controls (65.57 ± 2.31; $p<0.05$). These results suggested cardiomyopathy of the right ventricle in *Akap13*^{cKO} mice, with a more severe phenotype in female *Akap13*^{cKO} mice (Table ST.8a).

Right ventricular ejection fraction was also evaluated in *Akap13*$^{Het\text{-}MCM}$ mice and was found to be decreased in *Akap13*$^{Het\text{-}MCM}$ mice compared to control mice (n=20) (*Akap13*$^{Het\text{-}MCM}$ mice: 60.87% ± 1.83; Control: 65.23% ± 1.08) ($p<0.05$). *Akap13*$^{Het\text{-}MCM}$ mice were also stratified based on sex. Male *Akap13*$^{Het\text{-}MCM}$ mice showed decreased RVEF (*Akap13*$^{Het\text{-}MCM}$: 56.95% ± 3.58; Control: 63.30% ± 2.06) ($p<0.05$ one-way) (Table ST.8b). Female Akap13$^{Het\text{-}MCM}$ mice exhibited significantly decreased RVEF (*Akap13*$^{Het\text{-}}$

^{MCM}: 63.11 ± 1.45; Control: 68.19 ± 1.15) ($p<0.05$) compared to controls (n=9) mirroring the results of the *Akap13*$^{cKO\text{-}MCM}$ mice. These data suggested cardiomyopathy of the right ventricle in *Akap13*$^{Het\text{-}MCM}$ mice.

Right ventricular volume indices were also evaluated. The EDVI of the right ventricle was increased in *Akap13*$^{cKO\text{-}MCM}$ mice (1.78µL/g±0.36) compared to controls (1.50µL/g ±0.30; $p<0.05$) as was the ESVI (0.72µL/g ± 0.17) compared to controls (0.48 µL/g ± 0.1; $p<0.001$). When stratified based on time post-recombination, *Akap13*$^{cKO\text{-}MCM}$ mice in the <8 week post-recombination group showed the same pattern of right ventricular dilation seen with overall genotype comparisons: (EDVI: 1.78 ± 0.38; ESVI: 0.71± 0.16) compared to controls (EDVI: 1.44 ± 0.33; ESVI: 0.45 ± 0.09) (EDVI: $p=0.075$; ESVI: $p< 0.01$). Taken together, these data indicated dilation and reduced contractility of the right ventricle. *Akap13*$^{cKO\text{-}MCM}$ mice in the ≥8 week group had only modestly increased EDVI (1.77 ± 0.32) compared to controls (1.61 ± 0.18) ($p>0.05$). However, ESVI remained increased (0.74 ± 0.18) compared to controls (0.56 ± 0.05) ($p<0.05$ one-way). These data showed that right ventricular function continued to be affected over time. Right ventricular function was also evaluated in *Akap13*$^{Het\text{-}MCM}$ mice. No changes were observed with RV EDVI or ESVI ($p>0.05$).

When right ventricular EDVI and ESVI were stratified by sex, male *Akap13*$^{cKO\text{-}MCM}$ mice showed modestly increased EDVI (1.73 ± 0.36) compared to controls (1.52 ± 0.31) ($p>0.05$). ESVI was also increased (*Akap13*$^{cKO\text{-}MCM:}$ 0.71 ± 0.19; control: 0.51 ± 0.08) ($p<0.05$). These data indicated dilation and impaired contractility of the right ventricle in

male *Akap13*$^{cKO\text{-}MCM}$ mice. Female *Akap13*$^{cKO\text{-}MCM}$ mice showed similar but more severe outcomes. EDVI (1.84 ± 0.34) as well as ESVI 0.75 ± 0.14) were increased in female *Akap13*$^{cKO\text{-}MCM}$ mice compared to controls (EDVI: 1.47 ± 0.29; ESVI: 0.47 ± 0.10) where (EDVI: $p=0.059$ two-way; ESVI: $p<0.01$). These data suggested dilation and impaired contractility of the right ventricle. In sum, both male and female *Akap13*$^{cKO\text{-}MCM}$ mice developed biventricular dilated cardiomyopathy with compensatory left ventricular hypertrophy and impaired contractility. However, female *Akap13*$^{cKO\text{-}MCM}$ mice showed increased morbidity since they exhibited more severe cardiac dysfunction than respective *Akap13*$^{cKO\text{-}MCM}$ males (Table ST.7a).

Right ventricular function in *Akap13*$^{Het\text{-}MCM}$ mice were also stratified based on sex. Female *Akap13*$^{Het\text{-}MCM}$ mice (n=7) showed no changes in EDVI (*Akap13*$^{Het\text{-}MCM}$: 1.45 ± 0.12; Control: 1.47 ± 0.10) ($p=0.80706$), and modestly increased ESVI (*Akap13*$^{Het\text{-}MCM}$: 0.54 ± 0.050; Control: 0.47 ± 0.037) ($p>0.05$) (Table ST.7b). Male *Akap13*$^{Het\text{-}MCM}$ mice (n=4) also showed changes in EDVI (*Akap13*$^{Het\text{-}MCM}$: 1.95 ± 0.15; Control: 1.56 ± 0.14) ($p>0.05$) and modestly increased ESVI (*Akap13*$^{Het\text{-}MCM\ t}$: 0.77 ± 0.08; Control: 0.58 ± 0.07) ($p= 0.09$) compared to controls (n=11) (TABLE). These data showed that both male and female *Akap13*$^{Het\text{-}MCM}$ mice had modest dilation of the right ventricles and therefore showed a mild biventricular cardiomyopathy.

When stratified based on duration post-recombination, male *Akap13*$^{cKO\text{-}MCM}$ mice in the <8 weeks post-recombination group showed modestly increased ESVI (*Akap13*$^{cKO\text{-}MCM}$: 0.74 ± 0.19; control: 0.53 ± 0.03) ($p>0.05$). However, male *Akap13*$^{cKO\text{-}MCM}$ mice in the ≥8

weeks post-recombination group had increased EDVI (1.73 ± 0.14) compared to controls (1.47 ± 0.01; $p<0.05$, one-way). Taken together, these data suggested male *Akap13*$^{cKO\text{-}MCM}$ mice developed mild right ventricular dilation and contractility defects that partially improved over time although persisted. Conversely, female *Akap13*$^{cKO\text{-}MCM}$ mice in the <8 weeks post-recombination group showed profoundly increased EDVI and ESVI compared to controls (*Akap13*$^{cKO\text{-}MCM:}$ EDVI: 1.89 ± 0.2; ESVI: 0.76 ± 0.08; control: EDVI: 1.33 ± 0.26; ESVI: 0.40± 0.06) (EDVI: $p< 0.05$; ESVI: $p<0.001$). Female *Akap13*$^{cKO\text{-}MCM}$ mice in the ≥8 weeks post-recombination group showed modestly increased EDVI (1.8 ± 0.41) ($p>0.05$) and ESVI (0.75 ± 0.18) ($p>0.05$) compared with respective controls (EDVI: 1.71 ± 0.16; ESVI: 0.58 ± 0.04). These data showed that female *Akap13*$^{cKO\text{-}MCM}$ mice had a more severe right ventricular phenotype than male *Akap13*$^{cKO\text{-}MCM}$ mice, and that these defects were only partially improved with time post-excision (Table ST.8).

Taken together, these data showed biventricular dilated cardiomyopathy with compromised contractility in *Akap13*$^{cKO\text{-}MCM}$ mice. *Akap13*$^{Het\text{-}MCM}$ mice had a similar but less severe phenotype compared to *Akap13*$^{cKO\text{-}MCM}$ mice.

Summary of MRI data

Collectively, these MRI data showed that the *Akap13*$^{cKO\text{-}MCM}$ mice had severely impaired cardiac function with biventricular dilated cardiomyopathy, increased cardiac remodeling over time which resulted in compensatory left ventricular hypertrophy, and impaired contractility. Males were more likely to compensate with cardiac remodeling over time, however, they decompensated with cardiac stress testing. Females showed a more severe cardiac phenotype than males from the outset and were not able to adequately compensate with time or stress. Moreover, female *Akap13*$^{Het\text{-}MCM}$ also exhibited a disease phenotype while *Akap13*^{Het}-MCM male mice showed few phenotypic changes. Taken together, female *Akap13*$^{cKO\text{-}MCM}$ mice demonstrated increased morbidity over male *Akap13*$^{cKO\text{-}MCM}$ mice under these experimental conditions thus a sex-dependent phenotype was established.

Echocardiographic analyses showed impaired cardiac contractility and restrictive filling pattern of the left ventricle in Akap13^{cKO} mice

Echocardiography (ECHO) is a cardiac specific sonogram that uses ultrasound (high frequency) waves in order to produce a two-dimensional, three-dimensional, or Doppler ultrasound heart image on a visual display and is routinely used for heart disease diagnostics (Anavekar, 2009). Echocardiograms were conducted on anesthetized *Akap13^{cKO}* mice and controls in order to assess LV diastolic functional changes. Since LV dilation with compensatory LV hypertrophic remodeling was most pronounced in the *Akap13$^{cKO\text{-}MCM}$* mice ≥8 weeks post-recombination, particularly females, this group was focused on for analyses. Heart rate, body temperature, and respiration rates were monitored for each animal during the procedure. Measurements were obtained via a transthoracic approach from the parasternal long axis view (PSLAX). Relative wall thickness (RWT) was evaluated in order to categorize the type of hypertrophy exhibited. Relative wall thickness can be calculated using the measurement from Left Ventricular Posterior Wall at diastole (LVPWd) and the Left Ventricular End Diastolic Diameter (LVEDD) as follows:

$$2 \times \frac{LVPWd}{LVEDD}$$

LVPWd was increased in *Akap13$^{cKO\text{-}MCM}$* mice (n=3) (0.847mm ± 0.024) compared to controls (n=3) (0.679mm ± 0.038; $p<0.05$), and *Akap13$^{cKO\text{-}MCM}$* mice had modestly increased RWT (*Akap13$^{cKO\text{-}MCM}$* mice: 0.47 ± 0.036; control: 0.41 ± 0.012; p=0.15 one-way). However, no overall changes in the corrected LV mass (mg) were observed

(*Akap13*$^{cKO\text{-}MCM}$: 93.34mg ± 7.22; control: 90.72mg ± 10.95) (p=0.886). According to the literature, RWT measurements >0.42 and increased LV mass are criteria for concentric hypertrophy (Lang, 2006). However, if RWT is increased, but LV mass is unchanged, then the changes are defined as ventricular remodeling (Sherif F. Nagueh, 2009). Given these data, the three female *Akap13*$^{cKO\text{-}MCM}$ mice ≥8 weeks post-recombination exhibited left ventricular remodeling.

Fractional Shortening (FS) is a measure of heart function or contractility and is calculated by measuring the difference of the End-Diastolic Diameter (EDD) and End-Systolic Diameter (ESD) of the left ventricle. FS is evaluated by the following formula:

$$\frac{EDD - ESD}{EDD} \times 100$$

FS% were decreased in the *Akap13*$^{cKO\text{-}MCM}$ mice (n=3) (28.67% ± 1.50) compared to controls (n=5) (41.9 ± 3.67) ($p<0.05$). Additionally, *Akap13*$^{cKO\text{-}MCM}$ mice had increased left ventricular volume in diastole (*Akap13*$^{cKO\text{-}MCM}$: 56.04µL ± 7.38; control: 42.34µL ± 2.79) (p=0.06 one-way) and systole (*Akap13*$^{cKO\text{-}MCM}$: 25.69µL ± 5.32; control: 11.0µL ± 1.10) ($p<0.05$) which indicated dilation of the left ventricle associated with impaired contractility (Fig. 2.20a).

Furthermore, the ratio of the early (E)/late diastolic or atrial (A) left ventricular filling velocities, or E/A ratio, are used to measure left ventricular diastolic function, and along with mitral deceleration time (DT), grade diastolic dysfunction (where, E/A

<0.8=Grade I, 0.8-1.5=Grade II, ≥2=Grade III, and DT is reduced) (Fig. S.11). The transmitral valve inflow creates two separate waves with the E-wave appearing before the A. In normal hearts, the E-wave should have a larger amplitude than the A-wave (Fig. S.12). Recordings were taken at the level of the mitral annulus. Here we found *Akap13*$^{cKO\text{-}MCM}$ mice (n=3) had increased E/A ratio (2.93mm/s ± 0.23) compared to controls (n=8) (1.73mm/s ± 0.12) ($p<0.01$) (Fig. 3o). These findings were consistent in the *AKAP13*$^{cKO\text{-}TOC}$ mice (n=4) (*AKAP13*$^{cKO\text{-}TOC}$ 3.97 ± 0.64; control: 1.72 ± 0.28; $p<0.05$ one-way) (Fig. 2.20b-c).

Mitral E-wave Deceleration Time (DT) was decreased in female *Akap13*$^{cKO\text{-}MCM}$ mice (n=3, both) (*Akap13*$^{cKO\text{-}MCM}$: 13.40ms ± 2.07; control: 22.08ms ± 1.68; $p<0.05$) and in *AKAP13*$^{cKO\text{-}TOC}$ mice (n=4) compared to controls (n=3) (*AKAP13*$^{cKO\text{-}TOC}$: 19.07ms ± 2.68; control: 29.58 ± 0.241; $p<0.05$). When the results from both models and sexes were combined (n=7) (*AKAP13*^{cKO}: 13.83 ± 1.72; control: 25.81 ± 1.49; $p<0.01$) clearly demonstrated the decreased DT compared to controls (n=10) (Fig. 2.20d,e).

Mitral valve area (MVA) can be used, in part, to assess the stiffness of the left ventricle. MVA was increased in female *Akap13*$^{cKO\text{-}MCM}$ mice compared to control mice. (MVA: Female *Akap13*$^{cKO\text{-}MCM}$: 69.04mm^2 ± 16.64; female control: 35.04mm^2 ± 2.77; $p=0.1736$; *AKAP13*$^{cKO\text{-}TOC}$: 41.65mm^2 ± 6.02; control: 25.42mm^2 ± 0.71; $p=0.0935$; *AKAP13*^{cKO}: 62.98mm^2 ± 11.06; control: 33.76mm^2 ± 3.07; $p<0.05$). These data suggested changes concomitant to the increased stiffness of the LV (Fig. 2.20f,g).

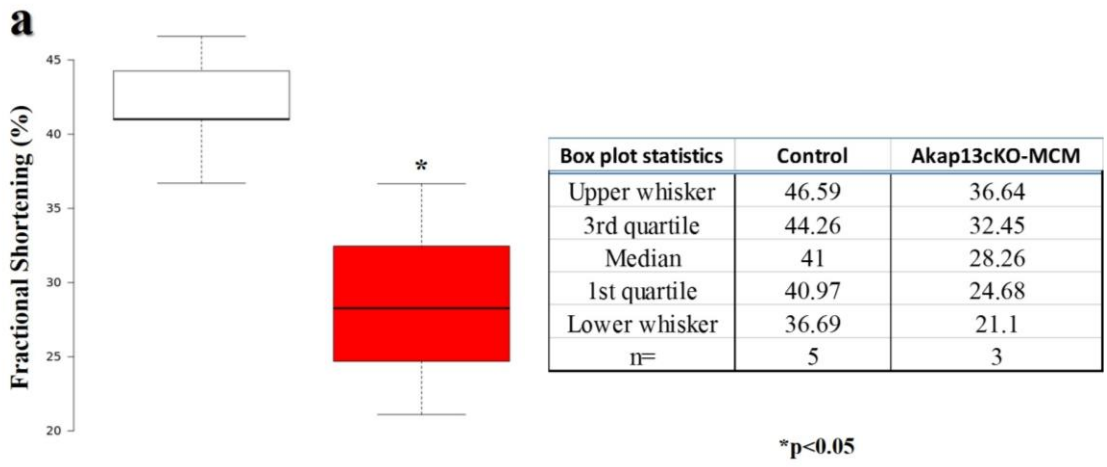

Box plot statistics	Control	Akap13cKO-MCM
Upper whisker	46.59	36.64
3rd quartile	44.26	32.45
Median	41	28.26
1st quartile	40.97	24.68
Lower whisker	36.69	21.1
n=	5	3

*p<0.05

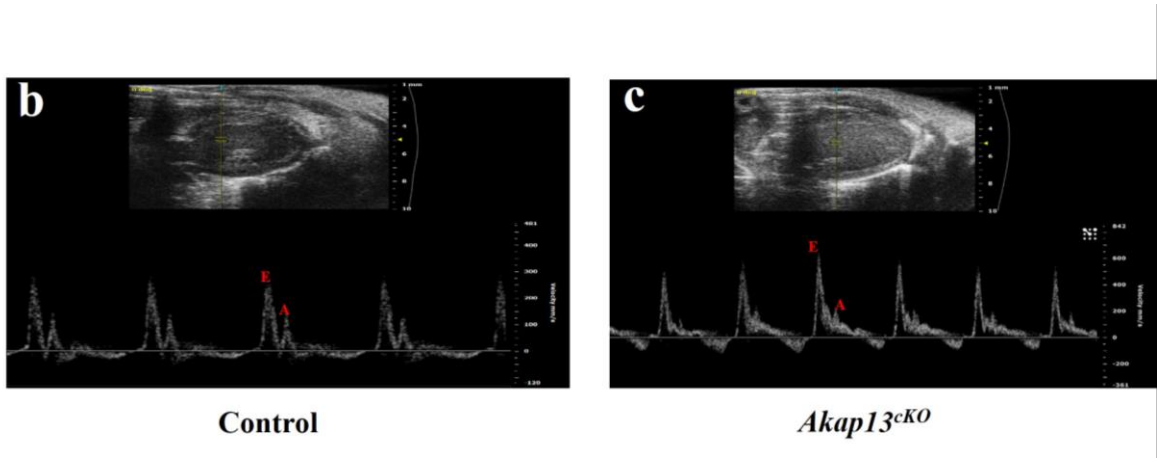

Control *Akap13^{cKO}*

Figure 2.20| **Echocardiography (Echo) showed restrictive filling pattern (Grade III) of the left ventricle in *Akap13$^{cKO\text{-}MCM}$* mice.** a) *Akap13$^{cKO\text{-}MCM}$* mice (n=3) had lower fractional shortening percentage (FS%) than control mice (n=5) ($p<0.05$). b) Echo, parasternal long axis (PSLAX) view of a control heart. Normal mitral inflow E- and A-waves shown below.

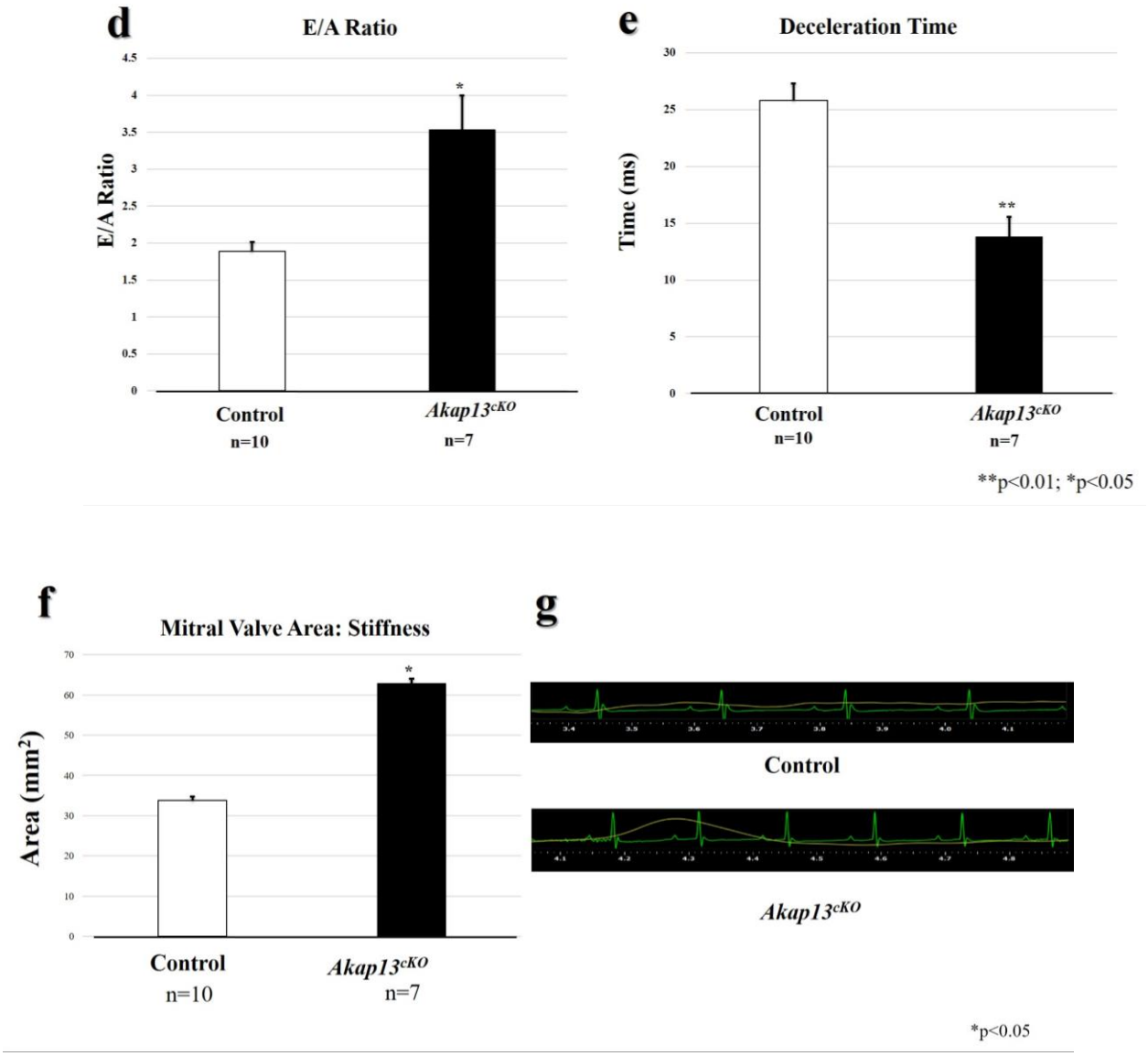

Figure 2.20 cont.| **Echocardiography (Echo) showed restrictive filling pattern (Grade III) of the left ventricle in *Akap13*$^{cKO\text{-}MCM}$ mice.** d) Echo, E/A ratio increased in *Akap13*$^{cKO\text{-}MCM}$ mice (n=7) compared to control mice (n=10) ($p<0.01$). e) Echo, *Akap13*$^{cKO\text{-}MCM}$ mice have decreased deceleration time compared to control mice ($p<0.05$). f) Echo, *Akap13*$^{cKO\text{-}MCM}$ mice (n=7) have increased mitral valve area compared to control mice (n=10) ($p<0.05$). g) Echo, electrocardiogram (ECG) strip showing (upper panel) control and (lower panel) *Akap13*$^{cKO\text{-}MCM}$ mice. *Akap13*$^{cKO\text{-}MCM}$ mice exhibited increased heart rate. Student's *t*-test used for statistical analyses.

Collectively, these echocardiographic data showed that female *Akap13*$^{cKO\text{-}MCM}$ mice ≥8 weeks post-recombination had dilated cardiomyopathy with compensatory hypertrophic remodeling of the left ventricle, impaired left ventricular systolic function, and diastolic dysfunction with restrictive pattern (Grade III) of the left ventricle. These findings were emulated in the *AKAP13*$^{cKO\text{-}TOC}$ mice (combined sexes), and were made even more apparent when the data from both models were combined. Left ventricular hypertrophy in the *Akap13*$^{cKO\text{-}MCM}$ mice ≥8 weeks post-recombination, as demonstrated by MRI and ECHO, was best appreciated by histological cross-section (Fig. S.13).

ECG analyses suggestive of cardiomyopathy with left atrial enlargement in Akap13^{cKO} mice

A 3-leads Electrocardiogram (ECG) was performed as an *in vivo* cardiac functional assessment to evaluate cardiac electrical activity in anesthetized *Akap13$^{cKO\text{-}MCM}$* mice (n=14) compared to control mice (n=18) (Fig. 2.21a,b). Alterations in cardiac electrical activity can indicate many underlying cardiac pathologies both chronic and acute in nature. ECG monitoring was performed at two different time points. Again, one group was monitored at < 8 weeks after cessation of the treatment inducing Cre-excision (either tamoxifen or doxycycline respective to the Cre), and the other group was monitored at ≥8 weeks post-recombination. Overall, when comparing *AKAP13^{cKO}* to control mice, *Akap13$^{cKO\text{-}MCM}$* mice exhibited tachycardia (*Akap13$^{cKO\text{-}MCM}$*: 518.64 bpm ± 20.47; Control: 457.56 bpm ± 16.26) ($p<0.05$), widened QRS intervals (*Akap13$^{cKO\text{-}MCM}$*: 10.80ms ± 0.62; Control: 8.74ms ± 0.34) ($p<0.01$), and prolonged QT intervals (*Akap13$^{cKO\text{-}MCM}$* QTcB: 63.43ms ± 6.02; QTcF: 37.726ms ± 2.58; Control QTcB: 48.02ms ± 3.34; QTcF: 31.774ms ± 1.1) (QTcB : $p< 0.05$; QTcF: $p< 0.05$) (Fig. 2.21c). Additionally, QRS decreased amplitude was observed in *Akap13$^{cKO\text{-}MCM}$* mice (*AKAP13^{cKO}* R amplitude: 441.06µV ± 58.36; Control: 643.45µV ± 36.24) ($p<0.01$). ST segment depression and T-wave inversion were detected in *AKAP13^{cKO}* mice compared to control mice (*Akap13$^{cKO\text{-}MCM}$* ST height: -16.44µV ± 20.52; Control: 34.18µV ± 9.56; T-amplitude: *Akap13$^{cKO\text{-}MCM}$*: -5.27µV ± 20.34; Control: 83.20µV ± 13.87) (ST height: $p<0.05$; T-amplitude: $p< 0.01$); 50% of *Akap13$^{cKO\text{-}MCM}$* mice had T-wave inversion whereas only 14% of control mice exhibited T-wave inversion (Fig. 2.21d). Furthermore, prolonged P duration in lead II

(*Akap13*$^{cKO\text{-}MCM}$: 19.494ms ± 1.12; Control: 16.25ms ± 0.88) ($p<0.05$) suggested left atrial enlargement (LAE) in *Akap13*$^{cKO\text{-}MCM}$ mice (Table 2.7). Taken together, these outcomes are consistent with cardiomyopathy with LAE in *Akap13*$^{cKO\text{-}MCM}$ mice (Table 2.7).

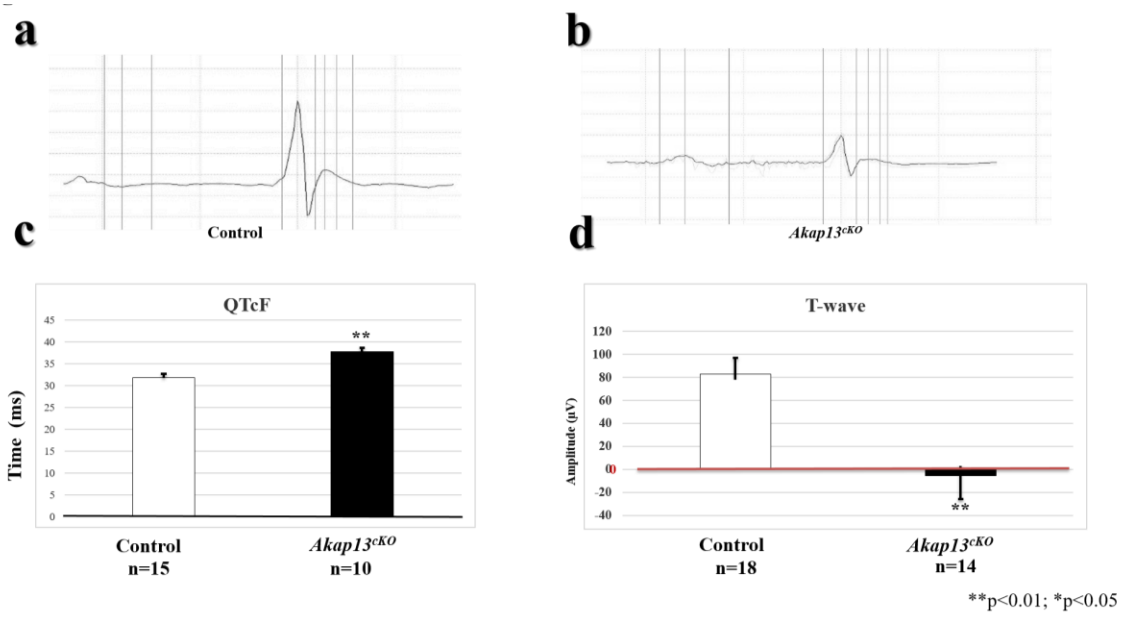

Figure 2.21| **Increased electrocardiogram (ECG) abnormalities in *Akap13*$^{cKO\text{-}MCM}$ mice.** a) ECG, Control mouse ECG waveform demonstrating a normal electrical pattern. b) ECG, *Akap13*$^{cKO\text{-}MCM}$ mice showed abnormal ECG waveforms. c) ECG, corrected QT (QTcF) was increased in *Akap13*$^{cKO\text{-}MCM}$ mice (n=10) compared to control mice (n=15) ($p<0.01$). d) T-wave abnormalities (including inversion) were seen with *Akap13*$^{cKO\text{-}MCM}$ mice compared to controls ($p<0.01$). Student's *t*-test used for statistical analyses.

	Summary of EKG p-values			
	OVERALL	<8 WEEKS	≥8 WEEKS	
Component	*Akap13* $^{cKO:MCM}$	*Akap13* $^{cKO:MCM}$	*Akap13* $^{cKO:MCM}$	Summary
Heart Rate (BPM)	0.0311	0.4057	0.0051	↑
QRS Interval (ms)	0.0057	0.0309	0.0457*	↑
QTcB(ms)	0.0298	0.5269	0.0138	↑
QTcF(ms)	0.0078	0.0493*	0.0109	↑
R Amplitude (µV)	0.0057	0.5176	0.0006	↓
ST Height (µV)	0.0271	0.0351*	0.5225	↓
T Amplitude (µV)	0.0012	0.0154	0.0292*	↓
Component	♂ *Akap13* $^{cKO:MCM}$	♂ *Akap13* $^{cKO:MCM}$	♂ *Akap13* $^{cKO:MCM}$	Outcome
Heart Rate (BPM)	0.0104	0.1870	0.0075	↑
QRS Interval (ms)	0.0075	0.0488	0.1459	↑
QTcB(ms)	0.0041	0.1227	0.0183	↑
QTcF(ms)	0.0170	0.1461	0.0283*	↑
R Amplitude (µV)	0.2400	0.7154	0.0311	↓
ST Height (µV)	0.0423	0.1586	0.1363	↓
T Amplitude (µV)	0.0057	0.0488*	0.0194	↓
Component	♀ *Akap13* $^{cKO:MCM}$	♀ *Akap13* $^{cKO:MCM}$	♀ *Akap13* $^{cKO:MCM}$	Outcome
Heart Rate (BPM)	0.8454	0.2962	0.3712	↑
QRS Interval (ms)	0.3002	0.1868	0.3449	↑
QTcB(ms)	0.7607	0.8693	0.3471	↑
QTcF(ms)	0.4518	0.5810	0.3756	↑
R Amplitude (µV)	0.5856	0.7939	0.0140	↓
ST Height (µV)	0.1915	0.2014	0.8106	↓
T Amplitude (µV)	0.0339*	0.0491*	0.4961	↓

Table 2.7| **Summary of EKG p-values.** Summary table showing increased ECG abnormalities in *Akap13*$^{cKO\text{-}MCM}$ mice compared to control mice. When the data were stratified based on age and time post-recombination, increased significant changes in ECG were seen with male *Akap13*$^{cKO\text{-}MCM}$ mice. These significant changes were suggestive of conduction defects, increased risk of adverse cardiac events, and increased risk of atrial fibrillation in the presence of left ventricular dysfunction (El-Chami MF, Brancato C, Langberg J, et al. QRS duration is associated with atrial fibrillation in patients with left ventricular dysfunction. Clin Cardiol 2010;33:132–8.).

5

When the ECG data were stratified based on sex, male *Akap13*$^{cKO\text{-}MCM}$ mice (n=7) exhibited tachycardia (523.3 bpm ± 26.09) compared to male controls (n=9) (437.58 bpm ± 12.62) ($p<0.05$). When these data were stratified based on time after cessation of treatment, male *Akap13*$^{cKO\text{-}MCM}$ mice (n=3) were more affected at ≥8 weeks (*Akap13*$^{cKO\text{-}MCM}$: 577.93 bpm ± 17.94; Control: 450.45 bpm ± 16.81) ($p<0.01$) than at <8 weeks post-recombination (n=4) (*Akap13*$^{cKO\text{-}MCM}$: 482.25 bpm ± 30.39; Control: 427.28 bpm ± 16.97) ($p=0.187$) (Control: ≥8 week: n=4; <8 weeks: n=5). However, female *Akap13*$^{cKO\text{-}MCM}$ mice (n=7) showed no differences in heart rate compared to controls (n=7) until ≥8 weeks after cessation of knock-out inducing treatment, where they trended toward tachycardia (*Akap13*$^{cKO\text{-}MCM}$: 554.8 bpm ± 36.53; Control: 441.4 bpm ± 41.62) ($p>0.05$). Additional ECG findings indicated striking differences between the sexes: males showed multiple, significant ECG abnormalities compared to females. These pathological alterations became increasingly significant with time so that mice of either sex had increased ECG abnormalities ≥8 weeks after treatment cessation.

Overall, male *Akap13*$^{cKO\text{-}MCM}$ mice exhibited significantly widened QRS interval (*Akap13*$^{cKO\text{-}MCM}$: 11.40ms ± 0.84; Control: 8.41ms ± 0.45) ($p<0.01$) with increased QRS amplitude (*Akap13*$^{cKO\text{-}MCM}$: 446.49µV ± 94.66; Control: 577.71µV ± 48.61) ($p<0.01$) and prolonged QT (*Akap13*$^{cKO\text{-}MCM}$: QTcB: 75.18ms ± 9.74; QTcF: 45.51ms ± 5.42; Control: QTcB: 43.96ms ± 2.08; QTcF: 31.58ms ± 1.38) (QTcB: $p<0.01$; QTcF: $p<0.05$). QT was prolonged even after correction for QRS prolongation. Male *Akap13*$^{cKO\text{-}MCM}$ mice also showed ST segment depression (*Akap13*$^{cKO\text{-}MCM}$: -8.13µV ± 16.40; Control: 33.42µV ±

8.53) ($p<0.05$) and 43% showed T-wave inversion with an overall flattening of the T-wave (*Akap13*$^{cKO\text{-}MCM}$: 4.31µV ± 12.57; Control: 88.94 µV ± 19.02) ($p< 0.01$) compared to 11% of control mice (Fig. 2.22).

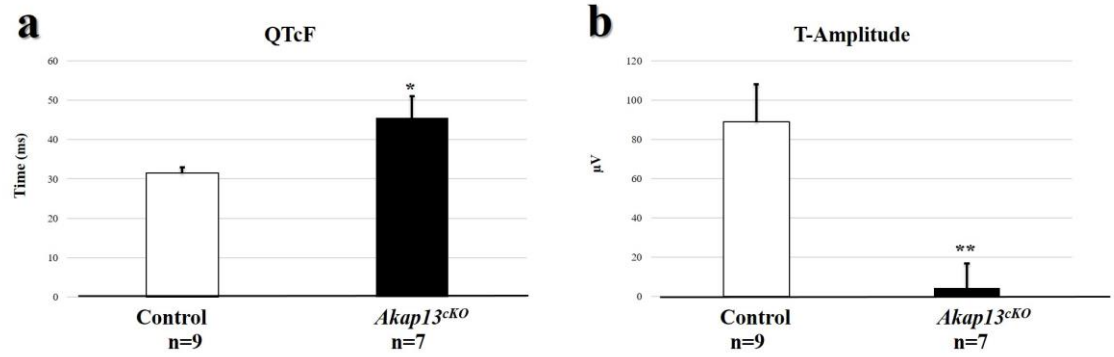

Figure 2.22| **Male *Akap13*$^{cKO\text{-}MCM}$ mice showed increased ECG abnormalities.** a) ECG, corrected QT (QTcF) was significantly increased in male *Akap13*$^{cKO\text{-}MCM}$ mice (n=7) compared to male control mice (n=9) ($p<0.05$). b) T-amplitude was decreased in male *Akap13*$^{cKO\text{-}MCM}$ mice (n=7) compared to male control mice (n=9). Student's *t*-test used for statistical analyses.

At <8 weeks, male *Akap13*$^{cKO\text{-}MCM}$ mice had widened QRS intervals (*Akap13*$^{cKO\text{-}MCM}$: 11.80ms ± 1.11; Control: 8.36ms ± 0.71) ($p<0.05$) with a trend toward a prolonged QT interval (*Akap13*$^{cKO\text{-}MCM}$: QTcB: 60.98ms ± 9.52; QTcF: 40.91ms ± 5.18; Control: QTcB: 42.90ms ± 3.60; QTcF: 30.96ms ± 2.43) (QTcB: p= 0.1227; QTcF: p= 0.1461). We observed a trend in ST depression (*Akap13*$^{cKO\text{-}MCM}$: -21.82µV ± 24.95; Control: 22.25µV ± 9.32) (p= 0.1586) accompanied by significant T-wave inversion (*Akap13*$^{cKO\text{-}MCM}$: -3.47µV ± 19.26; Control: 81.25µV ± 31.40) ($p<0.05$ one-way) in 50% of *Akap13*$^{cKO\text{-}MCM}$ mice compared to 20% of control mice. At ≥8 weeks we saw a persistent trend toward widening of the QRS interval (*Akap13*$^{cKO\text{-}MCM}$: 10.86ms ± 1.21; Control: 8.46ms ± 0.46) (p=0.1459) with decreased QRS amplitude (*Akap13*$^{cKO\text{-}MCM}$: 10.13 ± 78.73; Control: 47.38 ± 69.76) ($p<0.05$), prolonged QT interval (*Akap13*$^{cKO\text{-}MCM}$: QTcB: 89.37 ± 12.42; QTcF: 54.73 ± 9.67; Control: QTcB: 45.28 ± 0.91; QTcF: 32.36 ± 0.49) (QTcB: $p<0.05$; QTcF: $p<0.05$-one-way), and persistent ST depression (*Akap13*$^{cKO\text{-}MCM}$: 10.13µV ± 12.77; Control: 47.38µV ± 12.02) (p=0.1363) with flattening of the T-wave (*Akap13*$^{cKO\text{-}MCM}$: 14.68µV ± 11.74; Control: 98.55µV ± 15.81) ($p<0.05$) and T-wave inversion seen in 33.33% of *Akap13*$^{cKO\text{-}MCM}$ mice and 0% of control mice.

Female mice showed similar trends with ST depression (*Akap13*$^{cKO\text{-}MCM}$: -24.75µV ± 37.35; Control: 39.44µV ± 21.17) but were not significant (p=0.1915). However, female *Akap13*$^{cKO\text{-}MCM}$ mice (n=4) did show significant T-wave inversion compared to controls (n=4) before 8 weeks post-treatment (*Akap13*$^{cKO\text{-}MCM}$: -37.72µV ± 64.67; Control: 112.09µV ± 14.77) ($p<0.05$ one-way) where 50% of female *Akap13*$^{cKO\text{-}MCM}$ mice showed T-wave inversion, and 0% of control mice showed T-wave inversion. At ≥8 weeks, female

Akap13$^{cKO\text{-}MCM}$ mice (n=3) showed a generalized flattening of the T-wave (*Akap13*$^{cKO\text{-}MCM}$: 15.66µV ± 6.14; Control: 50.78µV ± 34.74) (P>0.05) compared to control mice (n=4) and decreased QRS amplitude (*Akap13*$^{cKO\text{-}MCM}$: 413.50µV ± 12.92; Control: 663.18µV ± 48.39) (p<0.05) (Fig. 2.23).

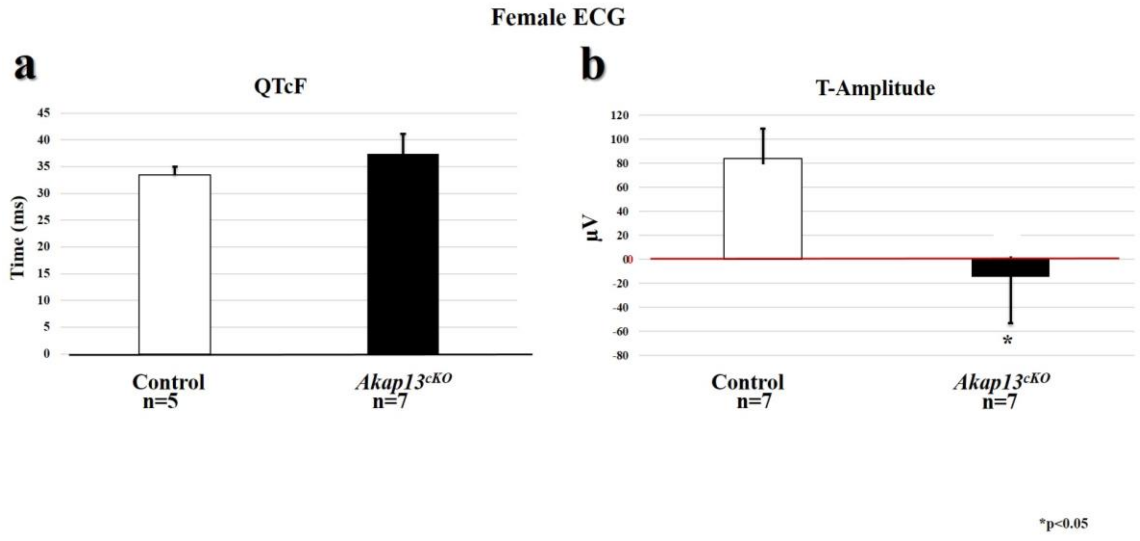

Figure 2.23| **Female *Akap13*$^{cKO\text{-}MCM}$ mice showed few ECG abnormalities.** a) ECG, corrected QT (QTcF) showed no differences between mice female *Akap13*$^{cKO\text{-}MCM}$ mice (n=5) compared to female control mice (n=7) ($p>0.05$). b) T-amplitude was decreased in female *Akap13*$^{cKO\text{-}MCM}$ mice (n=7) compared to female control mice (n=9) ($p<0.05$). Student's *t*-test used for statistical analyses.

Other ECG findings revealed that overall, *Akap13*$^{cKO\text{-}MCM}$ mice had significantly prolonged P waves on Lead II (*Akap13*$^{cKO\text{-}MCM}$: 18.87ms ± 1.27; Control: 15.58ms ± 0.64) ($p< 0.05$) which indicated left atrial enlargement. When stratified based on sex, both male and female *Akap13*$^{cKO\text{-}MCM}$ mice had significantly prolonged P waves (male *Akap13*$^{cKO\text{-}MCM}$: 241.52ms ± 0.97; male Control: 17.28ms ± 0.71; female *Akap13*$^{cKO\text{-}MCM}$: 19.30ms ± 1.44; female Control: 2.36ms ± 0.83) (male: $p<0.05$; female: $p<0.05$).

In summary, these ECG data showed that cardiac electrical activity defects were present in *Akap13*$^{cKO\text{-}MCM}$ mice. Alterations were consistent with cardiomyopathy and left atrial enlargement. Moreover, *Akap13*$^{cKO\text{-}MCM}$ males showed more abnormalities on ECG than *Akap13*$^{cKO\text{-}MCM}$ females.

Compensatory Tachycardia exhibited in *Akap13*^{cKO} mice

Next, we evaluated blood pressure, mean arterial pressure, and heart rate in awake mice via the tail vein. While hypertension can cause cardiomyopathy, we did not anticipate that *Akap13*$^{cKO\text{-}MCM}$ mice would have hypertension since a conditional, cardiomyocyte specific knockout was performed thereby reducing off-target effects, such as vascular contributions. Nonetheless, blood pressure had to be taken into consideration for a comprehensive assessment of the phenotype. As expected, *Akap13*$^{cKO\text{-}MCM}$ mice (n=6) exhibited no differences in systolic, diastolic, or Mean Arterial Pressure (MAP) compared with control (n=8) mice ($p>0.05$) (Fig. S.14). However, *Akap13*$^{cKO\text{-}MCM}$ mice (n=6) exhibited compensatory tachycardia (722.33 bpm ± 22.63) compared to control mice (n=12) (674.83 bpm ± 14.87) ($p<0.05$) (Fig. S.15). This finding was expected and was consistent with our HR ECG data.

Female *Akap13*^{cKO} mice had increased mortality

Survival analysis suggested that female *Akap13*$^{cKO\text{-}MCM}$ mice had an increased chance of mortality compared to male *Akap13*$^{cKO\text{-}MCM}$ mice since 40% of female mice died by 4 months post treatment (2/5 mice) whereas no male mice died of natural causes by this time point (0/6 mice) (p=0.051; one-way). Of these male mice, 2 were euthanized at 6 months post-treatment for other studies. However, the 4 male mice that were not euthanized for other studies were still alive at the time this dissertation was written (14 months post-treatment). The 3 surviving female mice were euthanized at 6 months and 9 months post-treatment for other studies (Fig. 2.24). These data, taken together with the cardiac functional data, suggest that *Akap13*$^{cKO\text{-}MCM}$ mice had failing hearts resultant from loss of *Akap13*, and that female *Akap13*$^{cKO\text{-}MCM}$ mice were more likely to succumb to the genetic insult than males.

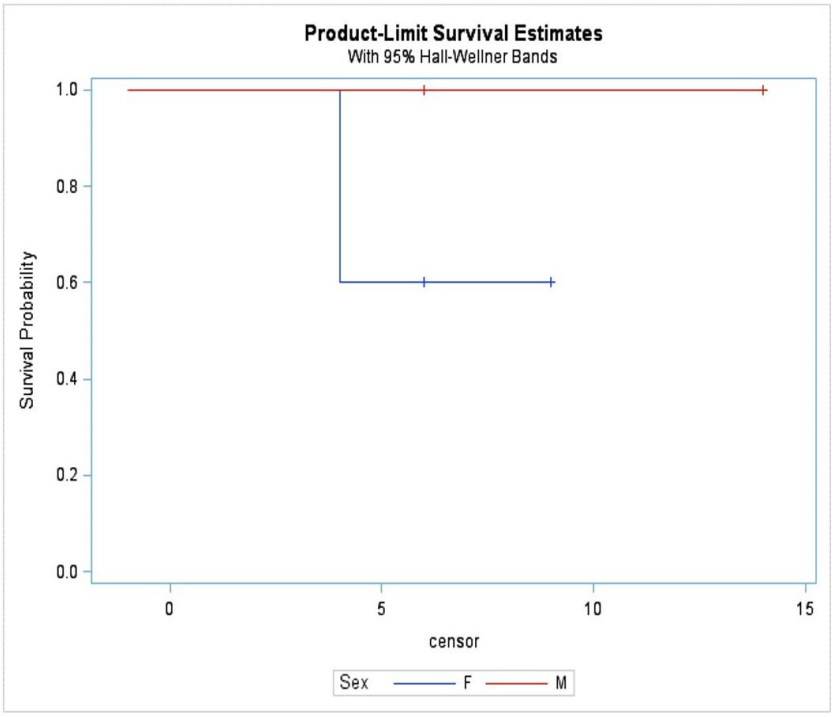

Akap13$^{cKO-MCM}$

Figure 2.24| **Survival Analysis showed increased mortality in female *Akap13$^{cKO-MCM}$* mice.** Kaplan-Meier survival curve, Female Akap13$^{cKO-MCM}$ had a 60% survival probability (p=0.05, one-way). Two out of 5 female Akap13$^{cKO-MCM}$ mice died (2/5 mice). No Male mice died during the measured time period (0/6 mice). (p=0.05, one-way) by Product-Limit Survival Estimates (SAS).

PKA activity was decreased in *Akap13*^{cKO} mice

Phosphotungstic Acid-Hematoxylin (PTAH), a stain used in histology labs for staining striated muscle fibers, such as cardiac tissue (Naaijenkins, 2015) revealed the same granular appearing cardiomyocytes appreciated with H&E. No overt increase in fibrosis was noted, but unequal staining of the cardiomyocytes in the *Akap13*$^{cKO\text{-}MCM}$ mice compared to controls was observed (Fig. S.16). Additionally, we stained *Akap13*$^{cKO\text{-}MCM}$ heart tissue sections with Masson's Trichrome, a commonly used three-color stain that results in blue collagen, pink to red muscle fibers, cytoplasm and erythrocytes, and black nuclei. These results suggested an increase in collagen and dysmorphic cardiomyocytes in *Akap13*^{cKO} mice ≥8 weeks post-recombination which also suggested disease progression over time as demonstrated by MRI (Fig. S.17). These special stains (PTAH and Trichrome) highlighted the morphological changes at the cellular, tissue, and organ levels that *Akap13*^{cKO} mouse hearts developed including ventricular chamber dilation and hypertrophic remodeling with increased collagen in *Akap13*$^{cKO\text{-}MCM}$ mice ≥8 weeks post-recombination. Dysmorphic cardiomyocytes were also observed which indicated that loss of *Akap13* resulted in structural and potentially functional cardiomyocyte and organellar changes and cytoskeletal disruption.

Over the years, robust data have shown cAMP-dependent Protein Kinase A (PKA) and RhoA to have highly conserved, defined roles in cytoskeletal arrangement and regulation of the cardiac sarcomere (Yamasaki, 2002) (Mayers, 2010). Likewise, AKAP13 interaction with both PKA and RhoA have been well described in the literature, and were

therefore key targets for AKAP13's role in cardiomyocyte signaling pathways and maintenance of the cardiac sarcomere. However, PKA and RhoA do not act in coordination with each other. In fact, data have shown PKA inhibits RhoA as well as lysophosphatidic acid (LPA) stimulation of SRF via disruption of actin filaments (Sauzeau et al., 2000) (Ellerbroek et al., 2003) (Qiao, 2003) (Oishi, 2012). In order to assess general PKA activity (not isoform specific), we performed an enzyme-linked immuno-absorbent assay (ELISA) with *Akap13*^{cKO} mouse heart extracts compared to control heart extracts. PKA was found to be significantly decreased in the cardiac isolates from *Akap13*^{cKO} mice compared to control mice (Fig. 2.25) ($p<0.05$). Moreover, initial findings suggested that RhoA activity was not decreased in *Akap13*$^{cKO\text{-}MCM}$ heart extracts (n=3) compared to control (n=3) ($p>0.05$) (Fig. 2.26). These results were consistent with prevailing data, and suggested that loss of *Akap13* dysregulated PKA activity more profoundly than RhoA activity.

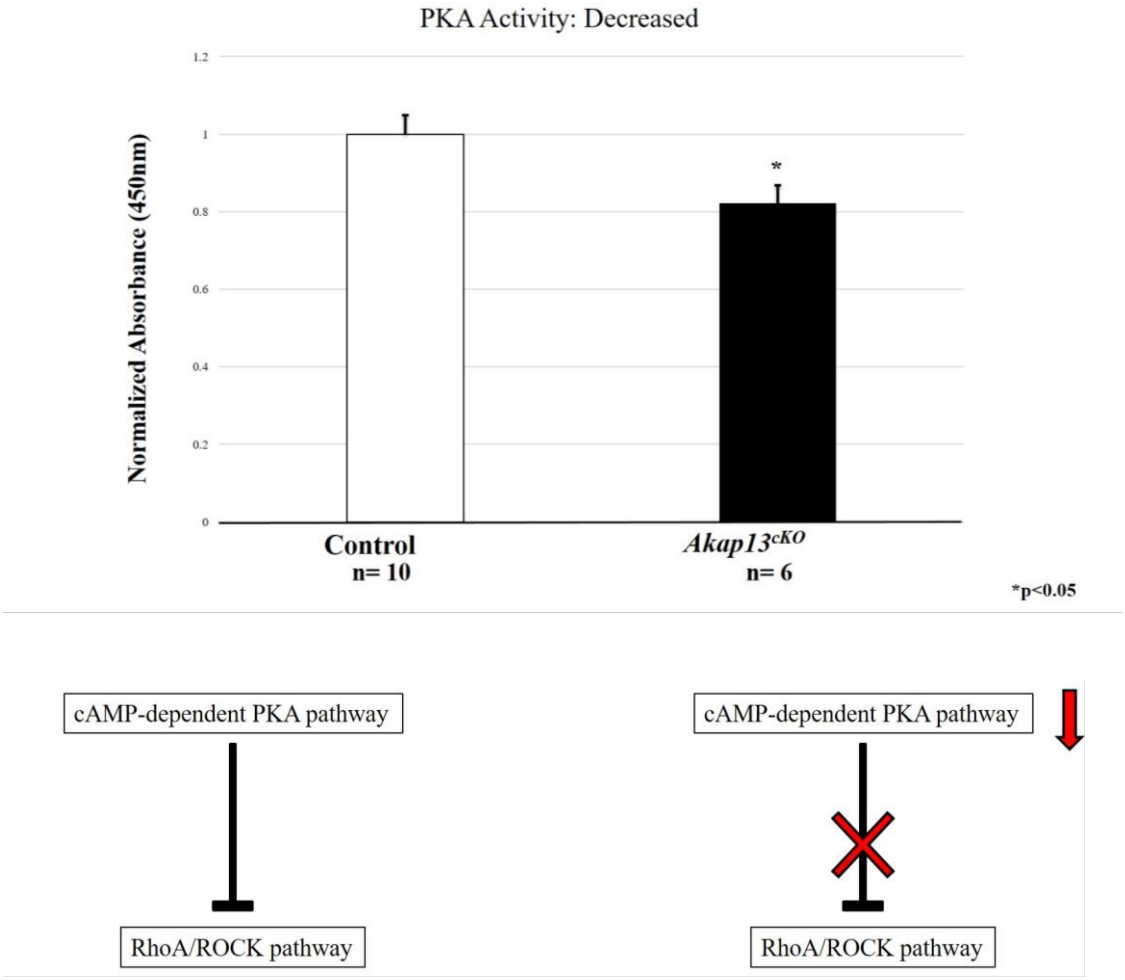

Figure 2.25| **PKA activity levels decreased in *Akap13^{cKO}* mice.** Upper panel, PKA activity measured by enzyme-linked immunosorbent assay (ELISA) showed decreased PKA activity in Akap13^{cKO} mice compared to control mice ($p<0.05$). Student's *t*-test used for statistical analyses. Lower panel, Diagram demonstrating the cAMP-dependent PKA pathway inhibition of the RhoA/ROCK pathway (left) and the de-repression of the RhoA/ROCK pathway with decreased activity of the cAMP-dependent PKA pathway (right).

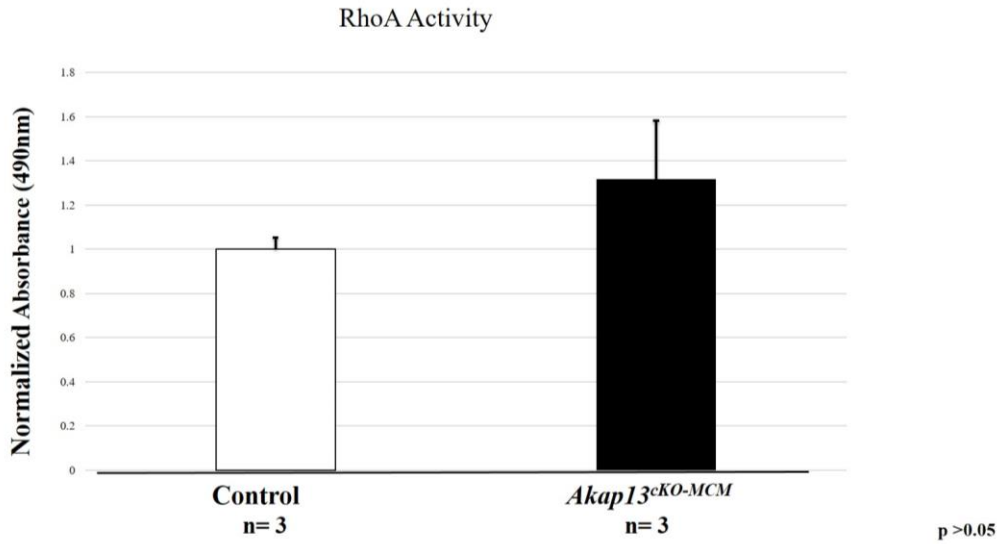

Figure 2.26| **RhoA activity was not altered in *Akap13*^{cKO} mice.** RhoA activity measured by enzyme-linked immunosorbent assay (ELISA) showed no significant changes in RhoA activity in Akap13$^{cKO\text{-}MCM}$ mice (n=3) compared to control mice (n=3) ($p>0.05$).

Proteomic and transcriptomic analyses indicated damage to key pathways required for normal actin assembly and mitochondrial function

To better understand AKAP13's mechanism of action, the Segars lab previously demonstrated AKAP13 binding and interaction with the following transcription factors: c-Fos, c-Jun, SRF, CREB, PPARγ and ERα. Since it has been shown that AKAP13 is essential for embryonic development (Mayers, 2010), we hypothesized that AKAP13's ability to bind to the aforementioned transcription factors was a critical regulatory step for appropriate gene regulation. In the targeted cardiac knockout of *Akap13*, these transcription factors, while likely present in normal quantities, may have been unable to effectively regulate genes in the absence of AKAP13. Given this hypothesis, we evaluated the cardiac proteome and transcriptome of $Akap13^{cKO\text{-}MCM}$ mice (n=6) from heart protein (n=3) and RNA isolates (n=3) compared to heart isolates from age and sex-matched control mice (n=3, both).

Proteomic and RNAseq data mining and pathway analyses were performed using Ingenuity Pathway Analysis (IPA), Metacore, and Pathway Studio to ensure the majority of publicly available bioinformatics software knowledge bases had been adequately queried. Proteomics analyses identified significant disruption of cellular pathways including mitochondrial oxidative phosphorylation as well as cytoskeletal dynamics (Fig. 2.27).

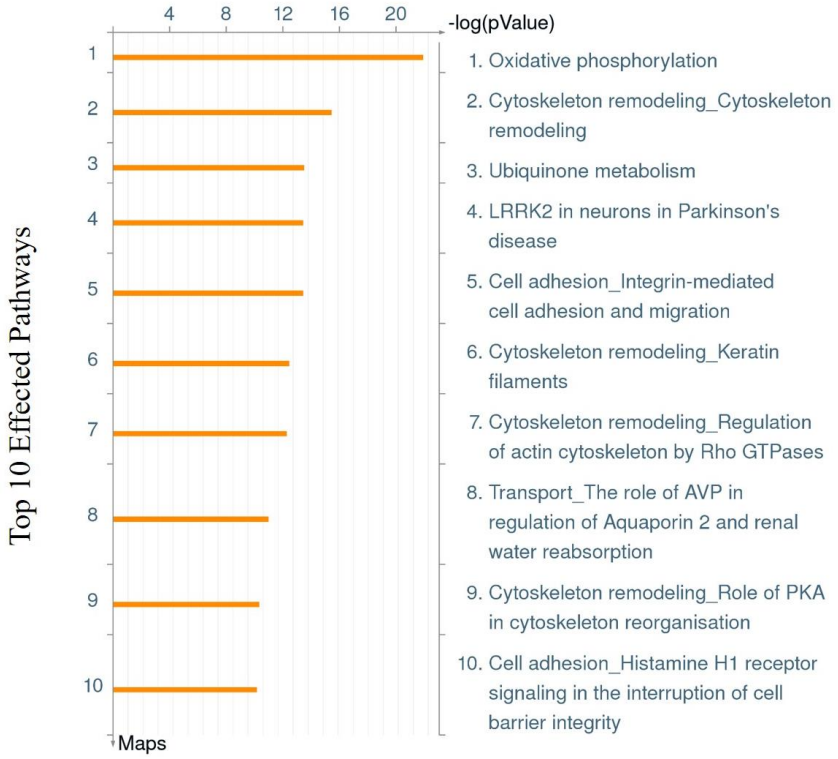

Figure 2.27| **Proteomics analysis demonstrate mitochondrial, cytoskeletal, and transcriptional pathway disruption in *Akap13*^{cKO}mice.** Proteomics analysis, cardiac tissue from 5-month-old control (n=3) and *Akap13*^{cKO} (n=3) mice was collected post-treatment (tamoxifen/doxycycline where appropriate). The pathway analysis demonstrated pathological changes in major mitochondrial processes (oxidative phosphorylation), and changes to the cytoskeleton.

PKA, specifically the RIIA isoform (*Prkar2a),* was found to have decreased peptide counts in our proteomics dataset in *Akap13*$^{cKO\text{-}MCM}$ heart protein isolates compared to control protein isolates (Supplemental). However, the RIA isoform (*Prkar1a)* was found to be increased in the same proteomic dataset, and is likely a compensatory reaction since AKAP13 preferentially binds to RIIA, but may bind to RIA when it has increased concentrations (Gold, 2006). RhoA levels were not found to be statistically altered in the *Akap13*$^{cKO\text{-}MCM}$ heart protein isolates compared to control protein isolates. These data supported the results from our PKA and RhoA functional analyses.

Moreover, several proteins partly responsible for mitochondrial fusion, cristae formation, cristae junctions, and mitochondrial transport including MFN1, subunits from the MICOS complex, TOM40, TIM10, and VDAC1 along with cytoskeletal proteins such as Class IIb Beta-Tubulin, and scaffold proteins such as alpha-1-syntrophin (*Snta1)* were reduced in *Akap13*$^{cKO\text{-}MCM}$ mice compared to control mice. Interestingly, *Snta1* has been linked to long-QT syndrome like the ECG phenotype exhibited by the *Akap13*^{cKO} mice. Likewise, many of the dysregulated genes had common transcriptional regulators including c-Fos, SRF, CREB, PPARγ and ERα (Table ST.9).

PGC-1 and ERR-induced regulator in muscle protein 1 (Perm1) protein levels were significantly decreased in *Akap13*$^{cKO\text{-}MCM}$ mouse heart extracts compared to control heart extracts per proteomic analysis. This was particularly interesting since PGC-1 has been implicated in cardiac mitochondrial dynamics. Cardiac specific PGC-1 knockout induces a strikingly similar mitochondrial phenotype as cardiac specific *Akap13* knockouts. Moreover, PGC-1 was shown to activate MFN1 transcription, a protein also decreased in

Akap13^{cKO} mice, via the transcription factor Estrogen-Related Receptor α (Martin, 2014). Other AKAPs, including the mitochondrial AKAP1, also had decreased peptide counts in *Akap13*$^{cKO\text{-}MCM}$ mice compared to control mice.

Similarly, RNA sequencing (RNAseq) showed that AKAP5 was downregulated in *Akap13*$^{cKO\text{-}MCM}$ mice compared to control mice. RNAseq analysis also showed dysregulation of mitochondrial genes including MT-*ND3*, *Slc7a1*, and *Lars2* as well as cytoskeletal genes such as *Tuba4a* and *Mylk4*, and perturbations of several transcription factors including E2F1 and Foxc1. Notably, the mitochondrial matrix protein Adenylate Kinase 4 (AK4) was downregulated in both RNAseq and proteomics datasets. (Table ST.10). Furthermore, key sarcomeric genes known for their involvement in the development of dilated cardiomyopathy were also shown to be dysregulated (Fig. 2.30).

Decreased mitochondrial membrane potential in cardiomyocytes isolated from *Akap13*$^{cKO\text{-}TOC}$ mouse hearts

Given the striking mitochondrial phenotype observed in many of *Akap13*$^{cKO\text{-}TOC}$ cardiac mitochondria, including partial or complete loss of cristae (Fig. 2.28), we sought to quantify the function of the mitochondria *in vitro*. To this end, we isolated cardiomyocytes from *Akap13*^{cKO} mouse hearts and stained them with live cell markers, Mitotracker green and MitotrackerCMX ROS, to quantify the mitochondrial membrane potential. The adult cardiomyocytes were observed using confocal microscopy, and even without quantification, the *Akap13*^{cKO} mice appeared to have increased mitochondria, but with decreased fluorescence intensity. After quantification, the fluorescence intensity ratio was found to be significantly decreased ($p<0.01$) in live mitochondria in *Akap13*^{cKO} cardiomyocytes (n=60) compared to control cardiomyocytes (n=60) (Fig. 2.29). These results indicated that mitochondria in *Akap13*^{cKO} cardiomyocytes had reduced membrane potential compared to mitochondria in control cardiomyocytes. Furthermore, live cell imaging showed an overall increase in the number of mitochondria in the *Akap13*^{cKO} cardiomyocytes in spite of the reduction in membrane potential (Baig-Ward, 2016, in preparation). Taken together, these data suggested that the mitochondria in *Akap13*^{cKO} isolated cardiomyocytes had decreased membrane potential compared to cardiomyocytes isolated from control mice. The increase in the mitochondrial population suggested a compensatory reaction, or a possible disruption in mitochondrial fusion/fission dynamics.

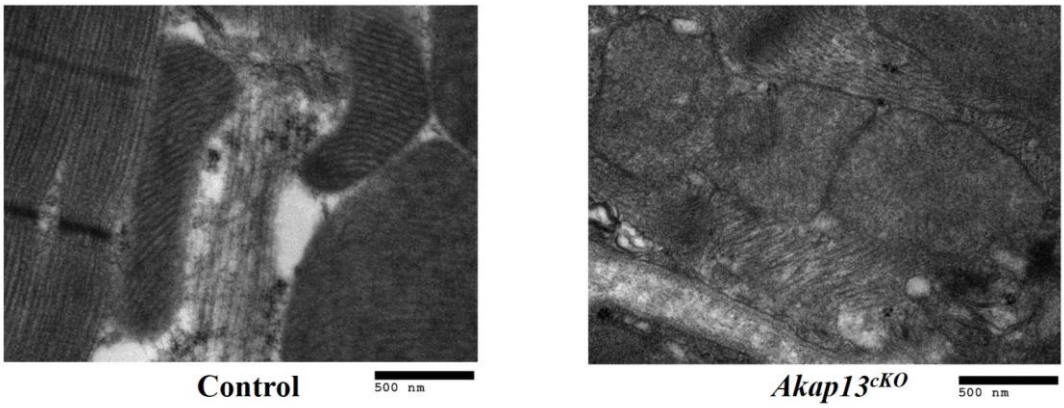

Figure 2.28| **Electron microscopy revealed significant loss of mitochondrial cristae in *Akap13*^{cKO} mice**. Electron micrograph, Control mouse cardiac tissue (left) demonstrated normal mitochondria with cristae, as expected. Akap13^{cKO} mouse heart tissue (right) showed loss of mitochondrial cristae in many of the mitochondria.

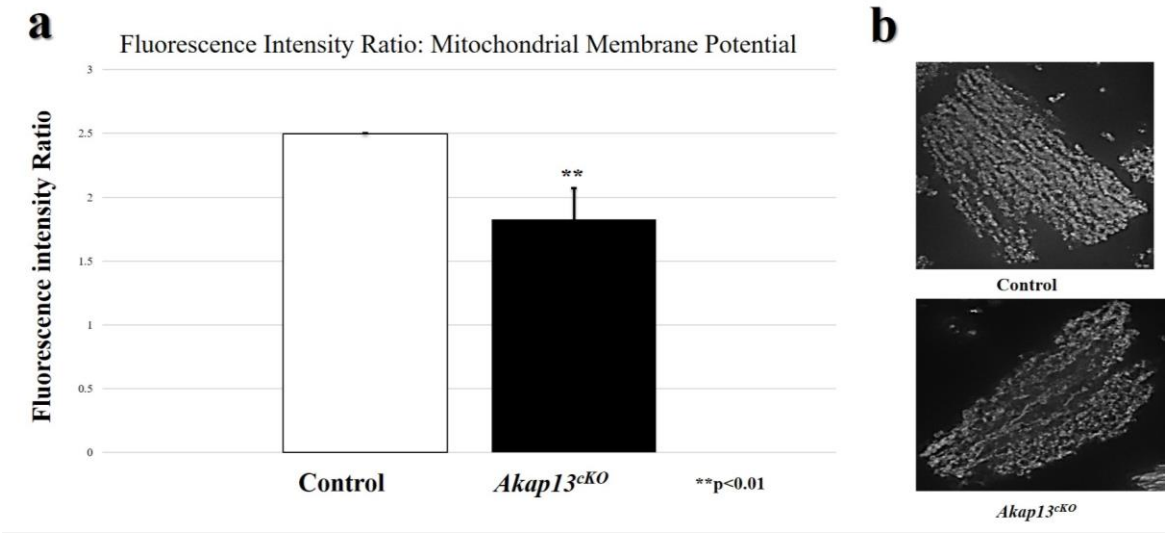

Figure 2.29| **Decreased mitochondrial membrane potential in adult cardiomyocytes isolated from *Akap13*^{cKO} mouse hearts.** a) Confocal microscopy, Fluorescence intensity ratio (as determined by MitotrackerCMX ROS and Mitotracker green ratios) was assayed as a measure of mitochondrial membrane potential. *Akap13*^{cKO} cardiomyocytes (n=60) had decreased mitochondrial membrane potential when compared to control (n=60) ($p<0.01$). B) Control (upper panel) and *Akap13*^{cKO} (lower panel) isolated cardiomyocytes are pictured.

Hallmarks of heart failure were detected in *Akap13*$^{cKO\text{-}MCM}$ mice

Myocyte Enhancer Factor 2c (*Mef2c)* is a developmental gene that encodes the 50kDa protein (MEF2C) essential for cardiogenesis. Initial Mef2c transcript analysis via RT-qPCR suggested *Mef2c* upregulation in *Akap13*$^{cKO\text{-}MCM}$ mouse heart isolates compared to controls (Fig. S.18). Similarly, RNAseq showed upregulation of myosin and other cytoskeletal and cardiac developmental genes (such as BMP10) in *Akap13*$^{cKO\text{-}MCM}$ mice compared to control mice which suggested a fetal gene response as reported in the heart failure literature (Dirkx, 2013) (Table ST.11). Furthermore, RNAseq demonstrated upregulation of Cyp2e1, a cytochrome implicated in heart disease and shown to be increased in dilated cardiomyopathy, and dysregulation of sarcomeric genes also known to be involved in dilated cardiomyopathy (Lu, 2012) (Fig.2.30). Other hallmarks of heart failure included increased levels of estrogen receptor alpha (ERα) and increased complement components.

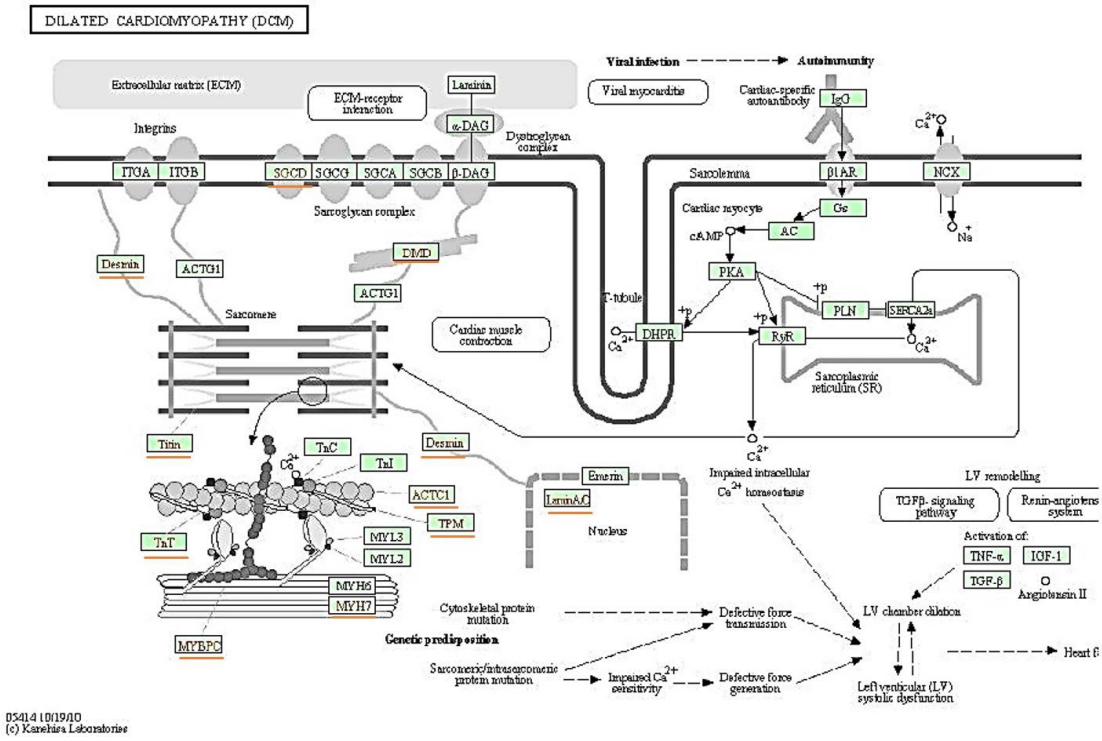

Figure 2.30| **Multiple sarcomeric components were altered in *Akap13*$^{cKO\text{-}MCM}$ mouse hearts.** RNAseq, next generation sequencing of RNA isolated from 5-month-old control (n=3) and Akap13$^{cKO\text{-}MCM}$ (n=3) pathway enrichment analysis identified several fundamental pathways affected in Akap13$^{cKO\text{-}MCM}$ mice including cytoskeleton/sarcomeric remodeling, fetal genes, cell adhesion, and calcium handling which demonstrated a dilated cardiomyopathy/heart failure phenotype.

PKA pathway, *Opa1*, and critical transcription factors altered in *Akap13*^{cKO} mice

Yeast two-hybrid analyses previously performed in our lab (unpublished data) suggested high stringency AKAP13 interactions with multiple mitochondrial and cytoskeletal proteins including AFG3L2 (paraplegin-like protein), COX8A (cytochrome c oxidase subunit VIII) and CTNNAL1 (catenin alpha like-1) which indicated that a physical interaction may be possible with these proteins (Figure 2.31a). Similarly, our lab previously demonstrated *Akap13* localization to actin filaments (Fig. S.19) in H9c2 rat cardiac cells. Mitochondria and actin are known to interact for normal mitochondrial morphology, movement, and function (Istvan R. Boldough, 2006). In fact, F-actin filaments transiently assemble on the outer mitochondrial membrane during the process of fission (Sunan Li, 2015). Furthermore, AFG3L2, a suggested AKAP13 binding partner, is an m-AAA protease involved in Opa1 cleavage. In the absence of AFG3L2, Opa1 isoforms are not properly processed, and results in fragmented mitochondria and reduced mitochondrial calcium uptake (Kondadi, 2014) (Maltecca, 2012).

To test whether AKAP13 is physically associated with the mitochondria, we performed western blot analysis using mitochondria isolated from control mouse hearts. The western blot showed two discrete, albeit faint, 310kDa AKAP13 bands suggesting that AKAP13 may be closely adherent to, or contained within, the mitochondria (Figure 2.31b). Given the size of the largest AKAP13 isoform (~310 kDa), it is doubtful that AKAP13 migrates into the mitochondria. However, due to mitochondrial interaction with F-actin, and AKAP13's ability to bind F-actin and other actin binding proteins, it is possible that AKAP13 is able to dock on the outer mitochondrial membrane and bring other effectors,

such as RhoA, CREB, PPARγ, PKA, PKN, PKD or the like closer to their targets (Lenoir, 2014) (Taglieri, 2014).

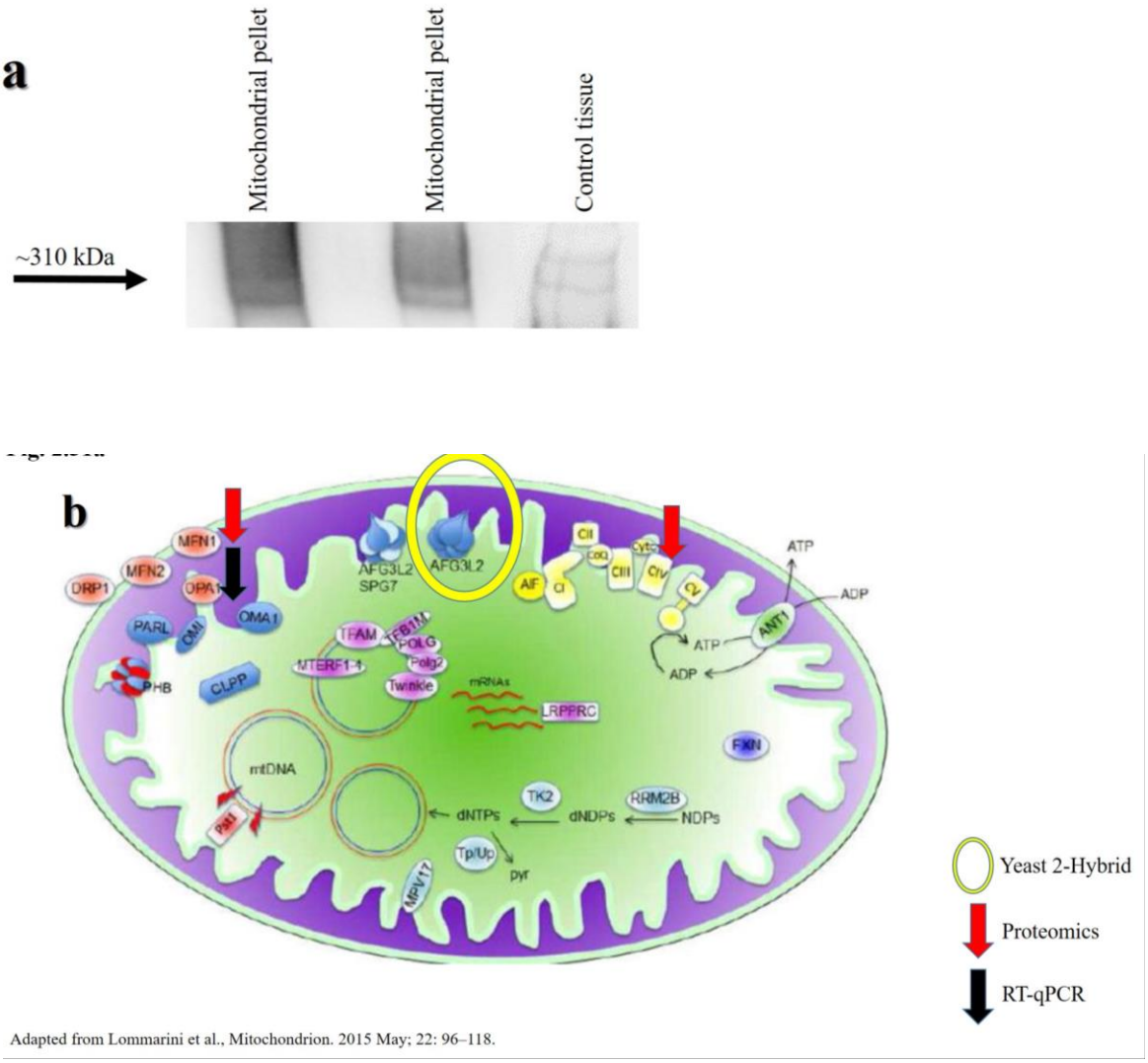

Figure 2.31| **AKAP13 protein detected in mitochondrial fraction isolated from mouse heart tissue.** a) Western blot, AKAP13 (~310kDa) was detected using an anti-AKAP13 polyclonal antibody in isolated mitochondria from control mouse hearts (n=3). Band tracing (ImageJ, lower panel) analysis detected the AKAP13 band. b) Schematic diagram of a mitochondria showing mitochondrial proteins affected in proteomics and RNAseq analyses. AKAP13 yeast two-hybrid putative binding partner indicated (yellow circle).

As mentioned above, Opa1, a dynamin-like 120kDa GTPase, migrates to the inner mitochondrial membrane, requires MFN1 for mitochondrial fusion (Cipolat, 2004), and is involved in cristae formation and apoptosis. Since cristae were absent in many mitochondria from cardiac tissue collected from *Akap13*$^{cKO\text{-}MCM}$ mice, MFN1 protein levels were decreased in our proteomics analysis, and high stringency yeast two-hybrid analyses indicated AFG3L2 as a putative AKAP13 binding partner, we performed RT-qPCR to assess the transcript levels of Opa1 in *Akap13*$^{cKO\text{-}MCM}$ mouse hearts compared to control hearts. *Opa1* transcripts were significantly reduced in *AKAP13*^{cKO} mice compared to controls which suggested Opa1 was down-regulated in *Akap13*$^{cKO\text{-}MCM}$ mice ($p<0.01$) (Fig. 2.32). Additionally, Opa1 transcript levels were quantified from *Akap13* siRNA knocked down H9c2 cells (Figs. S.20, S.21) between 12 and 24-hours post-lysophosphatidic acid (LPA) treatment by RT-qPCR. Notably, AKAP13 is known to act downstream of LPA (Mayers, 2010). Initial findings suggested that LPA upregulated *Akap13* (Fig. 2.33), as expected, but also upregulated Opa1 (Fig. 2.34). Both *Akap13 and Opa1* transcript levels increased with time. Similarly, previous studies have shown that LPA stimulates serum response factor (*Srf*), a transcription factor with a known role in immediate-early gene transcription, cardiac development, and the target of several key pathways involved in cell growth and differentiation, such as the MAPK pathway. For review, see Zarubin and Han (Han, 2005). We performed RT-qPCR to assess *Srf* transcript levels from *Akap13*$^{cKO\text{-}MCM}$ and control mouse heart isolates. *Srf* was downregulated in *Akap13*$^{cKO\text{-}MCM}$ mouse hearts compared to control mouse hearts (data not shown). These experiments were repeated in AKAP13 siRNA knocked down H9c2 cardiac cells, which also showed reduced Srf

message ($p<0.05$) (Fig. 2.35). These data were of particular interest since knockout of Srf results in embryonic lethality with disrupted cardiac sarcomeres (Miano, 2004) much like global *Akap13* knockout (Mayers, 2010).

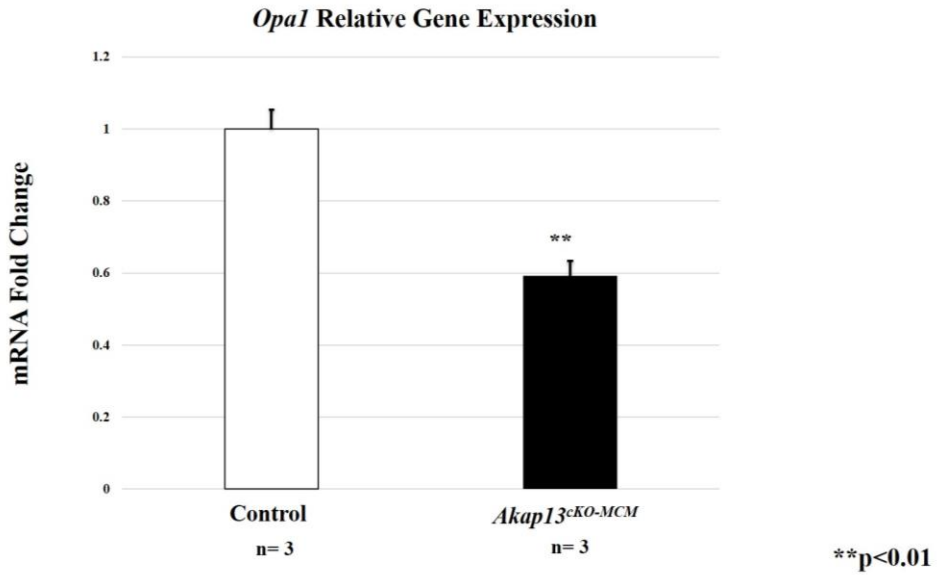

Figure 2.32| **Mitochondrial fusion protein, Opa1, gene expression levels reduced in *Akap13*^{cKO} mouse hearts.** RT-qPCR, Optic atrophy 1 (*Opa1*) is a gene whose protein product migrates to the inner mitochondrial membrane, and is partly responsible for mitochondrial morphology and function, including cristae formation and mitochondrial fusion. *Opa1* relative gene expression was decreased in *Akap13*$^{cKO-MCM}$ mouse hearts (n=3) compared to control mouse hearts (n=3) ($p<0.01$). Student's *t*-test used for statistical analyses.

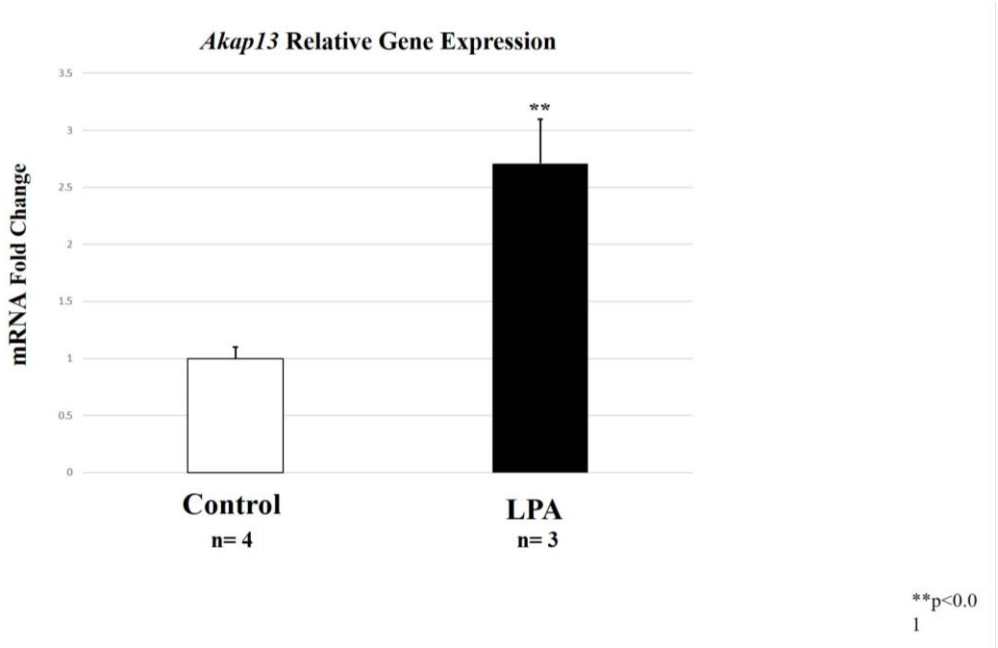

Figure 2.33| **LPA treatment increases *Akap13* mRNA expression in H9c2 rat cardiomyoblasts.** Results shown demonstrated previous findings from our group (Mayers, 2010). LPA treatment increases *Akap13* transcript levels in *Akap13* siRNA knocked down H9c2 cells ($p<0.01$). Student's *t*-test used for statistical analyses.

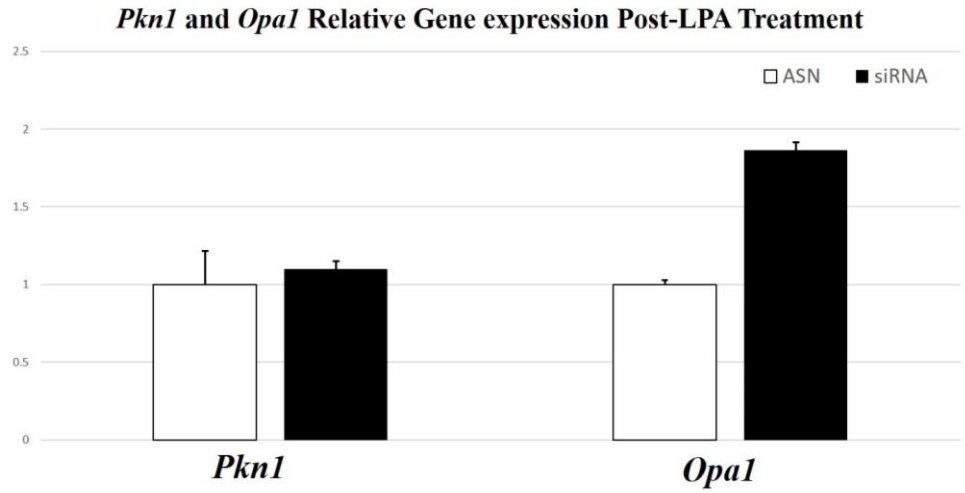

Figure 2.34| **LPA treatment increased *Opa1* relative gene expression in *Akap13* siRNA knocked down H9c2 rat cardiomyoblasts.** RT-qPCR, *Pkn1* and *Opa1* transcript levels were quantified in *Akap13* siRNA knocked down H9c2 rat cardiomyoblasts post lysophosphatidic acid (LPA) treatment. *Pkn1* transcript levels were unchanged after LPA treatment of *Akap13* siRNA knocked down H9c2 cells. *Opa1* transcript levels were increased in *Akap13* siRNA knocked down H9c2 cells.

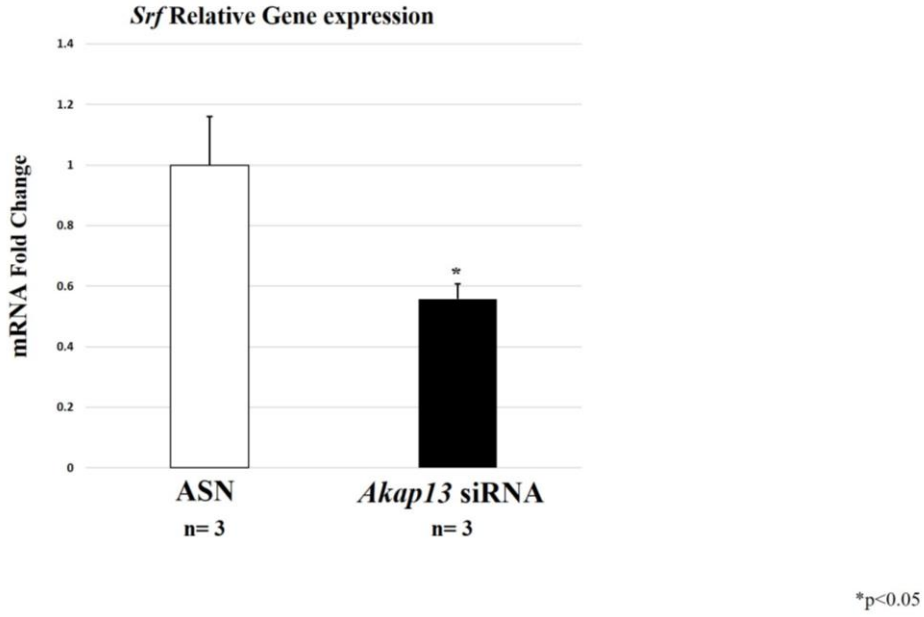

Figure 2.35| ***Srf* relative gene expression reduced in *Akap13* siRNA knocked down H9c2 rat cardiomyoblasts.** RT-qPCR, Serum response factor (*Srf*), a transcriptional activator (binds to serum response element (SRE)). *Srf* transcript levels were quantified in *Akap13* siRNA knocked down H9c2 rat cardiomyoblasts. *Srf* was significantly decreased in *Akap13* siRNA knocked down H9c2 rat cardiomyoblasts (n=3) ($p<0.05$) compared to control cells (n=3).

Further global assessment of the proteins and genes down regulated in both the proteomics and RNAseq datasets revealed common transcription factors for many of the genes including Elk-1 (14 genes) and Estrogen-Related Receptor α (13 genes) (Baig-Ward, 2016, in preparation). These transcription factors were implicated only in proteins downregulated in our proteomics dataset. They were not indicated in any of the upregulated genes or proteins from either the RNAseq or Proteomics datasets. However, SRF was mostly found in genes that had been upregulated indicating that this transcription factor may have been switched "on" by either loss of upstream repression (via PKA), dysregulation of co-factors such as ternary complex factors (Elk-1), or pathway redundancy.

Collectively, these data suggested dysfunction in mitochondrial genes, related proteins, and in critical cytoskeletal and cardiac genes resultant from the loss of *Akap13* in cardiac tissue. Furthermore, preliminary studies have suggested that LPA treatment was able to rescue both *Akap13* and *Opa1* in *Akap13* siRNA knocked-down H9c2 cardiac cells, and acts upstream of SRF. Moreover, *Srf* transcript levels were also found to be reduced in both $Akap13^{cKO\text{-}MCM}$ mouse heart extracts as well as *Akap13* siRNA knocked-down H9c2 cells.

AKAP13 modulated SRE- and Cre-luciferase activation

Given the possible AKAP13/mitochondrial interaction, roles of both RhoA and PKA in mitochondrial dynamics including motility (Istvan A. Boldough, 2006) and cardiac signaling, and to further examine our hypothesis that transcription factor interaction with AKAP13 is key for appropriate gene regulation, we performed SRE-luciferase (SRE-luc) and CRE-luciferase (Cre-luc) assays. H9c2 cells were serum deprived in 0.5% fetal bovine serum (FBS) for 20 hours. Cells were then transfected with either 0ng, 125ng, 250ng, or 375ng full length *Akap13* expression vector as well as SRE-luc (Promega) according to manufacturer directions (Promega, FuGENE6). Transfected cells either received no treatment or were treated with 10uM LPA. Fold change in SRE-luc activation was then measured in the cell lysates. In support of previous findings, these control experiments showed that SRE-luc activation was proportional to the concentration of AKAP13, with the largest fold change in SRE-luc activation seen after 375ng of AKAP13 combined with LPA treatment (Fig. S.22). Next, we wanted to ascertain which region of AKAP13 demonstrated the most robust SRE-luc activation. To this end, we transfected H9c2 cells with two separate regulatory regions of AKAP13 to deduce which domain was responsible for SRE-luciferase activation. We transfected the cells with either empty vector (RSV-0), the GEF domain of AKAP13 (Lbc), or the nuclear hormone interacting domain (NRID) (refer to Fig. S.3a for map). Cells were then treated with either Epinephrine or LPA. SRE-luc activation showed an almost 3.5-fold activation with the GEF domain plus LPA treatment ($p<0.05$). Less activation of SRE-luc was noted with the NRID. Conversely, epinephrine showed little change over control except for the NRID where it showed SRE-

luc repression (Fig. S.23). These experiments suggested that the GEF domain has the most robust SRE-luc activation of the domains queried, and was acting downstream of LPA. Furthermore, the results with epinephrine were particularly interesting since the G-protein coupled (GPCR) alpha -1A adrenergic receptors were downregulated in our RNAseq dataset. Since adrenergic receptors are known to signal through PKA/CREB, we performed a CRE-luc assay. H9c2 cells were serum deprived in 0.5% fetal bovine serum (FBS) for 20 hours. Cells were then transfected with either 0ng, 125ng, or 250ng, of full length *Akap13* expression vector. An 8-fold CRE-activation dose-response was seen when transfected with 250ng of AKAP13.

In summary, these data confirmed previous reports that AKAP13 acted downstream of LPA in H9c2 cells and showed robust activation of CRE-luc. Furthermore, these findings support the conclusion that AKAP13 played a key role in multiple pathways including interaction with AFG3L2 in regulation of mitochondrial fusion, and through a more regulatory level via interactions with SRF, CREB, and other transcription factors (Fig. 2.36).

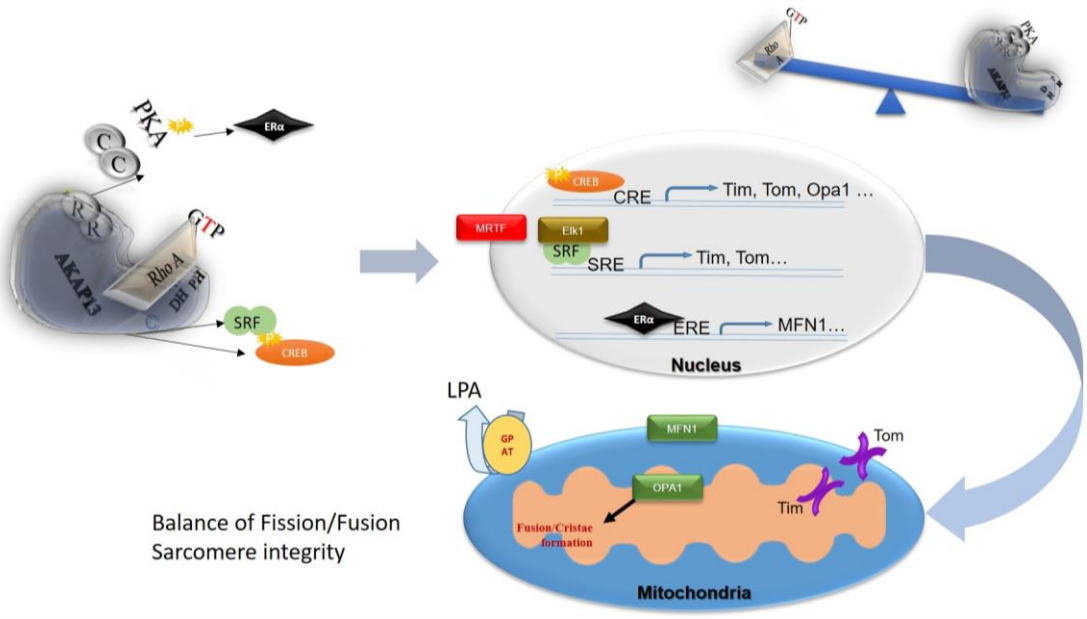

Figure 2.36| **Working molecular mechanism.** AKAP13 is known to modulate transcription factors and nuclear hormone receptors to affect gene expression. Additionally, AKAP13 rectifies cAMP-dependent PKA and RhoA signaling pathways dependent upon the metabolic needs of the cell. In the absence of AKAP13, gene expression is altered giving way to pathway dysregulation and ultimately a pathological gene program. Imbalance in the cAMP-dependent PKA and RhoA pathways would result.

CHAPTER 3: Discussion and Conclusion

We established an inducible, cardiac-specific *Akap13*^{cKO}mouse model using two different Cre-recombination strategies (α-MHC-MerCreMer and *Tnnt2*-rtTA; TetO-Cre). *Akap13*^{cKO}mice developed a biventricular dilated cardiomyopathy with compensatory hypertrophic remodeling of the left ventricle, decreased left and right ventricular systolic function, and abnormal left ventricular diastolic function as well as dilated left atria. Specifically, *Akap13*^{cKO}mice developed significantly reduced LVEF (both at rest and with dobutamine-induced stress), increased mass and volume indices, dilated ventricular chambers, reduced fractional shortening, alterations in E/A ratio and deceleration time indicating diastolic dysfunction with restrictive filling of the left ventricle, abnormal ECG including prolonged P duration, QRS, and QT intervals, and alterations in ST segments. Moreover, *Akap13*^{cKO} mice exhibited compensatory tachycardia. The severity of the cardiac phenotype, both early (<8 weeks post-induction of Cre-recombination) and as the disease progressed (≥8 weeks post-recombination), developed in a sex-dependent manner. Female *Akap13*^{cKO} mice displayed a more severe cardiac phenotype and were more likely to die post-recombination. Of note, ECG abnormalities were less prominent in female *Akap13*^{cKO} mice.

Ultrastructurally, *Akap13*^{cKO} heart tissue showed significantly disrupted sarcomeres and mitochondria. For much of the explanted cardiac tissue, sarcomeres were unrecognizable with partial z-discs punctuated throughout. Mitochondria were increased in number, and were of differing sizes, some smaller than normal, others considered mega-

mitochondria, and swollen. The majority of the mitochondria observed were completely or partially lacking cristae, and some were missing their outer membrane. Lamellar inclusions and increased lipids were also seen. Moreover, *Akap13*^{cKO} H&E stained cardiac tissue sections also demonstrated altered sarcomeres, as did immunohistochemical analyses. Dilated left ventricles were best appreciated in histological cross-section.

Confocal microscopy of live adult cardiomyocytes showed significantly decreased mitochondrial membrane potential and significantly increased numbers of mitochondria in *Akap13*^{cKO} adult heart cells compared to controls. Confocal analyses of H9c2 rat cardiomyoblasts with fluorescently labeled anti-AKAP13 and FITC-phalloidin (F-actin) showed AKAP13 localization to actin, as previously reported (Mayers, 2010). Furthermore, Western blot analysis of isolated cardiac mitochondria showed faint AKAP13 bands. These data suggested that AKAP13 may be closely adherent to the mitochondria via F-actin filaments, or may even migrate into the mitochondria. Given the size of the largest AKAP13 isoform (~310 kDa), migration into the mitochondria is unlikely. However, the smallest isoform, Brx (~170 kDa), is known to enter the nucleus. Other AKAPs, such as AKAP1, have established roles in mitochondrial dynamics (Jun, 2016). Additional studies with electron microscopy and immuno- or nanoparticle labeled AKAP13 antibodies would be an informative future study. Moreover, super-resolution microscopy could be performed in order to establish if AKAP13 localizes to mitochondria, and under what conditions.

The striking similarity of our results to the human dilated cardiomyopathy literature suggested that the *Akap13*^{cKO} model is a novel mouse model for targeted and potentially

translational research on cardiomyopathy, and is in line with the mission of the National Institutes of Health. Mitochondrial dysfunction is a known cause of cardiomyopathy, especially DCM. It has been reported that upwards of 600 rare genetic variants, including mitochondrial genes, have been associated with the various cardiomyopathies. This complexity is compounded by variable penetrance and incomplete expression, environmental factors, and the involvement of multiple signaling pathways and organelles (Jacoby, 2011) (Chen, 2012). Mutations in mitochondrial genes and proteins, such as mitochondrial fusion protein, OPA1, can lead to severe cardiac pathology (Chen, 2012). While mitochondria are dynamic organelles with short half-lives and are prone to morphological changes in disease states, such as alterations in size and cristae, few diseases, other than primary mitochondrial diseases, have shown the significant ultrastructural pathology similar to our data described here. The prominent ultrastructural alterations seen in the *Akap13*^{cKO} mouse model appear to be even more severe than those observed in many primary mitochondrial diseases. Given these data, a central regulatory role for the AKAP13 protein may be implicated.

Phenotypic changes in murine models deficient in *Opa1, Srf, Creb-1,* and PGC-1α/β have shown ultrastructural and cardiac alterations similar to, but not as severe as, the *Akap13*^{cKO} mouse model (Chen, 2012) (Miano, 2004) (Watson, 2010) (Arany, 2005) (Leone, 2005). In order to thoroughly investigate the genes and gene products altered in AKAP13^{cKO} mouse heart extracts in an unbiased manner, we performed proteomic and RNAseq analyses and RT-qPCR on identified gene targets. Ingenuity Pathway Analysis (IPA), Metacore, and Pathway studio analyses were performed on our differentially

expressed proteomic and RNSseq derived genes. Dysregulation of key genes and proteins involved in oxidative phosphorylation, cytoskeletal remodeling, regulation of the actin cytoskeleton by Rho GTPases, and cardiac dysfunction were indicated ($p<0.001$). Given these data, *Srf* transcript levels were assessed by RT-qPCR and were found to be reduced in *Akap13*^{cKO} mice and *Akap13* siRNA knocked down H9c2 cells ($p<0.05$, both). Similarly, *Opa1* transcript levels were assessed and were reduced in *Akap13*^{cKO} mice heart extracts and *Akap13* siRNA knocked down H9c2 cells ($p<0.05$, both). Likewise, decreased peptides for Perm1 *(PGC-1 and ERR-induced regulator)* were indicated in *Akap13*^{cKO} mice compared to control mice ($p<0.001$). Given these data, we do not suspect that the pathological sarcomeric and mitochondrial changes observed in AKAP13^{cKO} mice were secondary to heart failure, DNA damage response or other off target or treatment effects. Decreased expression of key target genes (*Srf, Opa1)* and gene products (MFN1, Perm1) were concomitant with the loss of *Akap13.* These data indicated that AKAP13 may be a key regulatory protein in cardiomyocyte signaling pathways involved in maintaining the cardiac sarcomere and mitochondrial dynamics.

Moreover, treatment with LPA, a known activator of AKAP13, RhoA, and SRF, upregulated AKAP13 expression in control and AKAP13 siRNA knocked down H9c2 rat cardiomyoblasts consistent with previous reports (Mayers, 2010). Additionally, LPA treatment increased SRE-luciferase activation in an AKAP13 dose-dependent manner. Higher doses of AKAP13 resulted in increased SRE-luciferase activation. Additionally, LPA treatment increased Opa1 message in *Akap13* siRNA knocked down H9c2 cells which suggested a common pathway between AKAP13 and OPA1. To probe downstream

of LPA receptors, Rho A and PKA activities were assayed in *Akap13*^{cKO} mouse heart extracts compared to control heart extracts. Enzyme-linked immuno-absorbent assay (ELISA) showed decreased PKA activity but unchanged RhoA activity. Furthermore, PKAR2A, the PKA isoform that AKAP13 preferentially binds to, was decreased in our proteomics dataset while PKAR1A was increased in a seemingly compensatory reaction. *Mybphl, Myl7, Myl4, Mef2c* and other genes with regulatory roles in heart development were found to be upregulated in *Akap13*^{cKO} mice. It is possible that a fetal gene response was seen with *Akap13*^{cKO} as an attempt to overcome the genetic insult, and protect the heart from further damage (RNAseq figure-table). A fetal gene response is often accompanied by heart failure (Dirkx, 2013) emphasizing the profound effect that the loss of *Akap13* had on the adult heart. Taken together, these data suggested that *Akap13* had an ongoing role in the adult murine heart, and was involved in cell signaling and pathway integration via interaction with actin and actin-associated proteins, and sarcomeric structure and organization via precise modulation of the PKA/RhoA pathways.

Our findings are supported by other reports which have also suggested that actin, desmin, SRF, RhoA, MEF2c, and intracellular Ca^{2+} are involved in sarcomere formation, cardiac signaling, dilation, and contractility (Mayers, 2010) (Greenstein, 2011); perturbations of these can lead to cardiomyopathy and other cardiac defects (Jacoby, 2011) (Miano, 2004). It is likely that expression and signaling involving these common pathway components are altered with the loss of *Akap13*, as we have previously reported (Koide, 2015) (Mayers, 2010). Notably, Protein A-Kinase Anchoring Proteins (AKAPs) are a key factor in cardiomyocyte development and serve as regulators of many signaling pathways. The

regulatory subunit of PKA, as mentioned earlier, is a known substrate of AKAPs. AKAPs bind the regulatory subunit of PKA and localize the bound PKA to discrete subcellular micro-niches allowing spatiotemporal regulation of various cell signaling cascades (such as those that utilize cAMP as a second messenger). That is, AKAPs act as scaffolds to sequester PKA and other molecules to distinct areas of the cell, and are involved in signaling crosstalk. This dissertation has demonstrated that the mitochondria and cardiac sarcomere may be additional target sites for AKAP13. However, substrate sequestration is not the sole function of every AKAP; functionality is influenced by the abilities of the individual AKAP. Furthermore, the active role of AKAPs in cell signaling are not limited to a particular type of cell or tissue; AKAPs have been shown to be important pathway components, from the plasticity of neurons to cardiomyocyte development to stimulating the production of cytokines and even cancer (aRubino 1998). The presence of AKAPs in various cell types emphasizes the importance of the active role of AKAPs in cell signaling beyond that of a simple scaffolding protein. However, *Akap13* is a unique AKAP: it is the only AKAP that has been found to have guanine nucleotide exchange factor (GEF) activity and modulate nuclear hormone receptors. The evolutionary conservation and widespread expression of *Akap13* along with its central role in coordinating otherwise chaotic signaling pathways suggest a critical if not a fundamental role in normal signaling cross-talk (Welch, 2010).

We interpreted these data to suggest that loss of AKAP13 may lead to reduction in transcription factor signaling, and specifically focused attention on SRF and CREB. These two factors are known to regulate crucial proteins involved in mitochondrial function, such

as OPA1, which was greatly reduced in the cKO cells. In support of a critical role of AKAP13 upstream of these factors, targeted loss of function of SRF (Miano, 2004) and OPA1 (Chen, 2012) produced a murine cardiac phenotype strikingly similar to the AKAP13 phenotype we observed. The similarity of phenotypes observed, the reduction in transcripts in the cKO cells, and the functional data regarding AKAP13 in H9C2 cells, suggest a mechanism whereby reduction in AKAP13 leads to impairment of a critical transcriptional mechanism regulating mitochondrial function.

One possible limitation to the interpretation of our results is that functional data in mice can be difficult to obtain and is a potential drawback to any cardiac study. In recent years, increasingly precise functional equipment and software have been designed and utilized for rodent functional testing. Because of this, various interpretations of functional tests can be found in the literature, but no real repository of rodent standard values, other than the paucity of data found in the Mouse Phenome Database published online by The Jackson Laboratory (Bar Harbor, ME) exists. The datasets currently found in the Mouse Phenome Database are often incomplete or obtained on small sample sizes. Because of this, the littermate and within-line sibling controls used in this dissertation were considered the best indication of standard values by which to directly compare our model. Notably, we have been asked by the MRI mouse core director at the National Heart Lung and Blood Institute (NHLBI) National Institutes of Health (NIH) (Bethesda, MD) to include our control mice data in a functional report to help establish mice reference values for MRI. Similarly, electrocardiogram (ECG) interpretation can vary from animal to animal, and even strain to strain. It has been shown in the literature where the T wave in lead I is

negative (Boukens, 2014). However, other reports (Sadhegi, 2002) (Ho, 2011), as well as our own data have indicated that the T waves, similar to humans, are more often positive in lead I. As stated above, normal values were established using the littermates and siblings of the *Akap13*^{cKO}mice. Statistical analyses and waveform interpretations were established per in depth literature review and the expert opinion of our cardiology collaborator (Dr. Alessandra Broferrio, MD) at NHLBI, NIH.

In conclusion, our data answered the question we had at the outset of this dissertation: Does AKAP13 have a role in the adult mouse heart? The data set forth in this dissertation identified *Akap13* as a critical gene required for normal adult mouse cardiac function and morphology. *Akap13* knockout lead to biventricular dilated cardiomyopathy with severely disrupted sarcomeric and mitochondrial phenotypes. Female *Akap13*^{cKO} mice exhibited a more severe cardiac phenotype with increased risk of morbidity post-induction of genetic recombination. Female *Akap13*$^{Het\text{-}MCM}$ mice also showed cardiac abnormalities whereas male *Akap13*$^{Het\text{-}MCM}$ mice did not. Furthermore, AKAP13 binds numerous transcription factors, such as c-fos, c-Jun, ERα, and CREB, a ubiquitous transcription factor in the absence of which produces dilated cardiomyopathy, mitochondrial dysfunction, and increased female morbidity (Watson, 2010), also similar to our model.

We interpret these findings to indicate that AKAP13 acts as a "regulator of regulators," coordinating, either directly or indirectly, transcription factor activation to facilitate a cardiac gene program unique to the developmental stage of the organism from the embryo (Mayers, 2010) through adulthood. It is likely that AKAP13 acts in multiple pathways to bring about the downstream effects highlighted in this dissertation. Here we

showed AKAP13 acting downstream of LPA in the PKA/RhoA pathways to modulate SRF and SRE-responsive genes. In the absence of AKAP13, PKA was decreased, and is likely no longer able to inhibit LPA stimulation of SRF, thereby allowing SRF to be de-repressed, and SRE-responsive genes to be inadvertently turned "on." This would disturb the usually tightly regulated transcriptional program. Additionally, reports in the literature have shown AKAP13 regulation of Estrogen Receptor α (ERα) both indirectly through a Cdc42-dependent mechanism, and directly through binding PKA and phosphorylating ERα (Rubino, 1998) (Toaldo, 2015). Dysregulation of ERα would result from loss of *Akap13* and may partially explain the more severe phenotype exhibited by female *Akap13*^{cKO} mice. These findings provide the first correlation between AKAP13 and a cardiomyopathy with a severe mitochondrial phenotype. Because of this, *Akap13* should be considered a candidate gene for complex familial DCM with mitochondrial phenotypes, and a candidate gene for sex-specific differences in heart disease. Future studies should focus on elucidating the mechanism of AKAP13, its role in mitochondrial dynamics, sex-specific differences in cardiomyopathy, and as a potential target for drug development and therapeutics.

CHAPTER 4: Materials and Methods

Animal care and use. All animal studies and procedures were approved by the Office of Animal Care and Use at the NICHD, NIH, and the ACUC at Johns Hopkins University School of Medicine. All animal tissue harvests were performed post-mortem; euthanasia procedures followed strict institutional guidelines.

Generation of *Akap13* conditional knockout murine model. A Cre-lox deletion strategy was used to generate $Akap13^{cKO}$mice. Lox p sites were inserted as previously described (Liu P, 2003); the *Akap13* guanine nucleotide exchange factor (GEF) domain was targeted for deletion. $Akap13^{cKO}$ mice were generated by crossing $Akap13^{Flox/Flox}$ mice with homozygous alpha-Myosin Heavy Chain-MerCreMer (α-MHC-MerCreMer) mice. Tamoxifen (40mg/kg body weight) was administered for 4 weeks through tamoxifen laced chow (Harlan Tekland) to induce cardiomyocyte-specific knockout for the α-MHC-MerCreMer model. An alternative $Akap13^{cKO}$ was generated by using Tetracycline- on cre (TOC); mice were given ad libitum access to doxycycline (1mg/mL) (Sigma) laced drinking water for one to two weeks. All mice had a C57Bl6/J background strain. Assays and imaging were conducted following cessation of tamoxifen or doxycycline treatment. gDNA was isolated from mouse tail tissue using the Wizard® Genomic DNA Purification Kit (Promega, Madison, WI, USA) per manufacturer's instructions. Polymerase chain reaction (PCR) was used for genotyping analysis as previously reported (Koide, 2015).

Southern Blot. For confirmation of our transgenic construct in the embryonic stem cells and in the *Akap13*$^{Flox/Flox}$ mice, we performed a Southern blot as previously reported (Koide, 2015).

***In situ* hybridization, Immunohistochemistry and Immunoblot.** Quantitative real time polymerase chain reaction (qRT-PCR) was performed to assess *Akap13* transcript levels for knockdown. Low levels of message in *Akap13*^{cKO} hearts compared with control mice suggested knockdown was achieved. *In situ* hybridization analyses were performed as previously described (Koide, 2015) in order to assess the distribution and knockdown of AKAP13 in paraffin embedded 4-5µm thick slices of control and *Akap13*^{cKO} mouse hearts, respectively. Hearts were collected from euthanized mice, and fixed in 10% neutral buffered formalin. Results substantiated those of qRT-PCR. Immunohistochemstiry (IHC) was used to ascertain protein levels in *Akap13*^{cKO} mice compared to controls. IHC was performed with MULTIVIEW® (mouse-HRP/rabbit-AP) IHC kit (Enzo Life Sciences, Boston, MA, USA) per manufacturer's instructions. AKAP13 antibodies were used as previously described (Mayers, 2010); anti-sarcomeric alpha-actinin (EA-53) (Abcam, Cambridge, MA, USA) was used as a control. Western blot was performed essentially as previously described (Rubino, 1998). AKAP13 and β-actin antibodies were used as previously described (Mayers, 2010). IHC and western blot both validated knockdown of AKAP13 protein.

RT-PCR. In order to evaluate the tissue specificity of the MCM and TOC, RNA was isolated from *Akap13*^{cKO} and control mice hearts, testes, ovaries, and livers using the RNeasy kit (Qiagen) for evaluation by reverse transcription polymerase chain reaction

(RT-PCR). The RNA was reverse transcribed using iScript (BioRad), followed by PCR. Primers used were as previously described (Koide, 2015).

Magnetic Resonance Imaging. Magnetic Resonance Imaging (MRI) was performed on *Akap13*^{cKO} and control mice at baseline and with stress. Mice were anesthetized with1-2% isoflurane and imaged with ECG, respiratory and temperature detection as described in standard MRI methods. Dobutamine stress testing was performed after acquiring gradient echo cine scans of the whole heart at baseline (typically 6 slices), without stress, then scanning 2 or 3 mid-ventricle slices under stress at two dobutamine infusion rates and comparing the ejection fractions and any wall motion abnormalities. Mice receive 0.2-0.3 mmol/kg Magnevist (Bayer HealthCare, Montville, NJ) i.v. at baseline and 0.2 mmol/kg at initiation of dobutamine stress. After the baseline scan mice are infused with 1/20 dobutamine (Eli Lilly, Indianapolis, IND) in 0.9% saline, 5% dextrose or 5% dextrose/0/9% saline at a dobutamine dose of 10µg/kg/min (0.010 mg/g/min) using an infusion pump (Cole-Parmer, Vernon Hills, Il.). After the heart rate reaches a steady state in 4-10 minutes, two or three slices, which are identical to 2-3 of the baseline slices at mid-ventricle, are imaged. Infusion rate is increased to 40µg/kg/min (0.040 mg/g/min) and the scans were repeated. Infusion was stopped and the mice were recovered. Cardiac functional analysis from the cine image data was performed. A full functional analysis is performed on the baseline data. Then for the mid ventricle slices of the baseline, low and high dose dobutamine scans, ejection fraction and wall motion are compared.

Echocardiograpy (Echo). All animals were under general anesthesia and body temperature was maintained at 37°C for the duration of the experiment. Animals were

induced at 4% isoflurane maintained with 1-2% isoflurane via nosecone. Sterile ophthalmic ointment was applied to prevent corneal desiccation while under anesthesia. The hair from the chest was removed using a chemical hair remover. The animal was placed in a supine position and secured with tape and Ultrasound gel was spread on the precordial region and the Vevo2100 (Visual Sonics, Toronto, CA) with a 40Hz transducer was used to acquire B-mode, M-mode, aortic valve, pulmonary valve and mitral valve visualizations. Mitral inflow recordings were obtained with the pulsed Doppler sample volume at the level of the mitral leaflet tips during maximal opening in diastole. Tissue Doppler recordings were measured with sample volumes at both the septal mitral annulus and lateral mitral annulus. The cardiac wall thickness and left ventricle size were determined by M-mode. The valves were measured with pulsed-wave Doppler mode. Animals were recovered in a warm cage until awake and ambulatory.

Electrocardiogram (ECG). All animals were under general anesthesia and body temperature was maintained at 37°C for the duration of the experiment. Animals were induced at 4% isoflurane and maintained at a rate of 1.5-2% isoflurane during ECG acquisition. Mice were placed in a supine position, and 29-gauge needle electrodes were inserted subcutaneously into all four limbs. Six leads were continuously recorded with Powerlab (ADInstruments, Colorado Springs, CO). Leads I and II were recorded directly via the needle electrodes and Leads III, aVR, aVL, and aVF were calculated automatically through LabChart 7.0 (ADInstruments) for one minute. Animals were placed in a warmed cage until awake and ambulatory. Each signal was analyzed using LabChart 7.0 ECG (ADInstruments) module software analysis using the Bazett formula. The QTc interval was

analyzed using the Fridericia formula. The ECG analysis module automatically detects PQRST onset, amplitude, and interval with default or customized detection settings.

Blood pressure. Systolic and diastolic blood pressures and Mean Arterial Pressure were measured in conscious mice using a computerized tail-cuff non-invasive system (Hatteras Instruments, Cary, NC) on a heated 37˚C platform. Mice were acclimated for three days every week in order to enhance reliability and reproducibility of the blood pressure measurements. Data obtained after acclimation period was recorded.

Histologic, light and fluorescent microscopic examination of cardiac tissues. Hearts were collected from post-mortem *Akap13*^{cKO} mice and controls, rinsed in 1XPBS, fixed in 10% neutral buffered formalin, and embedded in paraffin blocks. Paraffin-embedded 4-5µm slices were fixed to glass slides (with RNAse- cutting precaution) (Histoserv, Germantown, MD, USA). Haematoxylin/Eosin (H&E) stained mid-ventricular slices (Histoserv) were obtained from *Akap13*^{cKO} mice and controls; ventricular sizes and disrupted cardiomyocytes were quantified using ImageJ (NIH, Bethesda, MD, USA). To estimate possible cardiac infarct and necrosis, Phosphotungstic acid-haematoxylin (PTAH) stain for cardiac muscle fibers and collagen was performed on fixed, paraffin-embedded slices (Histoserv). Hearts were also fixed in OCT, snap-frozen, and frozen sections were prepared (Uniform Services University of the Health Sciences). Masson-trichrome, a connective tissue stain, was used to measure fibrotic areas in the cardiac tissue; collagen fibers stain blue, all other tissue stains red, and nuclei will appear black. Masson-trichrome stain (Histoserv) was performed on paraffin-embedded slices. All images of H&E, PTAH, and Masson-trichrome, stained sections were obtained with a Leica DMLS Binocular

Microscope (Leica Microsystems, Germany). For quantification, at least 4 independent images for each region of interest was used.

Apoptosis assay. To assess apoptosis in cardiac tissues, dUTP Nick End Labeling (TUNEL) In Situ Cell Death Detection Kit, Fluorescein (Roche, Indianapolis, IN, USA) was performed on paraffin-embedded slices per manufacturer's instructions. Fluorescent images were obtained using a Leica DMIRB Inverted Fluorescence Microscope (Leica Microsystems, Germany). For quantification 4 independent images for each region of interest were used and analyzed with ImageJ (NIH).

Transmission Electron Microscopy (TEM). *Akap13*^{cKO} and control heart tissue samples were prepared and observed as described (Wang, 2016). Image data was analyzed using ImageJ (NIH).

Bioinformatics: Proteomics. Tissue samples were homogenized in tris-buffered saline, followed by addition of an equivalent volume of lysis buffer (final concentrations: 1% SDS, 0.5% NP-40, 0.5% sodium deoxycholate). Samples were frozen for 4 h at -20 °C, transferred to 1.5 mL tubes and sonicated three times for 30 s at the lowest setting with sample cooling on ice between pulses. Samples were then boiled for 10 min and centrifuged to remove cell debris. Protein quantitation was performed on a 1/10 dilution of the sample solution using the BCA assay (ThermoFisher Scientific). Fifty micrograms of each sample were electrophoresed into the stacking portion of a 4-15% gel (Mini-PROTEAN TGX, Bio-Rad), excised from the gel and processed by in-gel digestion (I'll get you a reference for this). Briefly, gel bands were destained in 25 mM AMB, 50% acetonitrile (ACN, Sigma-Aldrich) at ambient temperature on a vortex platform. Gel bands

were dehydrated in 100% ACN and incubated in 25 mM AMB, 10 mM dithiothreitol (Sigma-Aldrich) at 56 °C for 30 min followed by alkylation with 25 mM AMB, 55 mM iodoacetamide (Sigma-Aldrich) in darkness for 45 min at ambient temperature. Gel slices were dehydrated in 100% ACN and rehydrated with 20 ng/μL sequencing grade modified trypsin (Promega, Madison, WI, USA), 25 mM AMB on ice for 45 min. Excess trypsin was removed, gel bands were washed with 500 μL of 25 mM AMB and in-gel digestion was performed at 37 °C for 16 h. Tryptic peptides were extracted with 70% ACN, 5% formic acid (Sigma-Aldrich) and peptide extracts were lyophilized by vacuum centrifugation and stored at -80 °C until analysis.

Samples were resuspended in 25 mM ammonium bicarbonate (Sigma Aldrich, St. Louis, MO) and were analyzed through five consecutive injections by LC-MS/MS on a nanoflow LC system (Easy-nLC 1000, ThermoFisher Scientific, San Jose, CA) coupled online with a Q Exactive MS (ThermoFisher Scientific). Samples were resolved on a 100 μm I.D. × 360 μm O.D. × 20 cm long capillary column (Polymicro Technologies, Phoenix, AZ), which was slurry packed in house with 5 μm, 100Å pore size C-18 silica-bonded stationary phase (Magic C18AQ, Bruker). Following pre- and analytical column equilibration, each sample was loaded onto a 2-cm reversed-phase (C-18) pre-column (ThermoFisher Scientific) at 3 μL/min at 3x the injection volume with mobile phase A (0.1% formic acid in water). Peptides were eluted at a constant flow rate of 200 nL/min by development a linear gradient of 0.33% mobile phase B (0.1% formic acid in acetonitrile) per min for 120 min and then to 95% mobile phase B for an additional 15 min. The columns were washed for

15 min at 95% mobile phase B and then quickly brought to 100% mobile phase A for the next sample injection.

The MS was configured to collect broadband mass spectra (m/z 375-1800) in profile mode using the lock mass feature for the polydimethylcyclosiloxane (PCM) ion generated in the electrospray process (m/z 445.12002). Mass spectrometric conditions were set as follows: electrospray voltage, 1.7 kV; no sheath and auxiliary gas flow; capillary temperature, 250 °C; S-Lens RF level, 60%; resolution, 70,000 at m/z 200. The ion selection threshold for the broadband scan was set at 1e6 with a maximum ion accumulation time of 50 ms. The ten most abundant ions were selected for MS/MS with the following settings: ion threshold, 1e6; intensity threshold, 5e3; maximum ion accumulation time, 200 ms; resolution, 17,500 at m/z 200; isolation window, 3 m/z; dynamic exclusion, 40 s; and a normalized collision energy (NCE) of 25.

Tandem mass spectra were searched against the SwissProt mouse protein database (downloaded on 09/25/2015, 16,719 sequences) from the Universal Protein Resource (www.uniprot.org) using Mascot Daemon/Server (v.2.3.2/v.2.3, Matrix Science Inc., Boston, MA) using the automatic decoy search option. The data were searched with a precursor mass tolerance of 10 ppm and a fragment ion tolerance of 0.6 Da. Cysteine carbamidomethylation (m/z 57.021464) was set as a fixed modification and methionine oxidation (m/z 15.994915) was set as a dynamic modification. A maximum of two missed tryptic cleavages were allowed. Identified peptides (PSMs, peptide spectral matches) were filtered using an ion score cutoff of 33 resulting in a false peptide discovery rate of less than 1% for all peptides identified (determined from the decoy database search). PSMs

whose sequence mapped to multiple protein isoforms were grouped as per the principle of parsimony. Results for each sample were normalized to the sample with the lowest total PSMs for the five replicate injections/analyses and protein abundance differences were determined by spectral counting, where the total PSMs identified for a given protein reflects overall abundance. For sample comparisons, statistical analyses for the enrichment of specific proteins among differentially expressed proteins were performed utilizing a z-statistic test on the log2-transformed spectral count ratios from normalized data. False positives (q values, FDR) were estimated using the R package "q value". These data were analyzed using Ingenuity Pathway Analysis (Qiagen), Metacore (Thomson Reuters, New York, NY, USA), and Pathway Studio (Elsevier, Amsterdam, Netherlands).

Adult cardiomyocyte isolation and protein and RNA extraction. Adult cardiomyocytes were isolated from *Akap13*^{cKO} mouse hearts and control hearts using an enzymatic digestion method (Cellutron, Baltimore, MD, USA). Cells were maintained in AS media (Cellutron), and were plated at the manufacturer's recommended cell density at least 6 hours before imaging. For protein and RNA isolation, adult cardiomyocytes were maintained in suspension culture for 30min-1 hour. Cells were pelleted by centrifugation at 1100rpm, and the AS medium was removed. Cells were re-suspended in either RIPA buffer (Invitrogen) supplemented with 4% protease and phosphatase inhibitors (Qiagen) for protein isolation, or Buffer RLT supplemented with β-mercaptoethanol per manufacturer's instructions (RNeasy, Qiagen, Valencia, CA, USA) for RNA isolation. For western blot, protein concentration was confirmed by BCA analysis (ThermoFisher); 500ng-1ug of protein lysate was loaded per lane. Immunoblotting essentially followed our

previously reported method (Rubino, 1998) except for the use of NuPAGE® Tris-Acetate gels and buffer system (ThermoFisher, Halethorpe, MD, USA) in lieu of the Tris-glycine system. RNA was isolated using the RNeasy kit. Manufacturer guidelines were followed for isolation and purification of RNA.

Bioinformatics: RNAseq. RNA from mouse hearts were isolated as described above. RNA Integrity Number (RIN) was assessed with a Bioanalyzer 1000 RNA chip (Agilent, Santa Clara, CA, USA); a minimum RIN value of 8.5 was established. Ribosomal rRNA removal, poly-A enrichment, and reverse transcription and library preparation were performed as previously described (Nuno L. Barbosa-Morais, 2012). Paul H. Driggers, PhD, kindly generated a differentially expressed gene list from the raw data files. These data were analyzed using Ingenuity Pathway Analysis (Qiagen), Metacore (Thomson Reuters, New York, NY, USA), and Pathway Studio (Elsevier, Amsterdam, Netherlands).

Cell Culture, cytoimmunofluorescence, confocal imaging, and quantitation. H9c2 cells were purchased from ATCC (Manassas, VA, USA) and maintained in DMEM medium (ATCC, Manassas, VA, USA) supplemented with 10% FBS, and 1% penicillin-streptomycin (Invitrogen). Staining procedures were followed as previously reported (Mayers, 2010). H9C2 cells and

Mitochondrial assays. Primary adult cardiomyocytes and H9c2 cells were imaged to assess the number of mitochondria and in mitochondrial membrane potential in primary adult cardiomyocytes from *Akap13*^{cKO} mice and control mice, and in *Akap13* siRNA knockdown (H9c2 cells). Mitochondrial membrane potential was also assessed by the JC-1 biochemical assay kit (ThermoFisher)

Immunoblot. Intact mitochondria were obtained using the Mitochondrial Isolation Kit (ThermoFisher). Mitochondria were then lysed following the manufacturer guidelines. For protein isolation from tissue, hearts were collected post-mortem and snap frozen in liquid nitrogen; snap frozen tissues were stored at -80°C. Tissue lysates were prepared the TissueRupter homogenizer (Qiagen)

Biochemical analyses. RhoA and PKA activity were analyzed in tissue lysates from *Akap13*^{cKO} mouse hearts and control hearts. To quantify active RhoA in the *Akap13*^{cKO} mouse hearts, Rho G-LISA (Cytoskeleton) was performed per the manufacturer's instructions. PKA activity was assessed using PKA activity assay Kit (ThermoFisher).

qRT-PCR. For analysis of mRNA transcripts of key genes, quantitative real time polymerase chain reaction (qRT-PCR) was performed as described in the literature (Koide, 2015). RNA was extracted from mouse hearts or H9c2 cells, where appropriate, with RNeasy (Qiagen). RNA was reverse transcribed to cDNA using iScript (BioRad). SYBR Green (BioRad) was used for RT-qPCR analysis per manufacturer's directions.

Statistical Data Analyses. Mean levels of test outcomes were compared by genotype and sexes using one-way ANOVA with Bonferroni adjustment for multiple comparisons and T-Tests where appropriate. These analyses were performed using the SAS (Statistical Analysis System) software version 9.3 (Cary, NC, USA). Student's *t*-test used for statistical analyses; (* where $p<0.05$, ** where $p<0.01$). Student's *t*-test, Mann-Whitney test for median comparison, and Chi-squared tests were used for statistical analyses as appropriate; * where $p<0.05$, ** where $p<0.01$). Biological replicates (n) were used in testing. Analyses are combined sex unless otherwise noted.

Primers List:

PCR primers:

5F 5’- GCG GAA GAA GGA GTC TCT TG -3’
7R 5’- TCA CCT TTG GTA CAT TGC AG -3’
8R3 5’- ATC GAC TTG CTA TCT GTC C -3’
MerCreMer-F: 5’- AGG TGG ACC TGA TCA TGG AG -3’
MerCreMer-R: 5’- ATA CCG GAG ATC ATG CAA GC -3’
TOC-F: 5’- GGC GCG GCA ACA CCA TTT TT -3’
TOC-R: 5’- TCC GGG CTG CCA CGA CCA -3’

RT-qPCR primers:

mAKAP13-F: 5’-TGG ATG AGC TGA TCA GTA TC- 3’
mAKAP13-R: 5’- TTG ACA GAC TGG TTG TGC TG-3’
m18S-F: 5’-CTT AGA GGG ACA AGT GGC G-3’
m18S-R: 5’-ACG CTG AGC CAG TCA GTG TA-3’
mGAPDH-F: 5’-GTT TGT GAT GGG TGT GAA CCA C-3’
mGAPDH-R: 5’-CTG GTC CTC AGT GTA GCC CAA-3’
Srf-F: 5’- CAC GAC CTT CAG CAA GAG GA-3’
Srf-R: 5’- CAA AGC CAG TGG CAC TCA TT-3’
PKN-F: 5’ –GAG AAG GCT ACT GCG GAG GA-3’
PKN-R: 5’ –CGG CCA CAA AGT CGA AAT C-3’
Opa1-F: 5’- TGA CAA ACT TAA GGA GGC TGT G-3’
Opa1-R: 5’- CAT TGT GCT GAA TAA CCC TCA A-3’

Literature Cited

Literature Cited

Hall. (1998). Rho GTPases and the actin cytoskeleton. *Science*, 509-514.

Anavekar, N. S. Oh JK. (2009). Doppler echocardiography: A contemporary review. *Journal of Cardiology*, 347–358.

Anzano, M.A., Byers SW, Smith JM, Peer CW, Mullen LT, Brown CC, Roberts AB, Sporn MB. et al. (1994) Prevention of Breast Cancer in the Rat with 9-cis-Retinoic Acid as a Single Agent and in Combination with Tamoxifen. Cancer Research, 54, 4614-4617.

Arany, He H, Lin J, Hoyer K, Handschin C, Toka O, Ahmad F, Matsui T, Chin S, Wu PH, Rybkin II, Shelton JM, Manieri M, Cinti S, Schoen FJ, Bassel-Duby R, Rosenzweig A, Ingwall JS, Spiegelman BM.. (2005). Transcriptional coactivator PGC-1 alpha controls the energy state and contractile function of cardiac muscle. Cell Metab. 2005 Apr;1(4):259-71.

Abdul Azeez KR, Knapp S, Fernandes JM, Klussmann E, Elkins JM. (2014). The crystal structure of the RhoA-AKAP-Lbc DH-PH domain complex. *Biochem. J.*, 1-9.

Bacskai BJ, Hochner B, Mahaut-Smith M, Adams SR, Kaang BK, Kandel ER, Tsien RY. (1993). Spatially resolved dynamics of cAMP and protein kinase A subunits in aplysia sensory neurons. *Science*, 222-226.

Baig. (2017). *In preparation.*

Baisamy L, Jurisch N, Diviani D. (2005). Leucine zipper-mediated homo-oligomerization regulates the Rho-GEF activity of AKAP-Lbc. *J Biol Chem*, 15405-15412.

Boukens BJ, Rivaud MR, Rentschler S, Coronel R. (2014). Misinterpretation of the mouse ECG: 'musing the waves of Mus musculus'. J Physiol. 2014 Nov 1;592(21):4613-26. doi: 10.1113/jphysiol.2014.279380. Review.

Carnegie GK, Soughayer J, Smith FD, Pedroja BS, Zhang F, Diviani D, Bristow MR, Kunkel MT, Newton AC, Langeberg LK, Scott JD. (2008). AKAP-Lbc mobilizes a cardiac hypertrophy signaling pathway. *Mol Cell.*, 169-179.

Charron F, Tsimiklis G, Arcand M, Robitaille L, Liang Q, Molkentin JD, Meloche S, Nemer M. (2001). Tissue-specific GATA factors are transcriptional effectors of the small GTPase RhoA. *Genes &Dev.*, 2702-2719.

Chen L, Liu T, Tran A, Lu X, Tomilov AA, Davies V, Cortopassi G, Chiamvimonvat N, Bers DM, Votruba M, Knowlton AA. (2012). OPA1 Mutation and Late-Onset Cardiomyopathy: Mitochondrial Dysfunction and mtDNA Instability. *Journal of the American Heart Association*, 1-12.

Chung AK, Das SR, Leonard D, Peshock RM, Kazi F, Abdullah SM, Canham RM, Levine BD, Drazner MH. (2006). Women Have Higher Left Ventricular Ejection Fractions Than Men Independent of Differences in Left Ventricular Volume. *Circulation*, 1597-1604.

Cipolat S, Martins de Brito O, Dal Zilio B, Scorrano L. (2004). OPA1 requires mitofusin 1 to promotes mitochondrial fusion. *Proc Natl Acad Sci USA.*

Curtis AB, Narasimha D. (2012). Arrhythmias in Women. Clinical Cardiology. 2 March 2012. 10.1002/clc.21975

Dirkx E, da Costa Martins PA, De Windt LJ. (2013). Regulation of fetal gene expression in heart failure. *Biochimica et Biophysica Acta*, 2414-2424.

Diviani D, Soderling J, Scott JD. (2001). AKAP-lbc anchors protein kinase A and nucleates Ga12-selective Rho-mediated stress fiber formation. *J Biol Chem*, 44247-44257.

Driggers PH, Segars JH, Rubino DM. (2001). The proto-oncoprotein Brx activates estrogen receptor beta by a p38 mitogen-activated protein kinase pathway. J Biol Chem. 2001 Dec 14;276(50):46792-7. Epub 2001 Sep 28.

Ellerbroek SM, Wennerberg K, Burridge K. (2003). Serine phosphorylation negatively regulates RhoA in vivo. J Biol Chem. 2003 May 23;278(21):19023-31.

Feliciello A, Gottesman ME, Avvedimento EV. (2001). The biological functions of A-kinase anchor proteins. *J Mol Biol.*, 457–467.

Frazao. (1999). America's Eating Habits: Changes and Consequences. . *Agriculture Information Bulletin No. (AIB750)*, 1-484.

Greenstein JL, Winslow RL. (2011). Integrative systems models of cardiac excitation-contraction coupling. *Circ. Res.* , 70-84.

Hazebroek M, Dennert R, Heymans S. (2012). Idiopathic dilated cardiomyopathy: possible triggers and treatment strategies. *Neth Heart J.*, 332–335.

Heidenreich PA, Trogdon JG, Khavjou OA, Butler J, Dracup K, Ezekowitz MD, Finkelstein EA, Hong Y, Johnston SC, Khera A, Lloyd-Jones DM, Nelson SA, Nichol G, Orenstein D, Wilson PW, Woo YJ; American Heart Association Advocacy Coordinating Committee; Stroke Council; Council on Cardiovascular Radiology and Intervention; Council on Clinical Cardiology; Council on Epidemiology and Prevention; Council on Arteriosclerosis; Thrombosis and Vascular Biology; Council on Cardiopulmonary; Critical Care; Perioperative and Resuscitation; Council on Cardiovascular Nursing; Council on the Kidney in Cardiovascular Disease; Council on Cardiovascular Surgery and Anesthesia, and Interdisciplinary Council on Quality of Care and Outcomes Research. (2011). Forecasting the future of cardiovascular disease in the United States. *Circulation*.

Hempel CM, Vincent P, Adams SR, Tsien RY, Selverston AI. (1996). Spatio-temporal dynamics of cyclicAMP signals in an intact neural circuitm. *Nature*, 166-169.

Heron. (2009). *Deaths: Final data for 2006.* Hyattsville, MD: National Vital Statistics Reports.

Hershberger. (2010). Clinical and genetic issues in dilated cardiomyopathy: A review for genetics professionals. *Genet Med*, 655-667.

Hershberger RE, Morales A, Siegfried JD. (2011). Heart Rate and Electrocardiography Monitoring in Mice. Curr Protoc Mouse Biol. 2011 Mar 1;1:123-139.

Huang S, Ingber DE. (2005). Cell tension, matrix mechanics, and cancer development. *Cancer Cell*, 175-176.

Istvan R Boldogh, Liza A Pon (2006). Interactions of mitochondria with the actin cytoskeleton. *Biochimica et Biophysica Acta*, 450-462.

Jacoby D, McKenna WJ. (2011). Genetics of inherited cardiomyopathy. *European Journal of Cardiology*, 296-304.

Jun YW, Park H2, Lee YK3, Kaang BK4, Lee JA3, Jang DJ1,2. (2016). D-AKAP1 is a signal-achored protein in the mitochondrial outer membrane. *FEBS* .

Kawamura S, Miyamoto S, Brown JH. (2003). Initiation and transduction of stretch-induced RhoA and Rac1 activation through caveolae: cytoskeletal regulation of ERK translocation. *J Biol Chem.*, 31111-31117.

Kino T, Souvatzoglou E, Charmandari E, Ichijo T, Driggers P, Mayers C, Alatsatianos A, Manoli I, Westphal H, Chrousos GP, Segars JH. (2006). Rho family Guanine nucleotide exchange factor Brx couples extracellular signals to the glucocorticoid signaling system.

Kirschner LS, Yin Z, Jones GN, Mahoney E. (2009). Mouse models of altered protein kinase A signaling. *Endocrine-Related Cancer*, 773-793.

Klussmann E, Edemir B, Pepperle B, Tamma G, Henn V, Klauschenz E, Hundsrucker C, Maric K, Rosenthal W. (2001). Ht31: the first protein kinase A anchoring protein to integrate protein kinase A and Rho signaling. FEBS Lett. 2001 Nov 2;507(3):264-8.

Koide H, Holmbeck K2, Lui JC3, Guo XC1, Driggers P1, Chu T1, Tatsuno I4, Quaglieri C1, Kino T1, Baron J3, Young MF2, Robey PG2, Segars JH1. (2015). Mice Deficient in AKAP13 (BRX) Are Osteoporotic and Have Impaired Osteogenesis.

Kondadi AK, Wang S, Montagner S, Kladt N, Korwitz A, Martinelli P, Herholz D, Baker MJ, Schauss AC, Langer T, Rugarli EI. (2014). Loss of the m-AAA protease subunit AFG_3 L_2 causes mitochondrial transport defects and tau hyperphosphorylation. *EMBO J. 2014 May 2;33(9):1011-26. doi: 10.1002/embj.201387009. Epub 2014 Mar 28.*

Konhilas JP, Leinwand LA. (2007). The effects of biological sex and diet on the development of heart failure. *Circulation*, 2747-2759.

Lang RM, Bierig M, Devereux RB, Flachskampf FA, Foster E, Pellikka PA, Picard MH, Roman MJ, Seward J, Shanewise J, Solomon S, Spencer KT, St John Sutton M, Stewart W; American Society of Echocardiography's Nomenclature and Standards Committee; Task Force on Chamber Quantification; American College of Cardiology Echocardiography Committee; American Heart Association; European Association of Echocardiography, European Society of Cardiology. (2006). Recommendations for chamber quantification. Eur J Echocardiogr (2006) 7 (2): 79-108. DOI: https://doi.org/10.1016/j.euje.2005.12.014
Published: 01 March 2006 Article history

Lenoir M, Sugawara M1, Kaur J1, Ball LJ2, Overduin M3. (2014). Structural insights into the acctivation of the RhoA GTPase by the lymphoid blast crisis (Lbc) oncoprotein. *J Biol Chem*, 23992-24004.

Leone TC, Lehman JJ, Finck BN, Schaeffer PJ, Wende AR, Boudina S, Courtois M, Wozniak DF, Sambandam N, Bernal-Mizrachi C, Chen Z, Holloszy JO, Medeiros DM, Schmidt RE, Saffitz JE, Abel ED, Semenkovich CF, Kelly DP. (2005). PGC-1 deficient mice exhibit multi-system energy metabolic derangements: Muscle

dysfunction, abnormal weight control, and hepatic steatosis. PLoS Biol. 3: 672–687.

Liu P, Jenkins NA, Copeland NG. (2003). A highly efficient recombineering-based method for generating conditional knockout mutations. *Genome Res.*, 476-84.

Lu D, Ma Y, Zhang W, Bao D, Dong W, Lian H, Huang L, Zhang L. (2012). Knockdown of cytochrome P450 2E1 inhibits oxidative stress and apoptosis in the cTnT(R141W) dilated cardiomyopathy transgenic mice. Hypertension. 2012 Jul;60(1):81-9. doi: 10.1161/HYPERTENSIONAHA.112.191478. Epub 2012 Jun 4.

Majumdar M, Seasholtz TM, Buckmaster C, Toksoz D, Brown JH. (1999). A rho exchange factor mediates thrombin and Ga12-induced cytoskeletal responses. *J Biol Chem*, 26815-26821.

Maltecca F, De Stefani D, Cassina L, Consolato F, Wasilewski M, Scorrano L, Rizzuto R, Casari G. (2012). Respiratory dysfunction by AFG3L2 deficiency causes decreased mitochondrial calcium uptake via organellar network fragmentation. *Human Molecular Genetics*, 3858–3870.

Colledge M, Scott JD. (1999). AKAPs: from structure to function. *Trends in Cell Biology*, 216–221.

Martin OJ, Lai L, Soundarapandian MM, Leone TC, Zorzano A, Keller MP, Attie AD, Muoio DM, Kelly DP. (2014). A Role for Peroxisome Proliferator-Activated Receptor gamma Coactivator-1 in the Control of Mitochondrial Dynamics During Postnatal Cardiac Growth. *Circulation Research*, 626-636.

Mauban JR, O'Donnell M, Warrier S, Manni S, Bond M. (2009). AKAP-scaffolding proteins and regulation of cardiac physiology. Physiology (Bethesda). 2009 Apr;24:78-87. doi: 10.1152/physiol.00041.2008.

Mayers CM, Wadell J, McLean K, Venere M, Malik M, Shibata T, Driggers PH, Kino T, Guo XC, Koide H, Gorivodsky M, Grinberg A, Mukhopadhyay M, Abu-Asab M, Westphal H, Segars JH. (2010). The Rho guanine nucleotide exchange factor AKAP13 (BRX) is essential for cardiac development in mice. *JBC*.

Miano JM, Ramanan N, Georger MA, de Mesy Bentley KL, Emerson RL, Balza RO Jr, Xiao Q, Weiler H, Ginty DD, Misra RP. (2004). Restricted inactivation of serum response factor to the cardiovascular system. *PNAS*, 17132–17137.

Montaner S, Perona R, Saniger L, Lacal JC. (1999). Activation of serum response factor by RhoA is mediated by the nuclear factor-kappaB and C/EBP transcription factors. *J Biol Chem. 1999 Mar 26;274(13):8506-15.*

B. A. Naaijkens,corresponding author P. A. J. Krijnen, E. Meinster, E. N. ter Horst, K. Vo, R. J. P. Musters, O. Kamp, H. W. M. Niessen, L. J. M. Juffermans, and A. van Dijk (2015). Acute myocardial infarction does not affect functional characteristics of adipose-derived stem cells in rats, but reduces the number of stem cells in adipose tissue. *Cell Tissue Research*, 623–632.

NHLBI. (2010). *The Heart Truth.* Washington, D.C.: United States Department of Health and Human Services.

Barbosa-Morais NL, Irimia M, Pan Q, Xiong HY, Gueroussov S, Lee LJ, Slobodeniuc V, Kutter C, Watt S, Colak R, Kim T, Misquitta-Ali CM, Wilson MD, Kim PM, Odom DT, Frey BJ, Blencowe BJ. (2012). The Evolutionary Landscape of Alternative Splicing in Vertebrate Species . *Science*.

O'Connor KL, Chen M, Towers LN. (2012). Integrin α6β4 cooperates with LPA signaling to stimulate Rac through AKAP-Lbc-mediated RhoA activation.*American Journal of Physiology Cell Physiology*.

Oishi A, Makita N, Sato J, Iiri T. (2012). Regulation of RhoA Signaling by the cAMP-dependent Phosphorylation of RhoGDIα. *The Journal of Biological Chemistry*, 38705-38715.

Park B, Nguyen NT, Dutt P, Merdek KD, Bashar M, Sterpetti P, Tosolini A, Testa JR, Toksoz D. (2002). Association of Lbc Rho Guanine Nucleotide Exchange Factor with α- Catenin-related Protein, α-Catulin/CTNNAL1, supports Serum Response Factor activation. *J Biol. Chem.*, 45361-45370.

Petroff MG, Kim SH, Pepe S, Dessy C, Marbán E, Balligand JL, Sollott SJ. (2001). Endogenous nitric oxide mechanisms mediate the stretch dependence of Ca+2 release in cardiomyocytes. *Nat Cell Biol.*, 867-873.

Pilote L, Dasgupta K, Guru V, Humphries KH, McGrath J, Norris C, Rabi D, Tremblay J, Alamian A, Barnett T, Cox J, Ghali WA, Grace S, Hamet P, Ho T, Kirkland S, Lambert M, Libersan D, O'Loughlin J, Paradis G, Petrovich M, Tagalakis V. (2007). A comprehensive view of sex-specific issues related to cardiovascular disease. *CMAJ.*, S1-44.

Pruitt KD, Brown GR, Hiatt SM, Thibaud-Nissen F, Astashyn A, Ermolaeva O, Farrell CM, Hart J, Landrum MJ, McGarvey KM, Murphy MR, O'Leary NA, Pujar S, Rajput B, Rangwala SH, Riddick LD, Shkeda A, Sun H, Tamez P, Tully RE, Wallin C, Webb D, Weber J, Wu W, DiCuccio M, Kitts P, Maglott DR, Murphy TD, Ostell JM. (2013). RefSeq: an update on mammalian reference sequences. *Nucleic Acids Res.*, 756-763.

Qiao J, Huang F, Lum H. (2003). PKA inhibits RhoA activation: a protection mechanism against endothelial barrier dysfunction. *Am J Physiol Lung Cell Mol Physiol.*, 72-80.

Rogers R, Norian J, Malik M, Christman G, Abu-Asab M, Chen F, Korecki C, Iatridis J, Catherino WH, Tuan RS, Dhillon N, Leppert P, Segars JH. (2008). Mechanical homeostasis is altered in uterine leiomyoma. *Am J Obstet Gynecol.*, e1-11.

Rubino D, Driggers P, Arbit D, Kemp L, Miller B, Coso O, Pagliai K, Gray K, Gutkind S, Segars J. (1998). Characterization of Brx, a novel Dbl family member that modulates estrogen receptor action.*Oncogene*.

Ruwhof C, van der Laarse A. (2000). Mechanical stress-induced cardiac hypertrophy: mechanisms and signal transduction pathways. *Cardiovasc Res.*, 23-37.

Sadeghi A, Doyle AD, Johnson BD. (2002). Regulation of the cardiac L-type Ca2 channel by the actin-binding proteins -actinin and dystrophin. Am. J. Physiol. Cell Physiol. 282, C1502–C1511.

Sah VP, Minamisawa S, Tam SP, Wu TH, Dorn GW 2nd, Ross J Jr, Chien KR, Brown JH. (1999). Cardiac-specific overexpression of RhoA results in sinus and atrioventricular nodal dysfunction and contractile failure. *J Clin Invest.*, 1627-34.

Sahai E, Alberts AS, Treisman R. (1998). RhoA effector mutants reveal distinct effector pathways for cytoskeletal reorganization, SRF activation and transformation. *EMBO J.*, 1350-1361.

Sauzeau V, Le Jeune H, Cario-Toumaniantz C, Smolenski A, Lohmann SM, Bertoglio J, Chardin P, Pacaud P, Loirand G. (2000). Cyclic GMP-dependent protein kinase signaling pathway inhibits RhoA-induced Ca2+ sensitization of contraction in vascular smooth muscle. J Biol Chem. 2000 Jul 14;275(28):21722-9.

Schmidt A, Hall A. (2002). Guanine nucleotide exchange factors for the Rho GTPases: turning on the switch. *Genes Dev.*, 1587-1609.

Scott JD, Santana LF. (2010). A-Kinase Anchoring Proteins: Getting to the Heart of the Matter. *Circulation*, 1264-1271.

Seeger TS, Frank D, Rohr C, Will R, Just S, Grund C, Lyon R, Luedde M, Koegl M, Sheikh F, Rottbauer W, Franke WW, Katus HA, Olson EN, Frey N. (2010). Myozap, a novel intercalated disc protein, activates serum response factor-dependent signaling and is required to maintain cardiac function in vivo.*Circulation Research*.

Segars JH, Marks MS, Hirschfeld S, Driggers PH, Martinez E, Grippo JF, Brown M, Wahli W, Ozato K. (1993). Inhibition of Estrogen-Responsive Gene Activation by the Retinoid X Receptor ,B: Evidence for Multiple Inhibitory Pathways. *Molecular and Cellular Biology*, 2258-2268.

Nagueh SF, Smiseth OA, Appleton CP, Byrd BF 3rd, Dokainish H, Edvardsen T, Flachskampf FA, Gillebert TC, Klein AL, Lancellotti P, Marino P, Oh JK, Alexandru Popescu B, Waggoner AD (2009). Recommendations for the Evaluation of Left Ventricular Diastolic Function by Echocardiography: An Update from the American Society of Echocardiography and the European Association of Cardiovascular Imaging.*Sherif F. Nagueh, MD, Chair†*, 165–193.

Sohal DS, Nghiem M, Crackower MA, Witt SA, Kimball TR, Tymitz KM, Penninger JM, Molkentin JD. (2001). Temporally Regulated and Tissue-Specific Gene Manipulations in the Adult and Embryonic Heart Using a Tamoxifen-Inducible Cre Protein. *Circulation Research*, 20-25.

Sterpetti P, Hack AA, Bashar MP, Park B, Cheng SD, Knoll JH, Urano T, Feig LA, Toksoz D. (1999). Activation of the Lbc Rho exchange factor proto-oncogene by truncation of an extended C terminus that regulates transformation and targeting. *Mol Cell Biol*, 1334-1345.

Li S, Xu S, Roelofs BA, Boyman L, Lederer WJ, Sesaki H, Karbowski M. (2015). Transient assembly of F-actin on the outer mitochondrial membrane contributes to mitochondrial fission. *The Journal of Cell Biology*, 109-123.

Taglieri DM, Johnson KR, Burmeister BT, Monasky MM, Spindler MJ, DeSantiago J, Banach K, Conklin BR, Carnegie GK. (2014). The C-terminus of the long AKAP13 isoform (AKAP-Lbc) is critical for development of compensatory cardiac

hypertrophy. J Mol Cell Cardiol. 2014 Jan;66:27-40. doi: 10.1016/j.yjmcc.2013.10.010.

Teramoto H, Malek RL, Behbahani B, Castellone MD, Lee NH, Gutkind JS. (2003). Identification of H-Ras, RhoA, Rac1, and Cdc2 responsive genes. *Oncogene*, 2689-2697.

Toksoz D, Williams DA. (1994). Novel human oncogene lbc detected by transfection with distinct homology regions to signal transduction products. Oncogene. 1994 Feb;9(2):621-8.

Uhlen M, Oksvold P, Fagerberg L, Lundberg E, Jonasson K, Forsberg M, Zwahlen M, Kampf C, Wester K, Hober S, Wernerus H, Björling L, Ponten F. (2010). Towards a knowledge-based Human Protein Atlas. *Nature Biotechnology*, 1248-1250.

Uhlén M, Fagerberg L, Hallström BM, Lindskog C, Oksvold P, Mardinoglu A, Sivertsson Å, Kampf C, Sjöstedt E, Asplund A, Olsson I, Edlund K, Lundberg E, Navani S, Szigyarto CA, Odeberg J, Djureinovic D, Takanen JO, Hober S, Alm T, Edqvist PH, Berling H, Tegel H, Mulder J, Rockberg J, Nilsson P, Schwenk JM, Hamsten M, von Feilitzen K, Forsberg M, Persson L, Johansson F, Zwahlen M, von Heijne G, Nielsen J, Pontén F. (2015). Proteomics. Tissue-based map of the human proteome. . *Science*, 1260419-1-1260419-9.

Salim S. Virani, MD, A. Nasser Khan, MD, Cesar E. Mendoza, MD, Alexandre C. Ferreira, MD, and Eduardo de Marchena, MD (2007). Takotsubo Cardiomyopathy, or Broken-Heart Syndrome. *Tex Heart Inst J.*, 76–79.

Yujuan Wang, Jakub W. Hanus, Mones S. Abu-Asab,4Defen Shen, Alexander Ogilvy, Jingxing Ou, Xi K. Chu, Guangpu Shi, Wei Li, Shusheng Wang, and Chi-Chao Chan,* (2016). NLRP3 Upregulation in Retinal Pigment Epithelium in Age-Related Macular Degeneration. *International Journal of Molecular Sciences*.

Peter A. Watson, Nicholas Birdsey, Gordon S. Huggins, Eric Svensson, Daniel Heppe, Leslie Knaub (2010). Cardiac-specific overexpression of dominant-negative CREB leads to increased mortality and mitochondrial dysfunction in female mice. *Am J Physiol Heart Circ Physiol*.

Wei L1, Zhou W, Croissant JD, Johansen FE, Prywes R, Balasubramanyam A, Schwartz RJ. (1998). RhoA signaling via serum response factor plays an obligatory role in myogenic differentiation. *J Biol Chem*, 30287-30294.

Welch EJ1, Jones BW, Scott JD. (2010). Networking with AKAPs. *Mol Interv.*, 86-97.

Wheeler-Jones. (2005). Cell signalling in the cardiovascular system: an overview. *Heart* , 1366-1374.

Wilson CR1, Tran MK, Salazar KL, Young ME, Taegtmeyer H. (2007). Western diet, but not high fat diet, causes derangements of fatty acid metabolism and contractile dysfunction in the heart of Wistar rats. *Biochem J.*, 457-467.

Wirtenberger M, Tchatchou S, Hemminki K, Klaes R, Schmutzler RK, Bermejo JL, Chen B, Wappenschmidt B, Meindl A, Bartram CR, Burwinkel B. (2006). Association of genetic variants in the Rho guanine nucleotide exchange factor AKAP13 with familial breast cancer.Carcinogenesis. 2006 Mar;27(3):593-8. Epub 2005 Oct 18.

Wong W, Scott JD. (2004). AKAP signalling complexes: focal points in space and time. *Nature Reviews Molecular Cell Biology*, 959-970.

Wu B, Zhou B, Wang Y, Cheng HL, Hang CT, Pu WT, Chang CP, Zhou B. (2010). Inducible Cardiomyocyte-Specific Gene Disruption Directed by the Rat Tnnt2 Promoter in the Mouse. *Genesis*, 63–72.

Yamasaki R, Wu Y, McNabb M, Greaser M, Labeit S, Granzier H. (2002). Protein kinase A phosphorylates titin's cardiac-specific N2B domain and reduces passive tension in rat cardiac myocytes. *Circ Res. 2002 Jun 14;90(11):1181-8.*

Zarubin T, Han J. (2005). Activation and signaling of the p38 MAP kinase pathway. Cell Res. 2005 Jan;15(1):11-8.

APPENDIX A

The following pages of this appendix contain supplementary figures and tables referenced in this dissertation. The nomenclature for supplementary figures includes an “S” in the figure code. The nomenclature for supplementary tables includes “ST” in the table code.

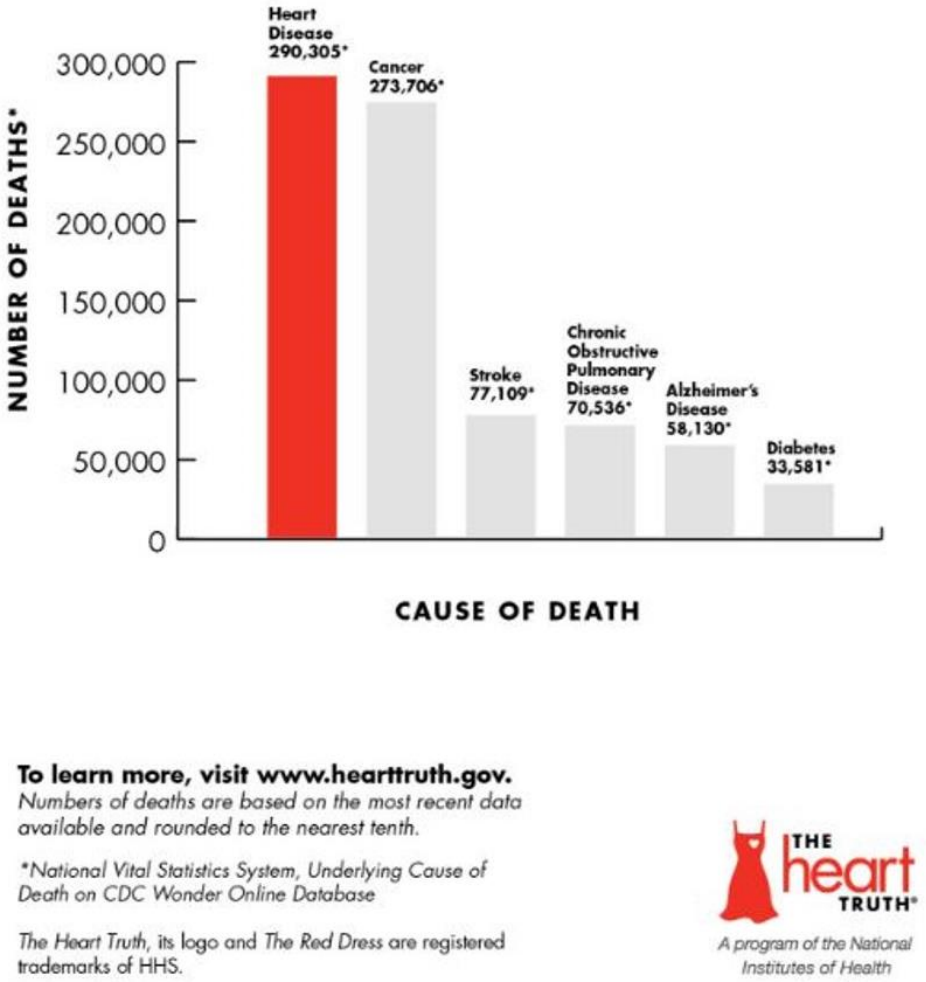

Figure S.1| **Heart Disease Statistics.** In the United States of America, heart disease is the number one cause of death in women. In 2010, it was estimated that one in four women died of cardiovascular disease (NHLBI, 2010).

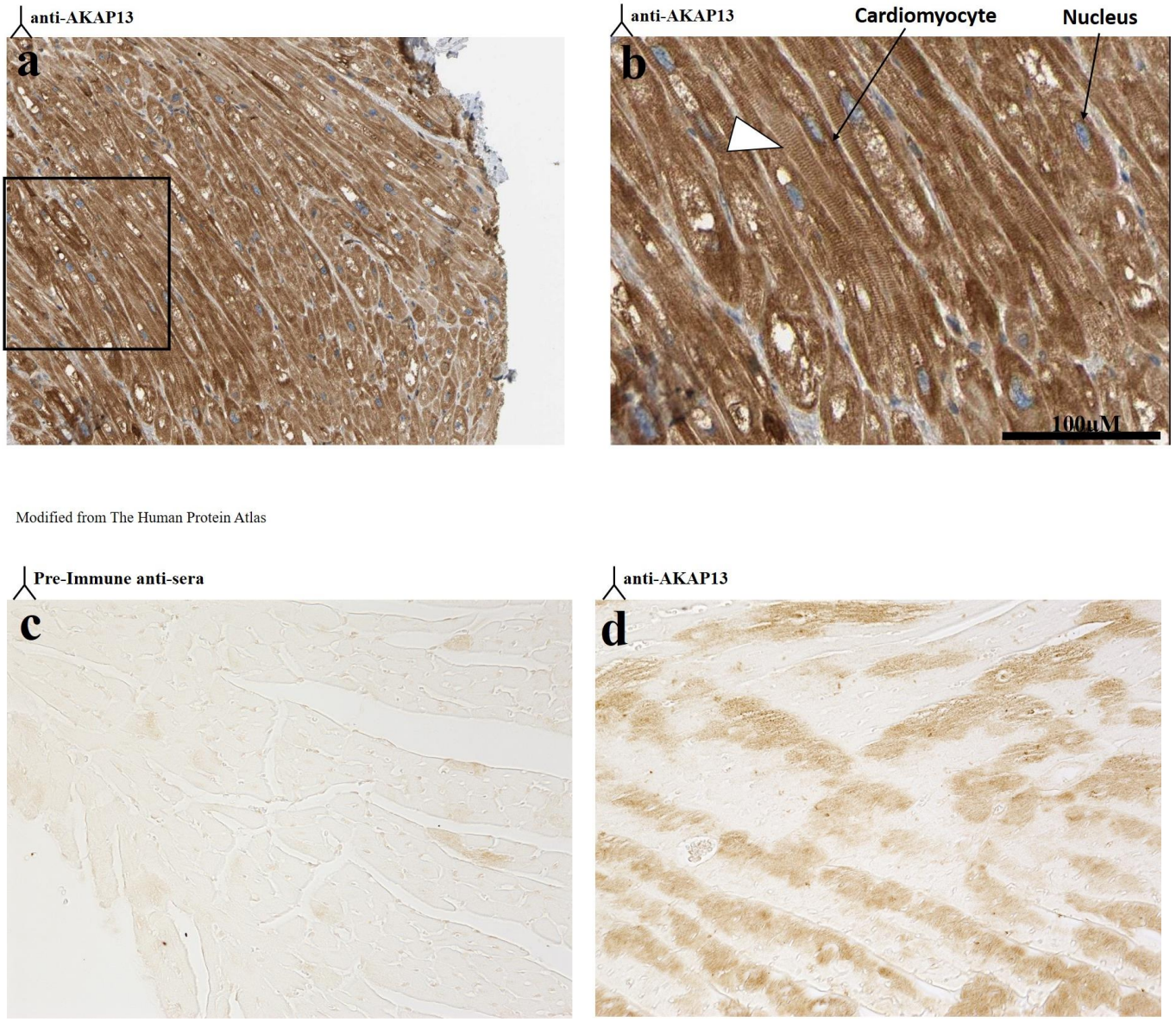

Figure S.2| **AKAP13 in adult myocardium.** a) Immunohistochemistry, Adult human myocardium showed strong protein staining for AKAP13. b) Enlargement of previous showed a striated AKAP13 banding pattern. c) Immunohistochemistry, Adult mouse myocardium with Pre-immune anti-sera. d) Immunohistochemistry, Adult mouse myocardium with anti-AKAP13 demonstrated strong AKAP13 presence.

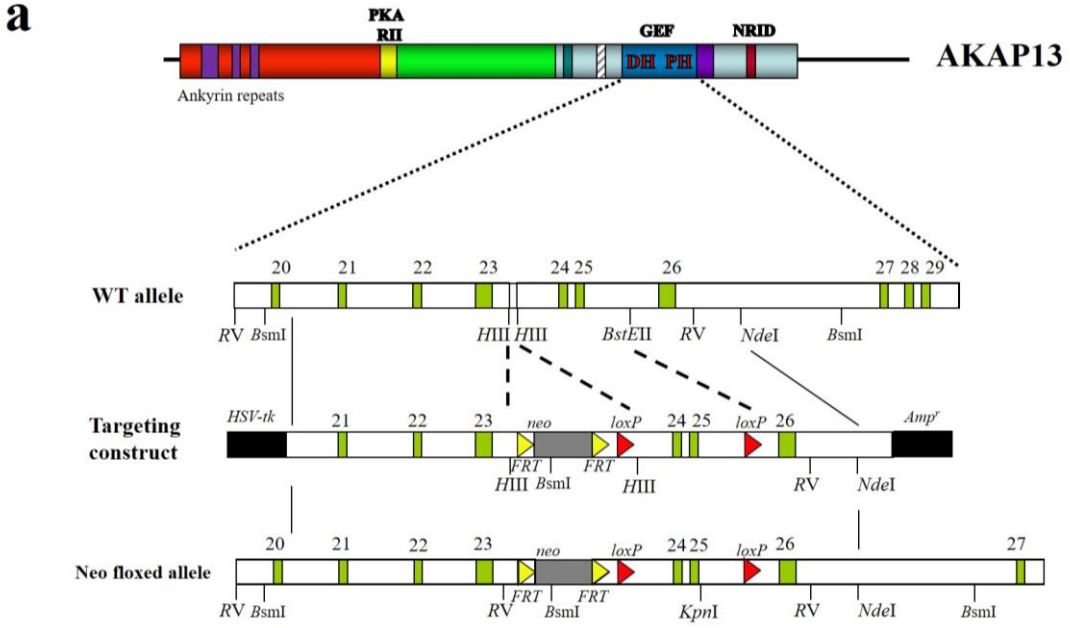
a
PKA
RII
GEF
NRID
AKAP13
Ankyrin repeats
DH PH
WT allele
Targeting construct
Neo floxed allele
HSV-tk
neo
loxP
FRT
Ampr
RV
BsmI
HIII
BstEII
NdeI
KpnI

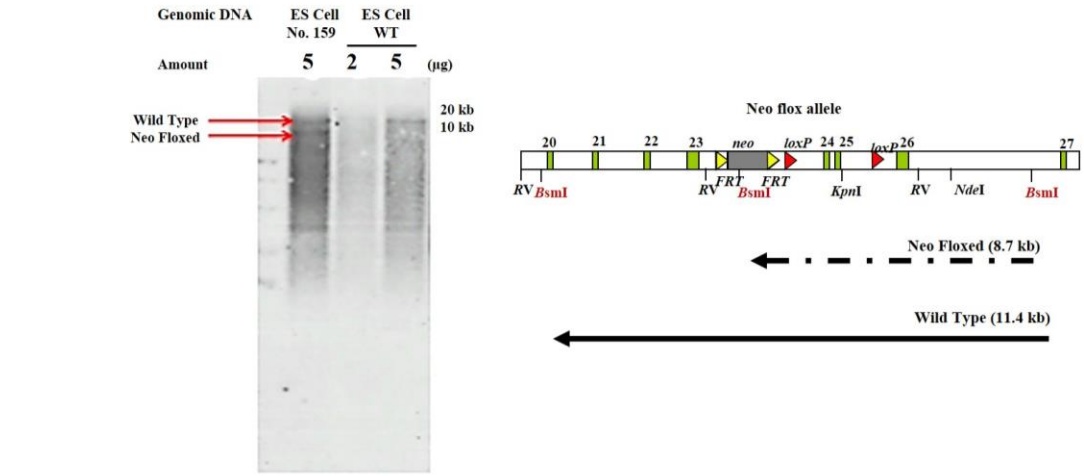
b
Genomic DNA
ES Cell No. 159
ES Cell WT
Amount
5
2
5
(µg)
Wild Type
Neo Floxed
20 kb
10 kb
Neo flox allele
Neo Floxed (8.7 kb)
Wild Type (11.4 kb)

c

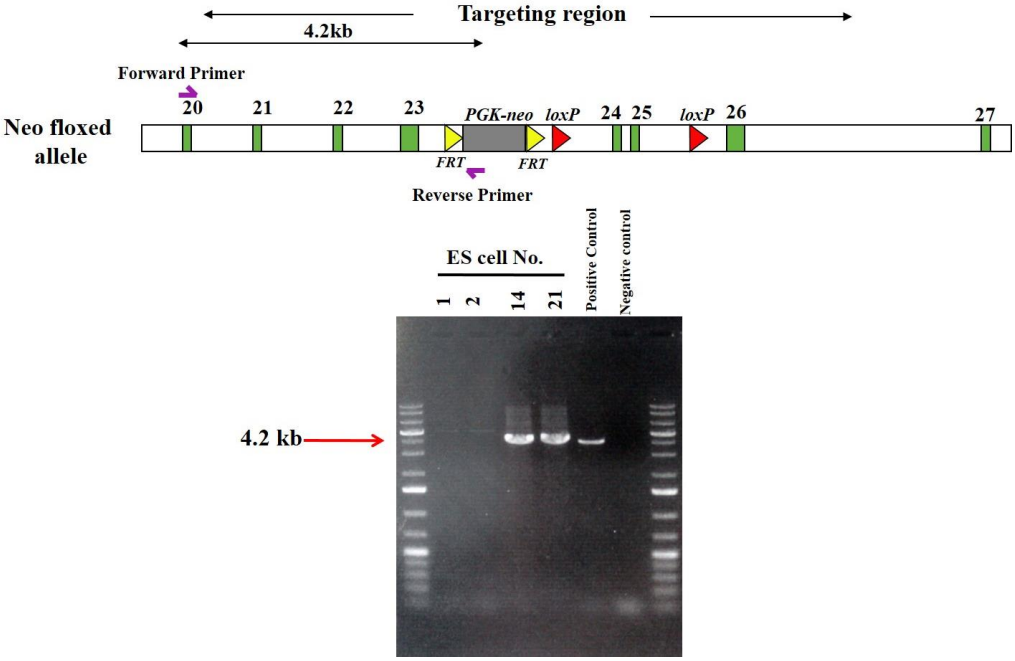
Targeting region
4.2kb
Forward Primer
Neo floxed allele
20
21
22
23
PGK-neo
loxP
24
25
loxP
26
27
FRT
FRT
Reverse Primer
ES cell No.
1
2
14
21
Positive Control
Negative control
4.2 kb

d

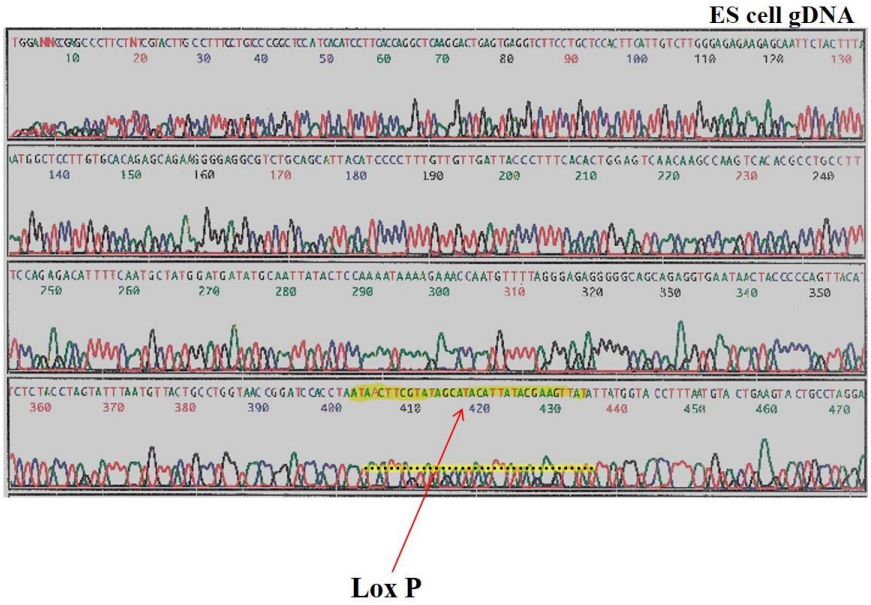
ES cell gDNA
Lox P

e

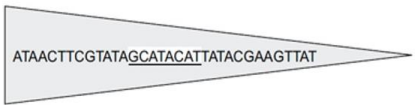
ATAACTTCGTATAGCATACATTATACGAAGTTAT

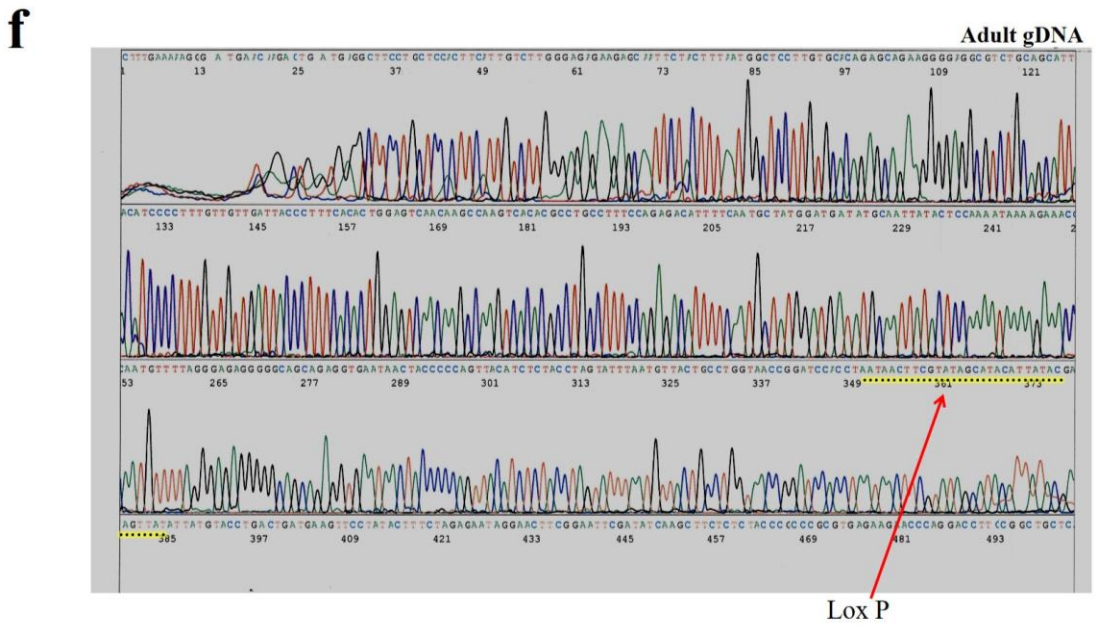

Figure S.3| **Establishment and validation of *Akap13* conditional knockout**. a) Targeting construct and floxed allele, A Cre-lox recombination strategy was used for targeted deletion of the GEF domain. The dashed lines show the areas of recombination between the WT allele and the targeting construct which resulted in the Neo floxed allele. FRT sites flanked the neomycin cassette and LoxP sites flanked the sequence designated for deletion, including exons 24 and 25 and adjacent regions. b) Southern Blot, BsmI digestion of ES Cell gDNA for validation of the neo floxed allele. c) Polymerase Chain Reaction (PCR), PCR validation of neo floxed allele; the desired PCR product size for the neo floxed allele was 4.2kb. d) Sequencing Analysis, sequence file shown is for ES cell gDNA validation of LoxP. e) Graphic showing LoxP sequence and directionality. f) Sequencing Analysis, sequence file shown for adult mouse gDNA validation of LoxP. Dotted, yellow line shows LoxP.

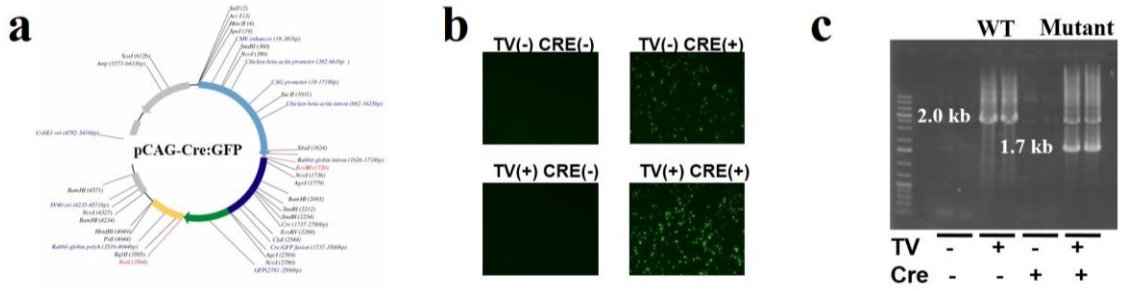

Figure S.4| **In vitro validation of recombination.** a) pCAG-Cre:GFP vector used for transfection of competent cells. b) Validation of targeting vector (TV) and pCAG-CRE:GFP vector through fluorescence. C) PCR, validation of desired recombination event. The PCR product for the mutant (floxed) allele is 1.7kb whereas the WT allele is 2.0kb.

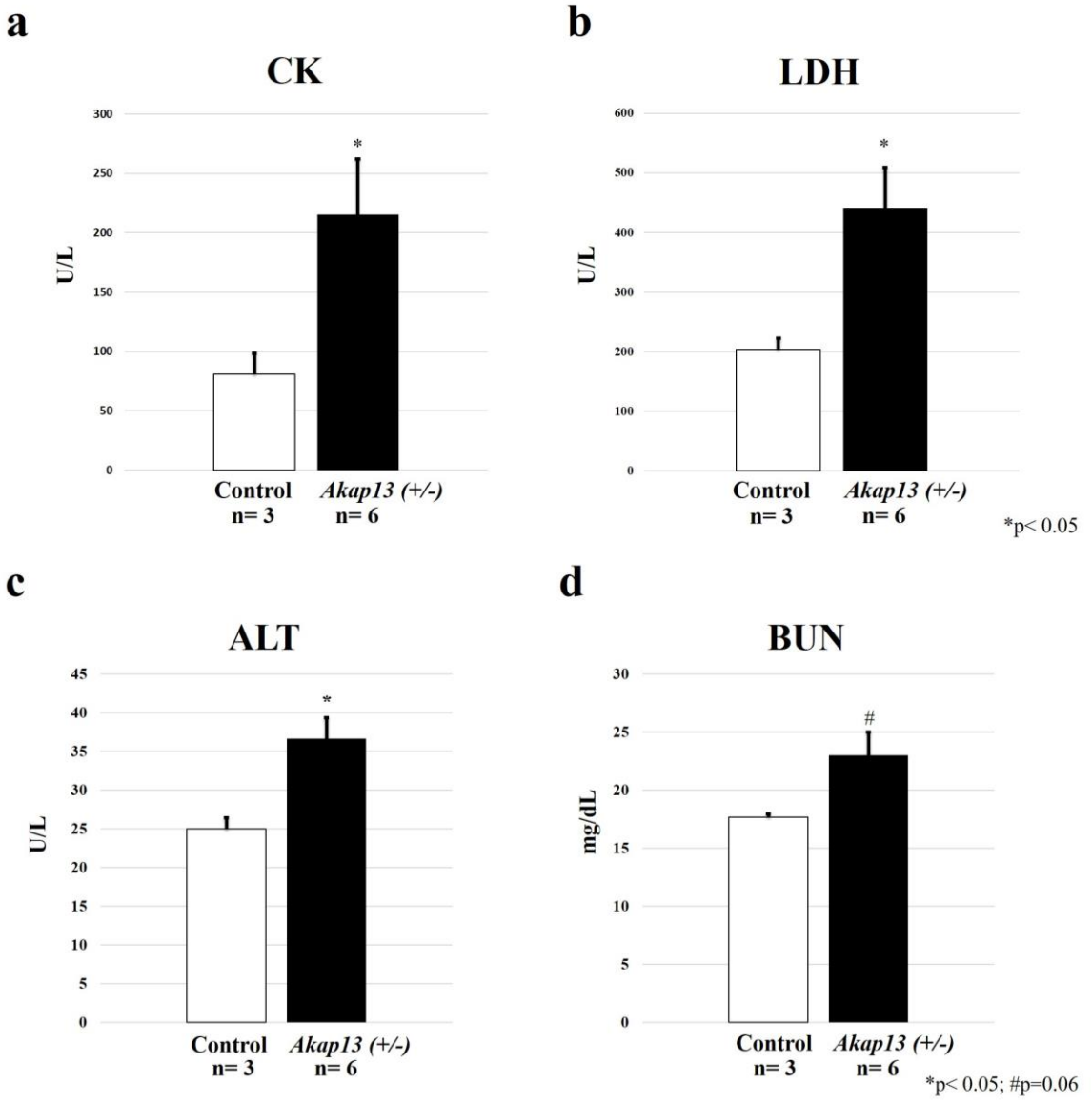

Figure S.5| **Blood Chemistry demonstrated multi-organ dysfunction in global *Akap13 (+/-) mice*.** a) Blood levels of Creatine Kinase (CK) indicated muscle damage in the *Akap13 (+/-)* mice compared to control mice ($p<0.05$). Historically, CK blood levels were used to diagnose myocardial infarction (MI).
b) Lactate Dehydrogenase (LDH) was increased in *Akap13 (+/-)* mice compared to control mice which suggested tissue damage ($p<0.05$). c) Alanine Aminotransferase (ALT) blood levels were elevated in *Akap13 (+/-)* mice compared to control mice ($p<0.05$). This indicated liver function may have been impaired in the haploinsufficient mice. d) Blood urea nitrogen (BUN) levels suggested kidney function was impaired in the *Akap13 (+/-)* mice compared to control mice ($p=0.06$).

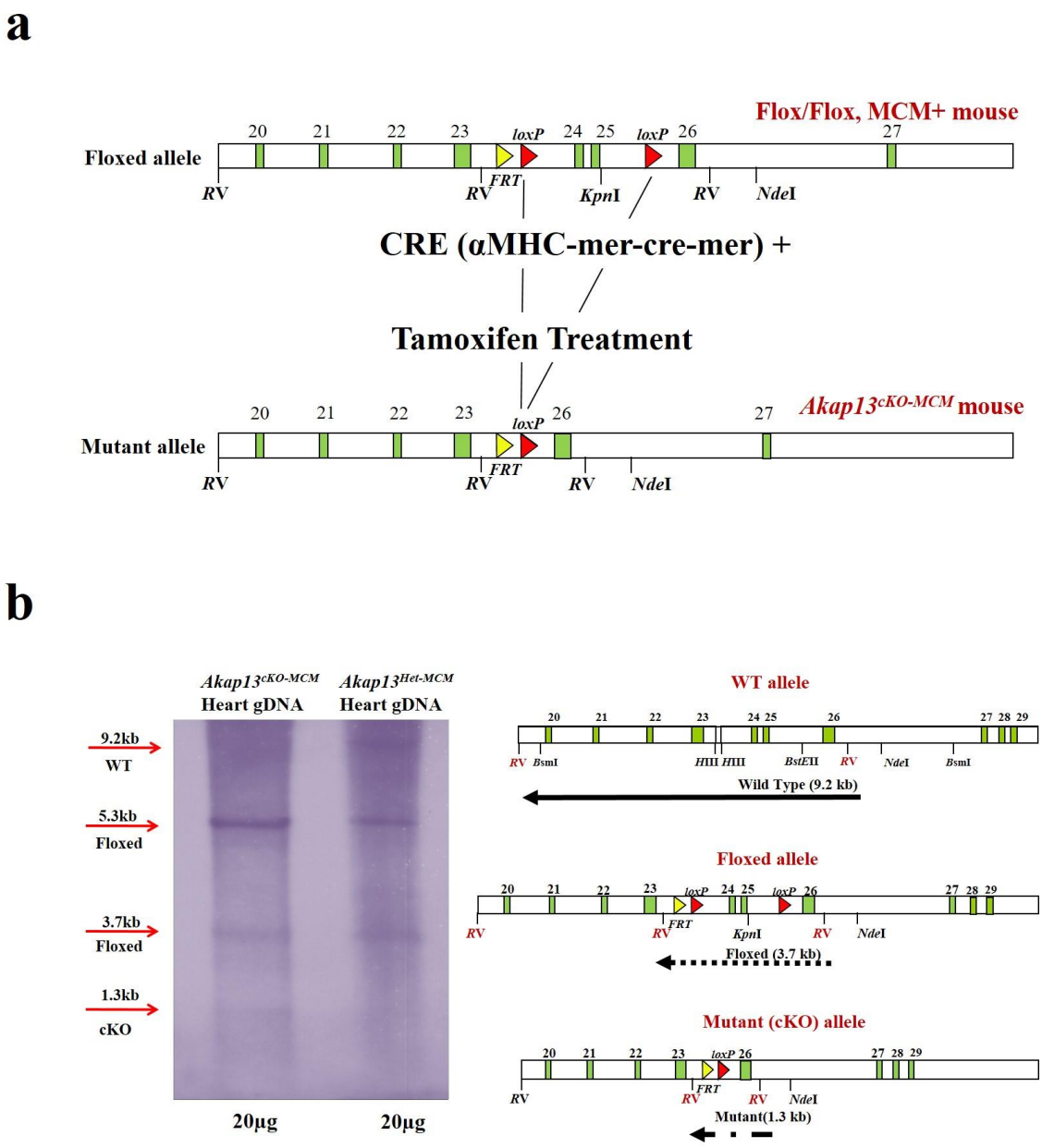

Figure S.6|**Southern Blot showed mutant allele in *Akap13*$^{cKO\text{-}MCM}$ mouse hearts.** a) Schematic diagram showing Cre-recombination of the floxed allele, induced by tamoxifen treatment, to produce the cardiomyocyte specific mutant allele. Red arrows indicate LoxP site(s). Yellow arrow indicates the FRT site. b) Southern blot showed the mutant (1.3kb) band in EcoRV digested gDNA from *Akap13*$^{cKO\text{-}MCM}$ mouse hearts, but was not readily visible in the *Akap13*$^{Het\text{-}MCM}$ hearts.

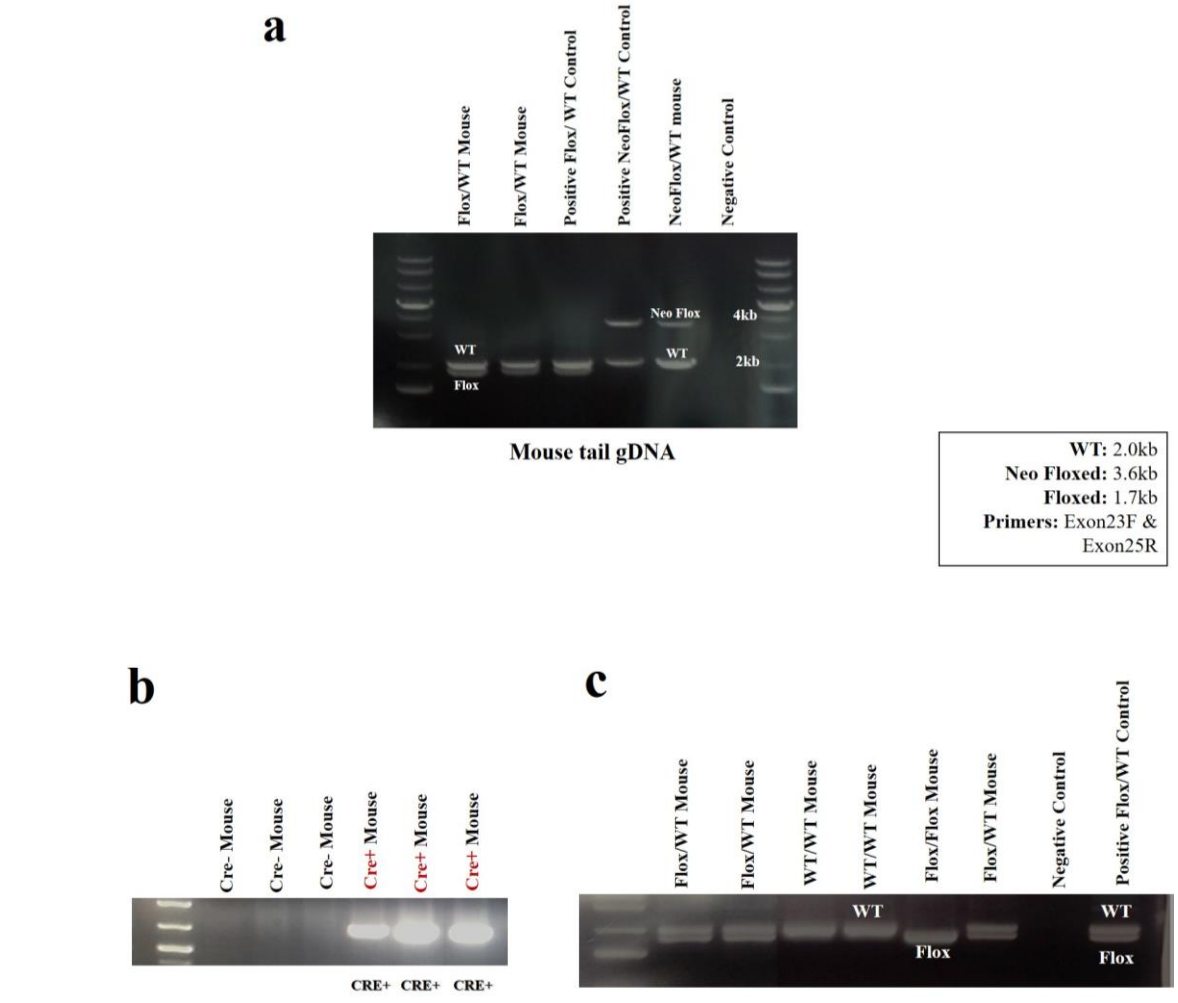

Figure S.7|**Genotyping.** a) PCR of mouse gDNA showed neo floxed (3.6kb), floxed (1.7 kb) and WT (2.0 kb) bands. b) PCR of mouse gDNA showed Cre positive bands (440bp). c) PCR of mouse gDNA showed homozygous floxed bands (1.7kb), homozygous WT bands (2.0kb), and heterozygous (Flox/WT) bands.

W/W, MCM+; TAM Diet v. Control, MCM+					
	W/W, MCM+		Control		p-value
LVEF	59.19	%	63.78	%	0.36
EDVI	2.67	µL/g	2.23	µL/g	0.30
ESVI	1.11	µL/g	0.81	µL/g	0.25
EDMI	3.89	mg/g	3.43	mg/g	0.32
ESMI	3.94	mg/g	3.30	mg/g	0.16
Total mice (n)	4		3		

Table ST.1|**Comparison of controls by Magnetic Resonance Imaging (MRI).** Here we showed W/W, MCM+ mice given tamoxifen compared with control mice expressing MCM. No statistical differences were observed with Magnetic Resonance Imaging (MRI) ($p>0.05$).

Control v. Control					
	Control < 8 weeks		Control ≥8 weeks		p-value
LVEF	65.98	%	66.83	%	0.73
EDVI	2.45	µL/g	2.13	µL/g	0.35
ESVI	0.84	µL/g	0.72	µL/g	0.45
EDMI	4.22	mg/g	3.88	mg/g	0.30
ESMI	3.68	mg/g	3.78	mg/g	0.79
Total mice (n)	3		6		

Table ST.2|**Comparison of controls by MRI.** Here we showed F/F, MCM- mice given tamoxifen compared with F/F, MCM+ mice on control chow. No statistical differences were observed with Magnetic Resonance Imaging (MRI) ($p>0.05$).

ECG Outcome	F/F, MCM-; Tam Diet	F/F, MCM+; Control Diet	p-value
Heart Rate (BPM)	442.36	446.63	0.93
QRS Interval (ms)	9.07	7.92	0.21
QTcB(ms)	47.23	41.03	0.14
QTcF(ms)	33.80	29.67	0.11
R Amplitude (µV)	618.79	712.53	0.27
ST Height (µV)	29.15	38.22	0.77
T Amplitude (µV)	66.85	112.67	0.29
Total mice (n)	8	4	

Table ST.3|**Comparison of controls by electrocardiogram (ECG).** Here we showed there were no statistical differences between types of control mice: F/F, MCM- given tamoxifen chow and F/F, MCM+ given control chow ($p>0.05$).

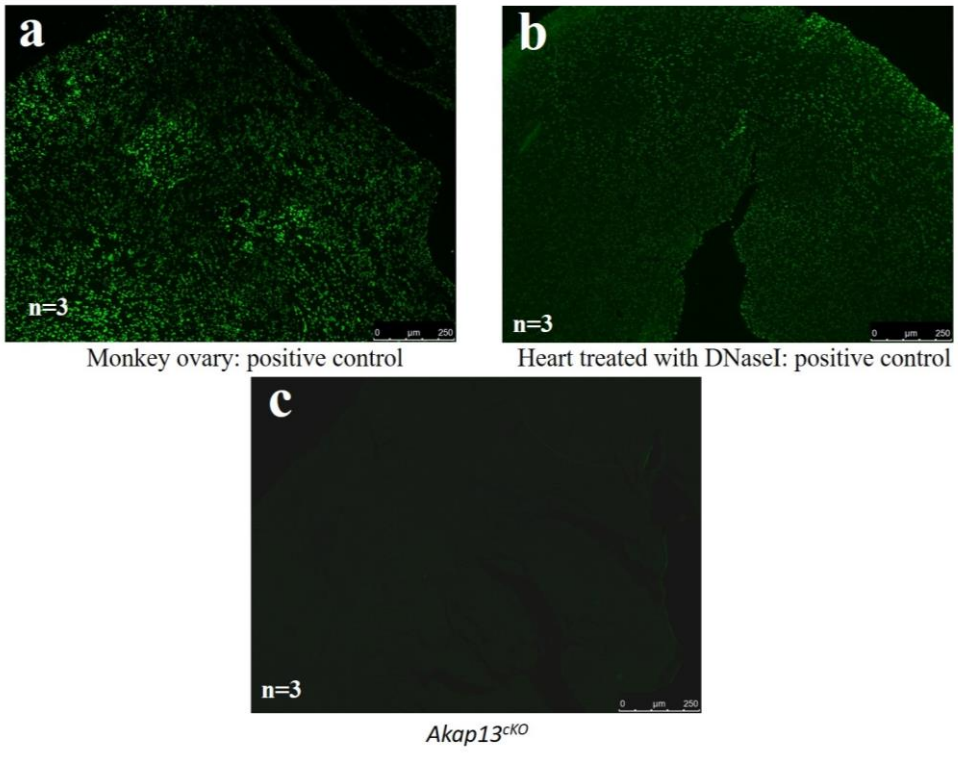

Figure S.8| **TUNEL showed no increase in apoptosis in *Akap13*$^{cKO\text{-}MCM}$ mouse hearts.** a) Monkey ovary was used as an intrinsically positive TUNEL control. b) Heart tissue sections treated with DNaseI for positive TUNEL control. c) *Akap13*$^{cKO\text{-}MCM}$ mouse hearts showed no increase in apoptosis.

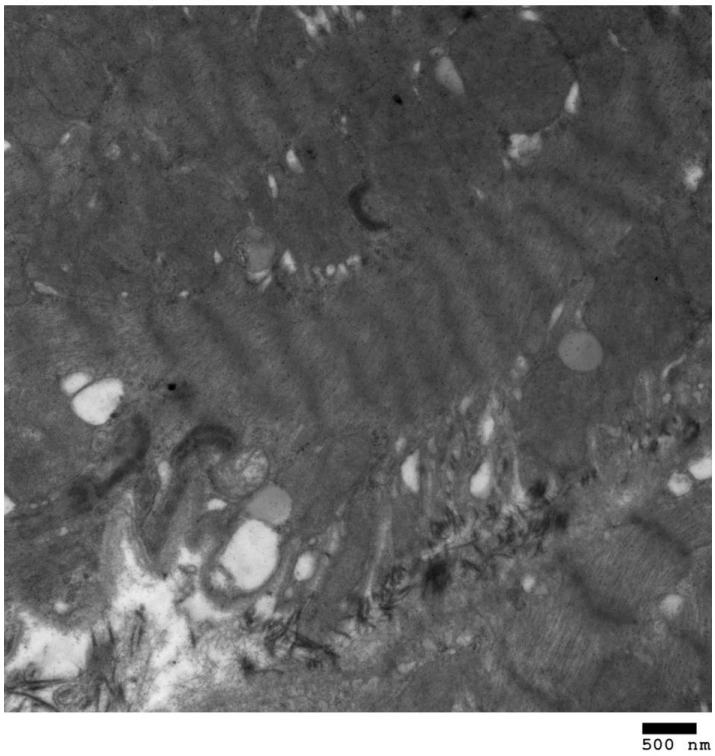

Figure S.9| **Sarcomeric disruption and increased lipid inclusions in *Akap13^{cKO}* mouse cardiac tissue.** Electron microscopy revealed significant disruption of the cardiac sarcomeres and ultrastructure. Lipid inclusions were also seen with increased frequency in Akap13^{cKO} mouse cardiac tissue compared to control mouse cardiac tissue.

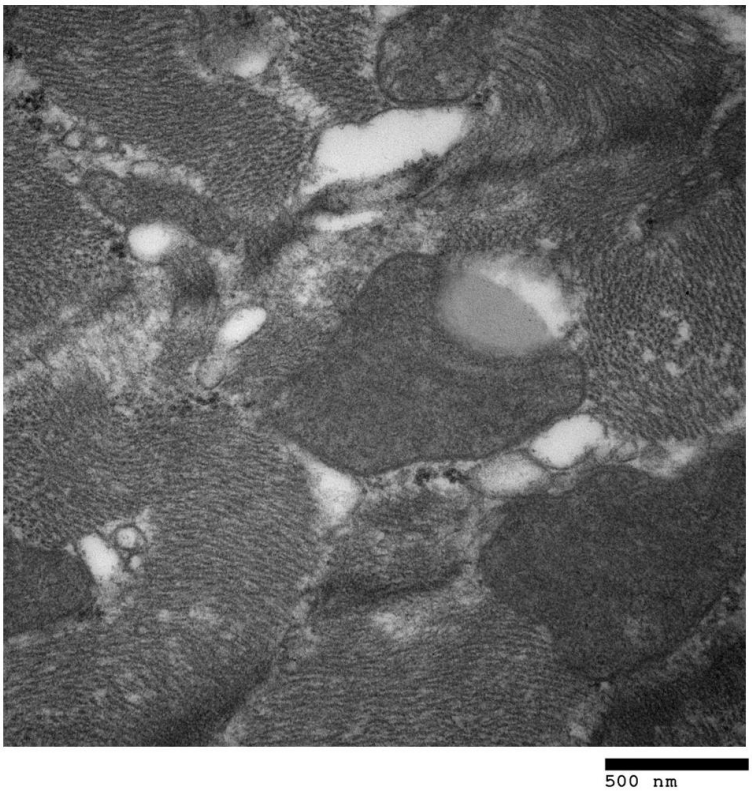

Figure S.10| **Increased lipid droplets in *Akap13*^{cKO} mouse cardiac tissue.** Electron micrograph, showed increased lipid droplets and blind ended sarcomeres.

Resting MRI			
	Control	***Akap13*** $^{cKO\ Het\text{-}MCM}$	**p-value**
LVEF (%)	63.79	60.07	0.33
EDVI (µL/g)	2.41	2.37	0.87
ESVI (µL/g)	0.88	0.97	0.65
EDMI (mg/g)	3.90	3.87	0.95
ESMI (mg/g)	3.88	3.81	0.84
Total Mice (n)	5	11	

Table ST.5| **Resting MRI Summary Table for *Akap13*$^{Het\text{-}MCM}$ mice.** No significance was seen when *Akap13*$^{Het\text{-}MCM}$ mice where analyzed as a group.

Stress MRI						
	Male			Female		
	Akap13 $^{cKO\ Het\text{-}MCM}$	Control	p-value	*Akap13* $^{cKO\ Het\text{-}MCM}$	Control	p-value
LVEF-10 (µg/mg/min)	73.81	73.34	0.87	61.1	76.43	0.0073
LVEF-40 (µg/mg/min)	78.88	79.55	0.87	68.00	83.76	0.00079
Total Mice (n)	3	5		6	8	

Table ST.6| **Stress MRI Summary Table for *Akap13*$^{Het\text{-}MCM}$ mice.** Significant differences are seen in female *Akap13*$^{Het\text{-}MCM}$ mice only.

Right Ventricular Assessment			
	Control	***Akap13*** $^{cKO\text{-}MCM}$	**p-value**
RVEF (%)	67.35	59.21	0.0000028
EDVI (µL/g)	1.50	1.78	0.035
ESVI (µL/g)	0.49	0.73	0.00012
Total Mice (n)	14	15	

Right Ventricular Assessment			
	Control	***Akap13*** $^{cKO\ Het\text{-}MCM}$	**p-value**
RVEF (%)	60.87	60.2	0.85
EDVI (µL/g)	1.60	1.64	0.88
ESVI (µL/g)	0.65	0.65	1.00
Total Mice (n)	6	11	

Table ST.7| **Resting MRI Summary Table for right ventricular function** Top) statistical differences in right ventricular function between *Akap13*$^{cKO\text{-}MCM}$ and control mice. Bottom) No statistical differences were seen in *Akap13*$^{Het\text{-}MCM}$ mice compared to control mice.

Right Ventricular Assessment						
	Male			Female		
	Control	*Akap13* ^{cKO}	p-value	Control	*Akap13* ^{cKO}	p-value
RVEF (%)	66.23	59.42	0.011	68.19	58.97	0.00015
EDVI (µL/g)	1.53	1.73	0.33	1.48	1.84	0.059
ESVI (µL/g)	0.51	0.71	0.046	0.47	0.75	0.0013
Total mice (n)	6	8		8	7	

Table ST.8| **Resting MRI Summary Table for right ventricular function in *Akap13*$^{cKO\text{-}MCM}$ mice.** a) Overall, *Akap13*$^{cKO\text{-}MCM}$ mice showed significant differences in all right ventricular measurements compared to control mice. b) Summary of right ventricular function stratified based on sex.

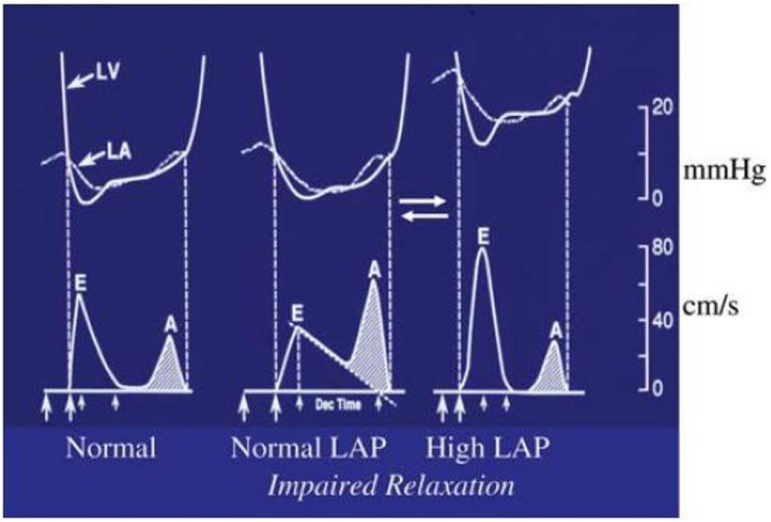

Figure S.11| **E- and A-waves indicate mitral inflow.** Normal (left) and pathologic (middle and right) E- and A-waves are shown. (European Journal of Echo., 2009)

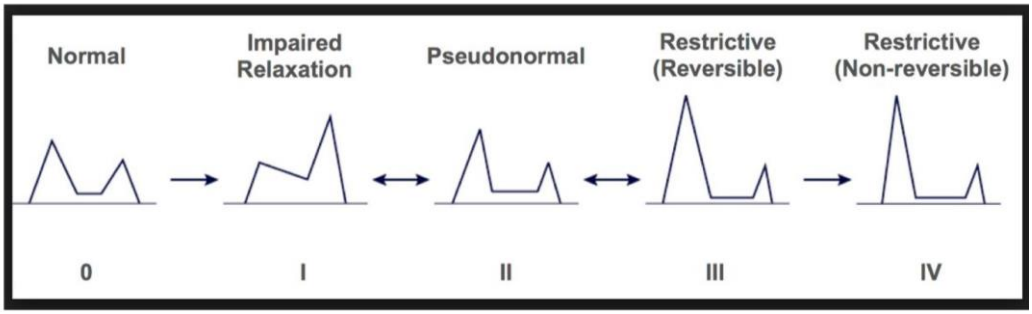

Figure S.12| **Diagram showing normal and pathologic filling patterns of the left ventricle.** Diagram showing grade I-IV pathologic filling patterns (https://123sonography.com/ebook/assess-diastolic-function).

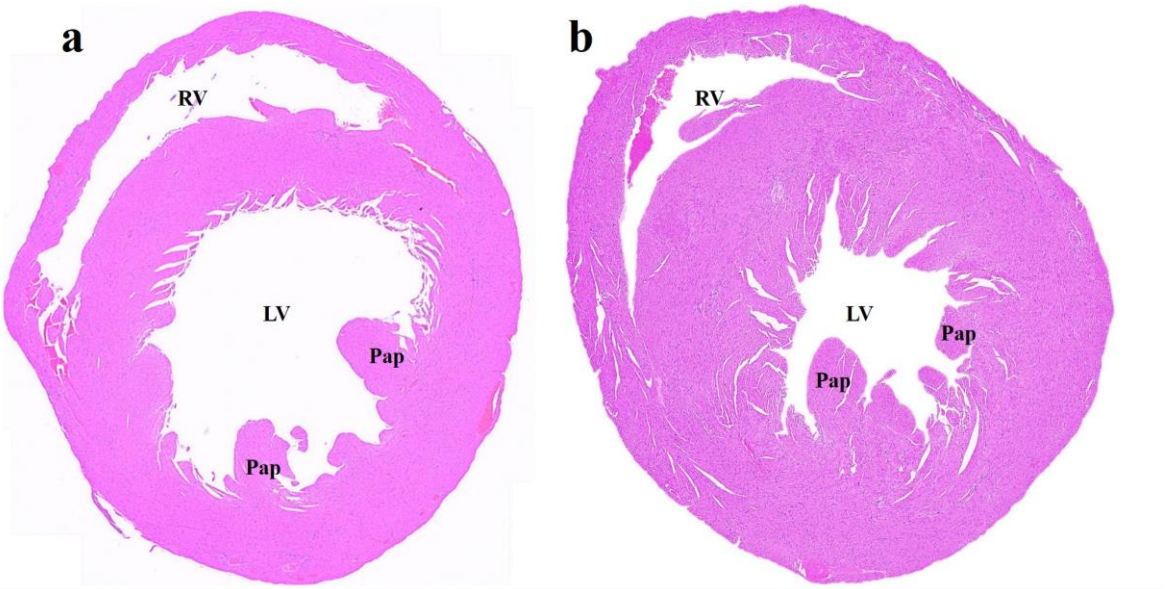

Figure S.13| **Compensatory hypertrophy in Akap13$^{cKO\text{-}MCM}$ mice ≥8 weeks post-recombination.** a) *Akap13^{cKO}* mice (n=4) <8 weeks post-recombination showed dilated left ventricles. b) *Akap13$^{cKO\text{-}MCM}$* mice ≥8 weeks post-recombination showed compensatory hypertrophy.

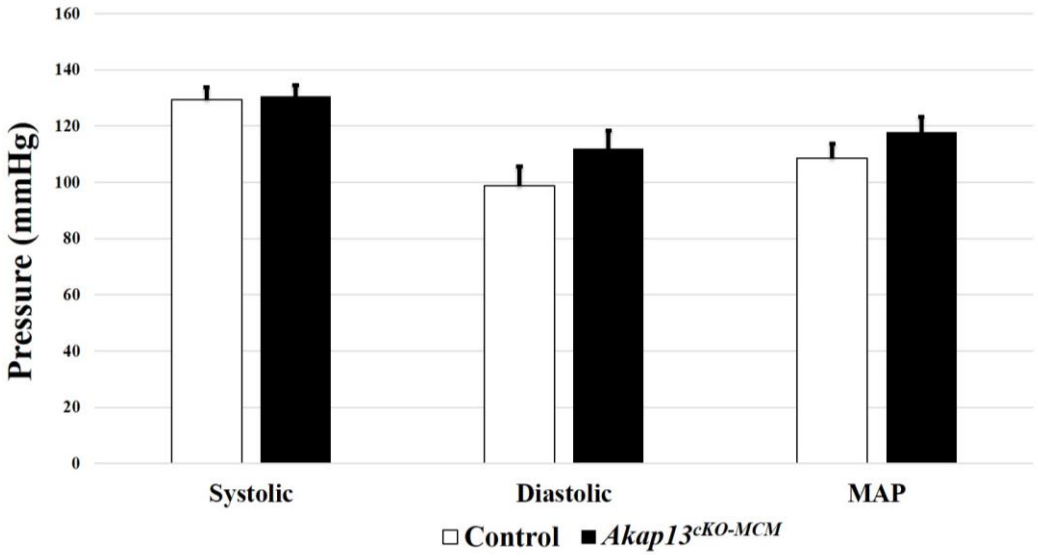

Figure S.14| **No changes in blood pressure or mean arterial pressure (MAP).** *Akap13*$^{cKO\text{-}MCM}$ mice (n=6) showed no significant differences in systolic pressure, diastolic pressure or MAP compared to control mice (n=8) ($p>0.05$). Mice were awake during testing and had been habituated to the test for 2-3 days before final evaluation. Blood pressure was assessed using a tail blood pressure cuff designed for rodents. Student's *t*-test used for statistical analyses.

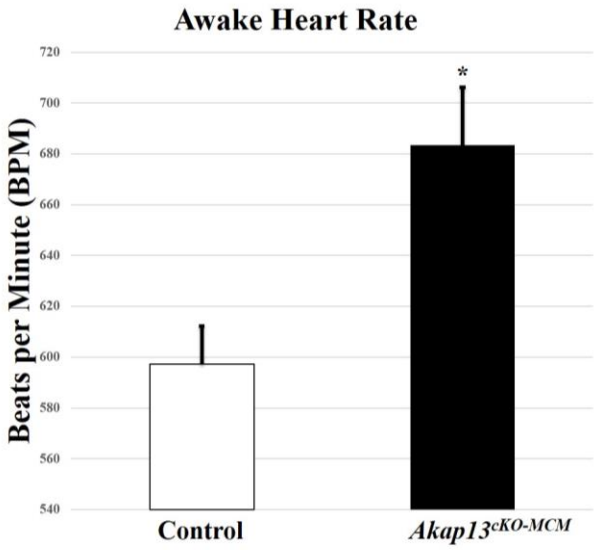

Figure S.15| **Tachycardia in awake Akap13$^{cKO\text{-}MCM}$ mice.** *Akap13$^{cKO\text{-}MCM}$* mice (n=6) had increased heart rate (tachycardia) compared to control mice (n=8). Mice were awake during testing and had been habituated to the test for 2-3 days before final evaluation. Heart rate was assessed using a tail cuff designed for rodents.

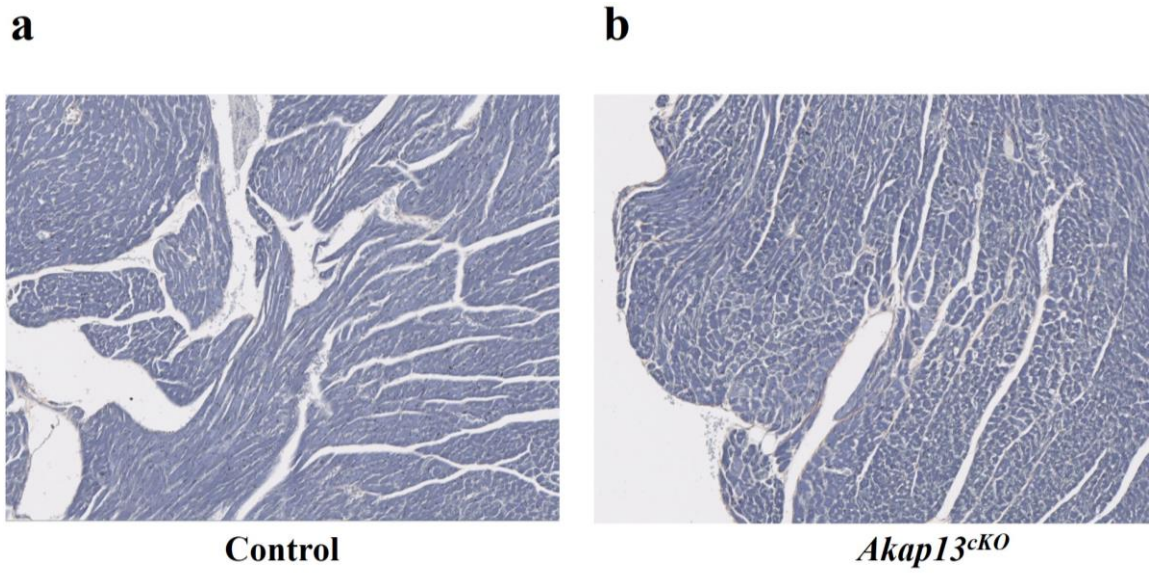

Figure S.16| **Phosphotungstic acid-haematoxylin (PTAH) stain showed dysmorphic cardiomyocytes.**
a) Control mouse heart tissue stained with PTAH. Cardiac muscle cells appear purple.
b) *Akap13*$^{cKO\text{-}MCM}$ mouse heart tissue stained with PTAH showed granular and irregular staining pattern in the cardiac muscle cells.

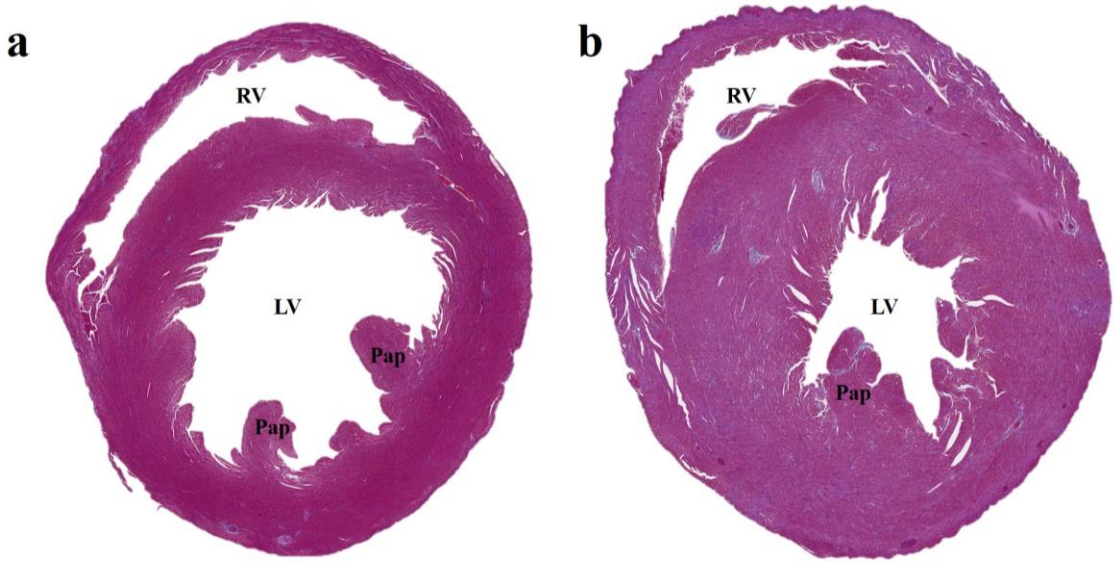

Figure S.17| **Trichrome stain showed increased collagen with time post-recombination in Akap13^{cKO} mice.** a) *Akap13^{cKO}* mice <8 weeks post-recombination showed dilated left ventricles with little collagen deposition (blue) with trichrome stain. b) *Akap13$^{cKO\text{-}MCM}$* mice ≥8 weeks post-recombination showed compensatory hypertrophy with increased collagen deposition (blue) with trichrome stain.

Proteomics		
Protein	**Log2 fold change (EdgeR)**	**p-Value**
PKA(RIA)	1.08	0.015
PKA(RIIA)	-0.89	0.040
RhoA	-0.020	1.00
MFN1	-1.40	0.0091
MICOS complex	-3.20	0.0026
TOM40	-2.16	0.00034
TIM10	-2.17	0.024
VDAC1	-0.71	0.00083
Class IIb Beta-Tubulin	-3.20	0.0018
SNTA1	-0.81	0.040
UQCR11	-5.00	0.00049

Table ST.9| **Proteomics summary table.** Proteomics analysis, cardiac tissue from 5 month old control (n=3) and Akap13^{cKO} (n=3) mice was used for assessing changes in the Akap13^{cKO} proteome. Pathway analysis demonstrated pathological changes in major mitochondrial processes (oxidative phosphorylation), fusion proteins (MFN1) and changes to the cytoskeleton. Additionally, changes were seen in PKA (RIIA).

RNAseq		
Transcript	Log(2) Fold Change	p-Value
Nppa (ANP)	3.37	0.000050
Bmp10	10.28	0.00035
Sln	5.110	0.000050
Mybphl	4.92	0.000050
Myl4	4.49	0.000050
Fgf12	3.90	0.000050
Ak4	-0.46	0.00055
Arhgap20	-0.50	0.00020
E2f1	-1.46	0.00020
Akap5	-1.20	0.00020
Kif23	-1.12	0.00090

Table ST.10| **RNAseq revealed signs of heart failure and dysregulation of transcription factors in *Akap13*$^{cKO\text{-}MCM}$ mice.** RNAseq, Next generation sequencing of RNA isolated from 5 month old control (n=3) and *Akap13*$^{cKO\text{-}MCM}$ (n=3) pathway enrichment analysis identified signs of heart failure (increased ANP, fetal gene response) and transcription factor dysregulation (AK4 and E2f1) in the Akap13$^{cKO\text{-}MCM}$ mice.

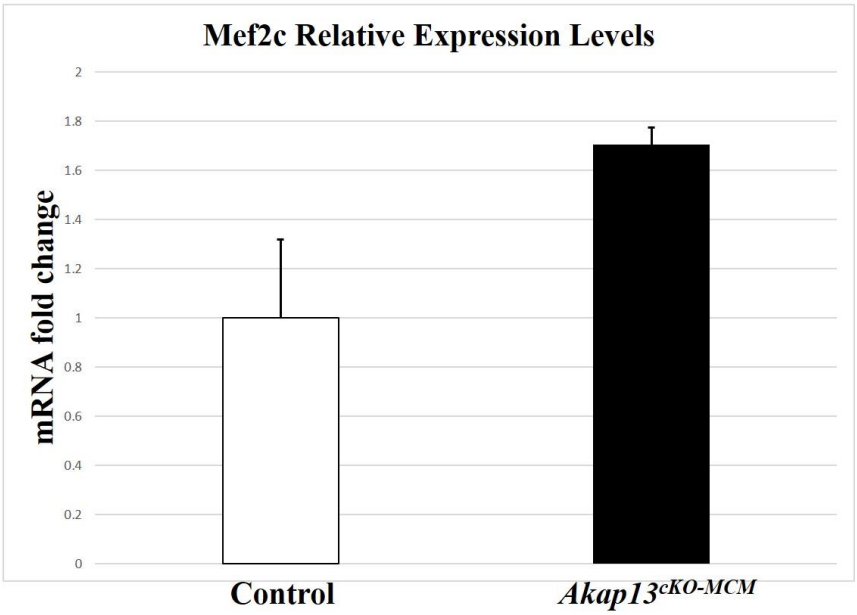

Figure S.18| **Mef2c transcript levels increased in *Akap13*$^{cKO\text{-}MCM}$ mouse hearts.** RT-qPCR, Preliminary quantitative analysis of MADS box transcription enhancer factor 2, polypeptide C (*Mef2c*) transcript levels showed upregulation of *Mef2c* in Akap13^{cKO} mouse hearts suggesting a cardiac fetal gene response as seen with proteomic and transcriptomic analyses.

Proteomics		
Protein	**Log (2) Fold Change**	**p-value**
Epidermal growth factor receptor (Egfr)	6.73	3.83E-12
HIG1 domain family member 1A, mitochondrial (Higd1a)	5.31	0.000123
Acyl-coenzyme A thioesterase 9, mitochondrial (Acot9)	5.28	0.00095
Complement factor H (Cfh)	4.98	1.24E-07
Non-POU domain-containing octamer-binding protein (Nono)	4.97	0.00098
Complement factor B (Cfb)	4.96	2.60E-06

Table ST.11| **Cardiac proteomic analyses revealed signs of heart failure in *Akap13*$^{cKO\text{-}MCM}$ mice.** Cardiac proteomic analyses also showed increased signs of heart failure including increased complement and growth factors. Some mitochondrial proteins (Higd1a) were also significantly increased which suggested that mitochondrial proteins were not all decreased, rather, specific pathways were being affected.

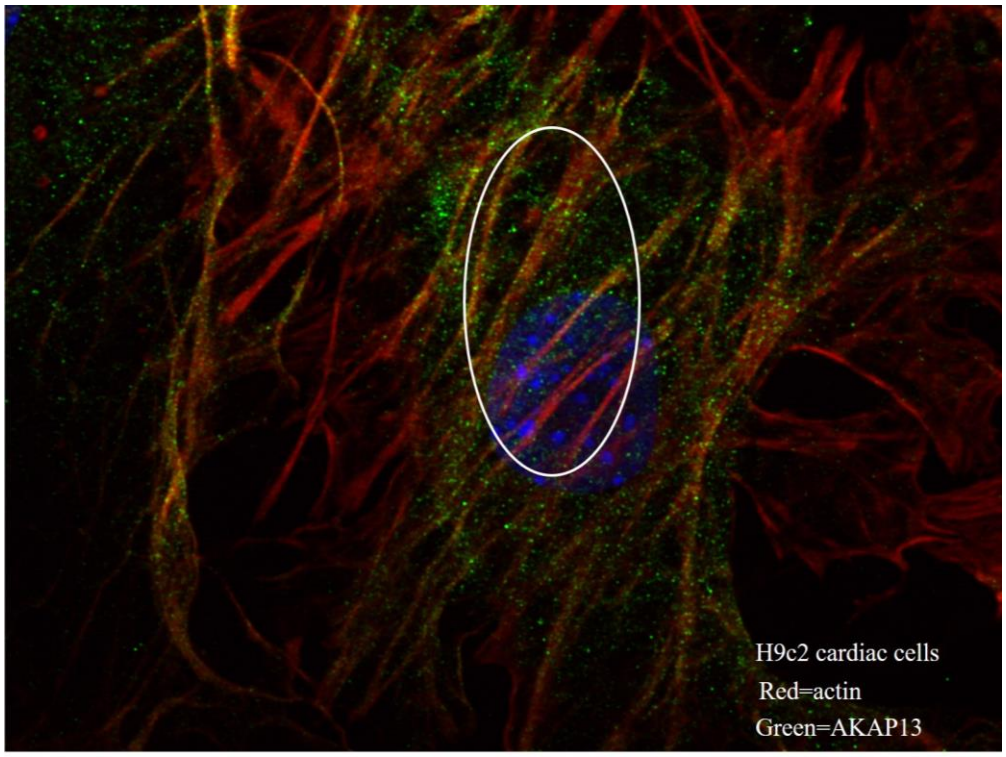

Figure S.19| **AKAP13 localizes to actin in H9c2 cells.** H9C2 (rat cardiomyoblasts) dual labeling showed AKAP13 (green) co-localization (yellow) to actin filaments (red); the nucleus was stained with DAPI (blue).

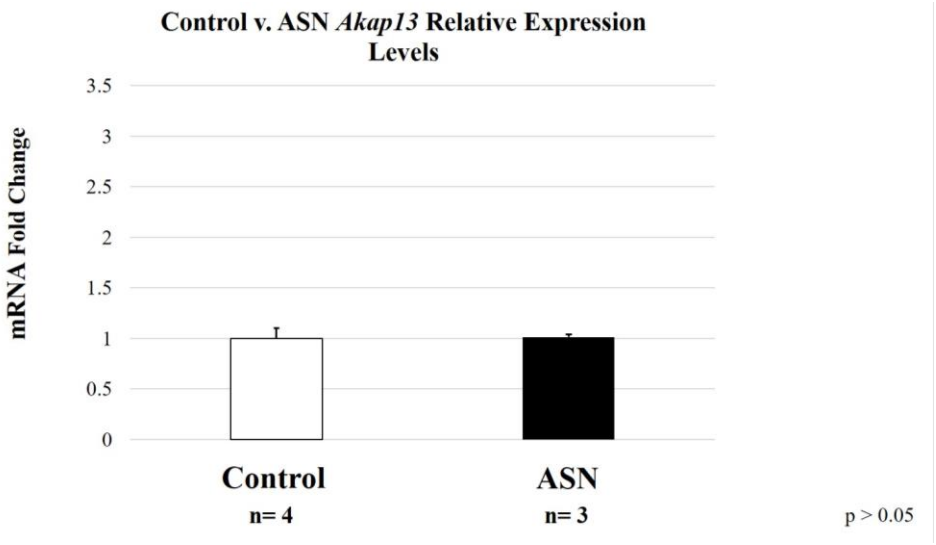

Figure S.20| **Control and All Stars Negative (ASN) showed no changes in *Akap13* transcript levels.** a) RT-qPCR, Endogenous levels of *Akap13* mRNA transcripts were knocked down using small interfering RNA (siRNA). ($p<0.001$). Student's *t*-test used for statistical analyses. b) RT-qPCR, Endogenous levels of *Akap13* mRNA transcripts were quantified in control (no transfection) and ASN transfected H9c2 cells. No changes in endogenous *Akap13* transcripts were observed ($p>0.05$). Student's *t*-test used for statistical analyses.

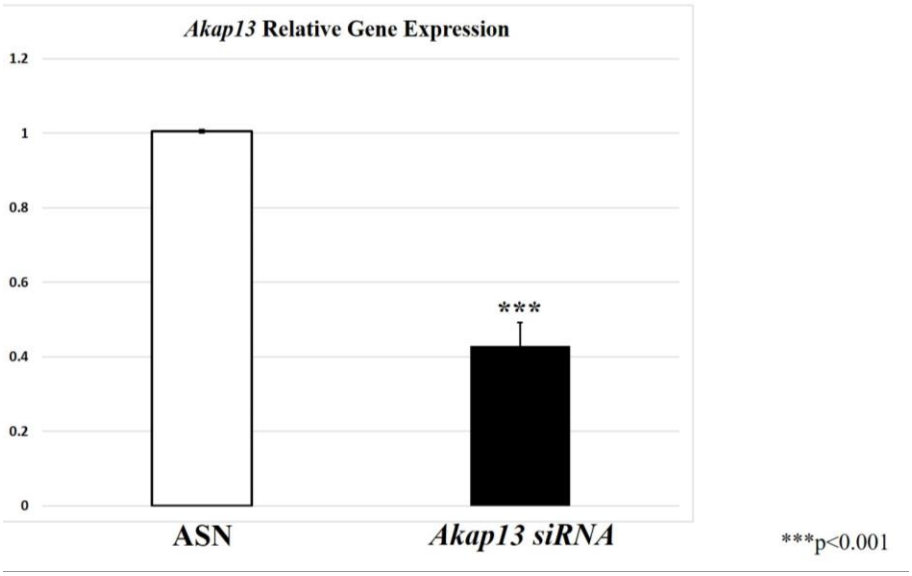

Figure S.21| ***Akap13* knockdown.** RT-qPCR, Endogenous levels of *Akap13* mRNA transcripts were knocked down in H9c2 cells using small interfering RNA (siRNA). ($p<0.001$). All Star's Negative (ASN) transfected H9c2 cells were used for control. Student's *t*-test used for statistical analyses.

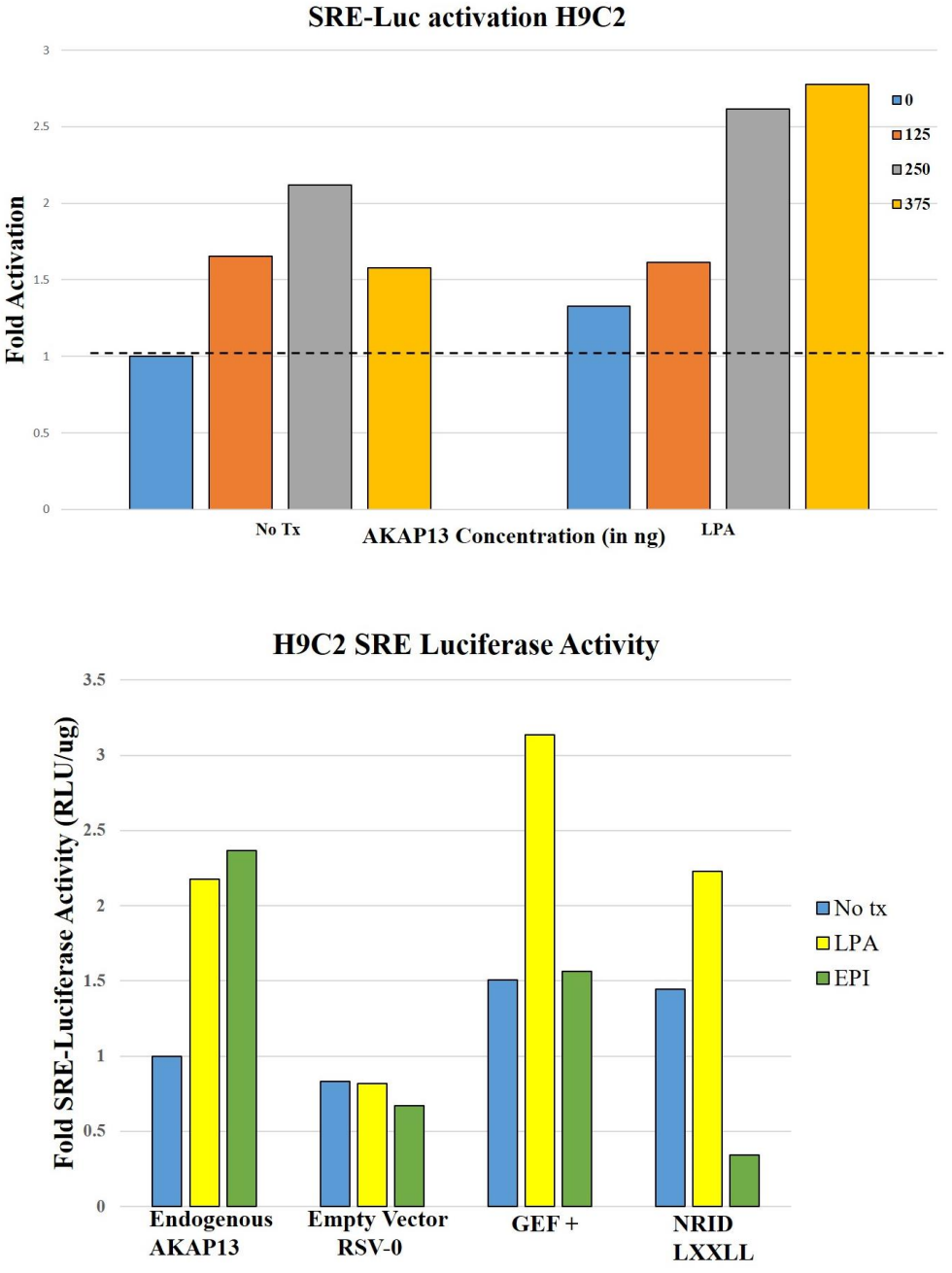

Figure S.22| **Overexpression of AKAP13 activated SRE-luciferase.** Upper) Overexpression of AKAP13 showed increased fold-activation of SRE-luciferase at 125ng, 250ng, and 375ng of AKAP13, consistent with published data (Mayers, 2010). Lower) Overexpression of AKAP13 domains showed increased SRE-luciferase activation with the GEF domain more so than the nuclear hormone receptor interacting domain (NRID) with lysophosphatidic acid (LPA) treatment.

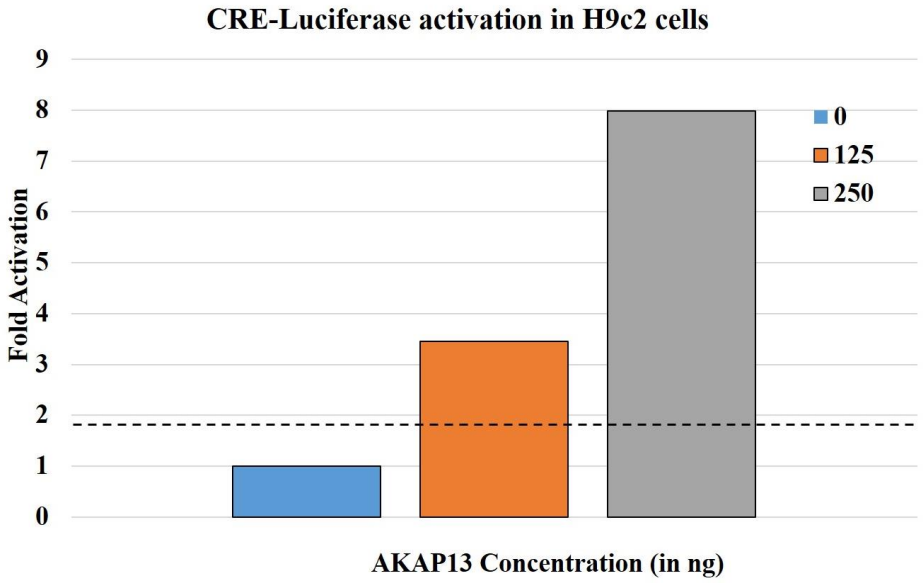

Figure S.23| **Dose-response seen with overexpression of AKAP13 with robust CRE-luc activation.** Overexpression of AKAP13 in H9c2 cells showed a robust increased fold-activation of CRE-luciferase at 125 ng and especially 250 ng AKAP13 (8-fold activation).

APPENDIX B

The following pages of this appendix contain tables for the TetOnCre (TOC) mouse model. Data are provided where available. This second Cre was introduced later during the project, so all assays that were performed using the MCM mouse model were not necessarily performed with the TOC mouse model. Tables are included here for completeness.

Resting MRI: TOC Model					
	Akap13 $^{cKO\text{-}TOC}$		**Control**		**p-value**
LVEF	59.02	%	67.05	%	0.0042
EDVI	2.13	µL/g	1.88	µL/g	0.068
ESVI	0.87	µL/g	0.622	µL/g	0.0062
EDMI	3.68	mg/g	3.46	mg/g	0.039
ESMI	3.68	mg/g	3.39	mg/g	0.040

Resting MRI: TOC Model. *Akap13*$^{cKO\text{-}TOC}$ (n=7) and Control (F/F, TOC+; no treatment; and F/F, TOC- with doxycycline treatment) (n=5). Left Ventricular Ejection Fraction (LVEF); End-Diastolic Volume Index (EDVI); End-Systolic Volume Index (ESVI); End-Diastolic Mass Index (EDMI); End-Systolic Mass Index (ESMI).

Resting MRI: TOC Model- Female					
	Akap13 $^{cKO\text{-}TOC}$		**Control**		**p-value**
LVEF	59.54	%	69.8	%	0.030
EDVI	2.21	µL/g	1.99	µL/g	0.077
ESVI	0.90	µL/g	0.60	µL/g	0.015
EDMI	3.64	mg/g	3.62	mg/g	0.88
ESMI	3.63	mg/g	3.48	mg/g	0.79

Resting MRI: TOC Model- Female. *Akap13*$^{cKO\text{-}TOC}$ (n=4) and Control (F/F, TOC+; no treatment; and F/F, TOC- with doxycycline treatment) (n=4). Left Ventricular Ejection Fraction (LVEF); End-Diastolic Volume Index (EDVI); End-Systolic Volume Index (ESVI); End-Diastolic Mass Index (EDMI); End-Systolic Mass Index (ESMI).

Resting MRI: TOC Model- Male					
	Akap13 $^{cKO\text{-}TOC}$		**Control**		**p-value**
LVEF	61.47	%	63.84	%	0.85
EDVI	1.91	µL/g	1.92	µL/g	0.78
ESVI	0.75	µL/g	0.70	µL/g	0.86
EDMI	3.50	mg/g	3.32	mg/g	0.83
ESMI	3.56	mg/g	3.37	mg/g	0.63

Resting MRI: TOC Model- Male. *Akap13*$^{cKO\text{-}TOC}$ (n=8) and Control (F/F, TOC+; no treatment; and F/F, TOC- with doxycycline treatment) (n=4). Left Ventricular Ejection Fraction (LVEF); End-Diastolic Volume Index (EDVI); End-Systolic Volume Index (ESVI); End-Diastolic Mass Index (EDMI); End-Systolic Mass Index (ESMI).

VITA

Kimberlyn Maravet Baig-Ward was born on August 25, 1983 in Bryan, Texas. She is a citizen of the United States of America, and currently resides in Annandale, VA with her two children, Camden Ward (5) and Amerlyn Ward (3), and pets (Max, Brodie, and Dolly). Ms. Baig-Ward attended Texas A&M University where she graduated in 2007 *Magna Cum Laude* with Foundation Honors, University Honors, and as an Honors Undergraduate Research Fellow. Ms. Baig-Ward went on to pursue an Intramural Research Training Award (IRTA) from 2007-2008 at the National Institutes of Health (NIH) in Bethesda, MD before beginning the MD/PhD dual degree program at Virginia Commonwealth University School of Medicine in 2008 as an individual Graduate Partnership Program student with the NIH. Later in her training, Ms. Baig-Ward followed her PhD advisor to Johns Hopkins University School of Medicine to complete her PhD research in Baltimore, MD.

During her PhD training, Ms. Baig-Ward had several abstracts accepted at national conferences including the American Society for Reproductive Medicine (ASRM) and the Society for Reproductive Investigation (SRI). Ms. Baig-Ward also participated in a national symposium (Mitochondria Communication, Taos, NM) in 2017. Ms. Baig-Ward is currently submitting several first author research publications from this body of work and from her additional projects (Neuro/Behavioral) not discussed in this dissertation. She has been a co-author on several papers and book chapters, including a research article in-

press from her collaborative efforts during her time at Johns Hopkins University School of Medicine.